2016

The Relationship Between High-Cycle Fatigue and Tensile Properties in Cast Aluminum Alloys

Huseyin Ozdes
University of North Florida, huseyin.ozdes@gmail.com

THE RELATIONSHIP BETWEEN HIGH-CYCLE FATIGUE AND TENSILE PROPERTIES IN CAST ALUMINUM ALLOYS

by

Hüseyin Özdeş

A thesis submitted to the School of Engineering

in partial fulfillment of the requirements for the degree of

Master of Science in Mechanical Engineering

UNIVERSITY OF NORTH FLORIDA

COLLEGE OF COMPUTING, ENGINEERING AND CONSTRUCTION

December, 2016

Certificate of Approval

This thesis titled “The Relationship between High-Cycle Fatigue and Tensile Properties in Cast Aluminum Alloys” by Hüseyin Özdeş is approved by:

Date

_____ _____
Dr. Murat Tiryakioğlu, CQE, Advisor

_____ _____
Dr. Alexandra Schönning, Committee Member

_____ _____
Dr. Paul Eason, PE, Committee Member

Accepted for the School of Engineering:

_____ _____
Director of the School of Engineering
Dr. Murat Tiryakioğlu, CQE

Accepted for the College of Computing, Engineering and Construction

_____ _____
Dr. Mark A. Tumeo, PE
Dean of the College of Computing, Engineering and Construction

Accepted for the University:

_____ _____
Dr. John Kantner
Dean of the Graduate School

Dedication

…to my beloved wife and son.

Acknowledgements

I would first like to thank my thesis advisor Dr. Murat Tiryakioğlu for keeping his office door always open whenever I had trouble or question about my research. He consistently motivated me throughout the hard work that was put into this investigation. Without his guidance and comments, I would have not enjoyed the time spent on this study.

I gratefully acknowledge the Alotech scholarship awarded for my studies and thank Mr. John Grassi for his unending support for my research.

Lastly, I greatly appreciate the support received from my family and my colleagues. Their support has always been valuable to me.

Table of Contents

List of Tables

List of Figures

Nomenclature

Symbol		Meaning
β_0, β_1	:	Alloy dependent coefficients
γ	:	Walker parameter
Γ	:	Gamma function
$\varepsilon_f^{'}$	:	Fatigue ductility coefficient
$\Delta\varepsilon$	:	Total strain range
$\Delta\varepsilon_e$	:	Elastic strain range
$\Delta\varepsilon_p$	:	Plastic strain range
ΔK_{th}	:	Threshold in crack propagation
$\overline{\sigma}$	:	Mean value of the Weibull distribution for stress (MPa)
σ_0	:	Scale parameter of the Weibull distribution for stress (MPa)
σ_a	:	Stress amplitude, alternating stress (MPa)
$\sigma_{a \mid ax}$	:	Uniaxial stress amplitude (MPa)
$\sigma_{a \mid rb}$	:	Rotating bending stress amplitude (MPa)
σ_{eq}	:	Equivalent stress at R=-1 (MPa)
σ_f	:	Fatigue strength at given cycles (MPa)
$\sigma_f^{'}$	:	Fatigue strength coefficient (MPa)
σ_m	:	Mean stress (MPa)
σ_{max}	:	Maximum stress (MPa)
σ_{min}	:	Minimum stress (MPa)
σ_T	:	Threshold value below which no failure is expected
σ_y	:	Yield strength (MPa)
A_i	:	Largest area of defect (mm^2)
b	:	Fatigue strength exponent, elastic exponent, Basquin exponent
c	:	Fatigue ductility exponent, plastic exponent
d	:	Diameter of the inner section of specimen (mm)
D	:	Specimen diameter (mm)
e_F	:	Elongation to fracture
$e_{F(max)}$	:	Ductility potential, defect-free elongation
f_1, f_2	:	Specimen geometry dependent functions
E	:	Elastic modulus, Young's modulus (GPa)
f	:	Probability density function
f_L, f_U	:	Probability density function of lower and upper distribution
F	:	Fatigue life correction factor
H_v	:	Vickers hardness (MPa)
K_t	:	Stress concentration factor
m	:	Shape parameter, Weibull modulus
N_0	:	Scale parameter of the Weibull distribution for equivalent fatigue life
N_{eq}	:	Equivalent fatigue life

$\overline{N_{eq}}$	:	Mean value of the Weibull distribution for equivalent fatigue life
N_f	:	Cycles to failure, fatigue life
N_i	:	Crack initiation life
N_p	:	Crack propagation life
N_T	:	Transition life
p	:	Fraction of the lower distribution
P	:	Probability of failure at given stress or fatigue life
Q_T	:	Quality index
$\overline{Q_T}$	:	Mean value of the Weibull distribution for quality index
R	:	Ratio of minimum stress to maximum stress
R^2	:	Coefficient of determination
R_A	:	Reduction in area
S_T	:	Tensile strength (MPa)
$S_{T(max)}$	:	Maximum tensile strength, defect-free tensile strength (MPa)
V	:	Volume of the specimen (mm^3)
W	:	Energy absorbed per volume by specimen, strain energy density (MJ/m^3)
w_p	:	Micro-strain energy per cycle (J/m^3)

Abbreviation		**Meaning**
BWQ	:	Boiling water quench
CWQ	:	Cold water quench
DAS	:	Dendrite arm spacing
FB	:	Fluidized bed
FSP	:	Friction stir processing
HCF	:	High-cycle fatigue
HIP	:	Hot iso-statically press processing
LCF	:	Low-cycle fatigue
ML	:	Maximum likelihood estimation
OA	:	Over-aged
PA	:	Peak-aged
RT	:	Room temperature
SWT	:	Smith-Watson-Topper method
UA	:	Under-aged

Abstract

Cast aluminum alloys are common in automotive and aerospace applications due to their high strength-to-density ratio. Fracture data for cast aluminum alloys, such as fatigue life, tensile strength and elongation, are heavily affected by the structural defects, such as pores and bifilms. There have been numerous studies in which either fatigue performance or tensile deformation were characterized and linked to casting defects. However, a comprehensive study that correlates tensile and fatigue properties has not been reported. The present study is motivated to fill this gap.

The main objective of the investigation is to analyze the link between tensile and fatigue performance of commonly used cast aluminum alloys, and determine whether fatigue performance of cast aluminum alloys can be predicted. To accomplish this task, four research questions were developed: (i) how well do equations developed to account for mean stress effects perform in cast aluminum alloys, especially in datasets with various levels of structural quality, (ii) is the strong correlation between fatigue life and structural quality index obtained from tensile data reported for A206 alloy castings applicable to other aerospace and automotive casting alloys, (iii) how do methods to estimate high cycle fatigue from tensile data perform with aluminum castings, and (iv) can the axial fatigue performance of an A356-T6 casting be predicted from rotating beam fatigue data.

Among the three mean stress correction models analyzed by using seven datasets from the literature, the one developed by Walker with an adjustable exponent has provided the best fit. It has been hypothesized that the adjustable Walker parameter is related to the structural quality index, Q_T, estimated from tensile data. Results have shown that there is indeed a strong correlation between Q_T and the Walker parameter. Moreover the parameters of the

Weibull distribution estimated from corrected data have been found to be strongly influenced by the mean stress correction method used.

Tensile and fatigue life data for 319, D357 and B201 aluminum alloy castings reported in the literature have been reanalyzed by using a maximum likelihood method to estimate Basquin parameters in datasets with run-outs, Weibull statistics for censored data and mean stress correction. After converting tensile data to Q_T, a distinct relationship has been observed between the expected fatigue life and mean quality index for all alloys. Moreover, probability of survival in fatigue life has been found to be directly linked to the proportions of the quality index distributions in two different regions, providing further evidence about the strong relationship between elongation, i.e., structural quality, and fatigue performance [1]. Specimen geometry has been found to make the largest difference whereas the two aerospace alloys, B201 and D357, with distinctly different microstructures, have followed the same relationship, reinforcing the findings in the literature that fatigue life in aluminum castings is mainly determined by the size distribution and number density of structural defects.

Six methods to predict fatigue life from tensile data have been compared by using data from the literature as well as the experimental A356 data developed in this study. Results have shown that none of the six methods provide reliable results. The consistently poor performance of the methods developed for steels and wrought alloys can be attributed to the major structural defects, namely bifilms, in aluminum castings. A new method to estimate the S-N curve from tensile data have been developed by using data for seventy-one S-N curves have been collected and Basquin parameters have been determined. Analysis showed that there is a strong relationship between QT and the Basquin exponent.

The Basquin parameters estimated by using the empirical relationships developed in the present study have provided better fits to the same datasets tested for the six methods. Hence the model developed in this study is proposed as the most reliable method to estimate high cycle fatigue properties.

Finally, three methods to convert rotating bending fatigue test results to uniaxial fatigue data have been investigated by using the data developed in this study. Results have indicated that the method developed by Esin, in which both the fatigue life and alternating stress are corrected, provide the best estimate.

Analyses of fracture surfaces of broken specimens via scanning electron microscopy have shown that tensile, axial fatigue and rotating beam fatigue properties are all strongly influenced by the same structural defects, confirming the validity of the approach taken in this study.

1. Introduction

Typically, structural components subjected to loads have been designed such that maximum stresses during the lifetime of the component do not exceed the tensile yield strength of the material so that only elastic strains are developed. However, there are usually local stress concentrations due to surface imperfections, design flaws and/or microstructural discontinuities in the structure, such as inclusions and pores. Thus, local stresses can be well in excess of the yield strength, and after some repeated loading, cracks can form and propagate until final rupture. This progressive failure is referred to as fatigue.

Fatigue was originally identified as a problem in the early 1800s by engineers who observed that some bridge and railroad sections were starting to crack although stresses were well under the yield strength. The engineers could not identify the reason for this type of failure, thus concluded that the metal was "tired", coining the word "fatigue" [2].

Today, fatigue failures are the most common failure type in service, which account for 90% of the failures reported [3, 4]. Nevertheless, there is no requirement for fatigue performance in any military or industrial specification, to the author's knowledge. Instead many industrial standards and specifications such as MIL-A-21180D [5] require a number of nondestructive tests as well as tensile tests be conducted for quality assurance purposes.

To examine properties of machined parts, there is a number of mechanical tests available to materials engineers. The most common one is the tensile test, which provides data for mechanical properties such as Young's modulus (E), yield strength (σ_Y), tensile strength (S_T) and elongation (e_F). To evaluate fatigue performance, fatigue tests need to be conducted to determine cycles to failure (N_f), at a given stress amplitude (σ_a) and mean

stress (σ_m), which are usually determined based on the tensile yield strength. Unlike other property tests in which loads are applied gradually, in fatigue test, specimens are subjected to alternating stresses to simulate the conditions under which the part would be in service [6]. In high-cycle fatigue ($N_f > 10^5$ cycles), where the maximum stresses are well below the yield strength (as in service), it is not unusual for a single test to take days, even weeks, to produce a single data point. To this respect, fatigue testing has become costly and time consuming.

On the other hand, another type of mechanical test, which is more readily available, tensile testing takes significantly lower time to run and it has been studied over years. Researchers have made attempts [7-12] to obtain fatigue properties from tensile test results. There have been some accomplishments on steel, yet aluminum alloys still stand as problematic.

2. Background

2.1. Tensile Testing

Tensile testing is the most commonly used mechanical test to determine the mechanical properties of metals. In this test, a specimen is stretched at a predetermined strain rate, usually 0.001 to 0.005 s^{-1}. The load or stress necessary to deform the specimen at that rate is recorded versus strain. A typical stress-strain curve for a steel specimen is presented in Figure 1, which shows the engineering and true stress-strain behavior. Note that maximum engineering stress, i.e., ultimate tensile strength, is the point where necking occurs after which engineering stress decreases with increasing strain. True stress, however, increases steadily until final fracture takes place.

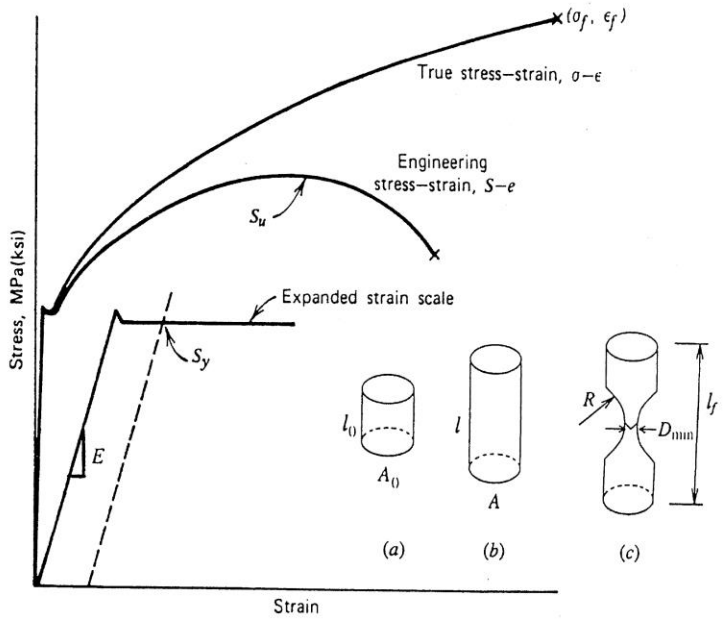

Figure 1. Schematic illustration of the tensile stress-strain curve, both engineering and true, and specific points of interest to engineers [13].

2.2. Fatigue Testing

To evaluate the fatigue performance of a material, fatigue tests are run at a predetermined stress ratio, R:

$$R=\frac{\sigma_{min}}{\sigma_{max}} \tag{1}$$

where, σ_{min} is minimum stress and σ_{max} is maximum stress in the spectrum, respectively. Some stresses used in fatigue testing terminology and different R ratio's spectra are illustrated in Figure 2.a and b, respectively. Different R ratios cause different mean stresses which have a significant effect on fatigue results [3, 14-20].

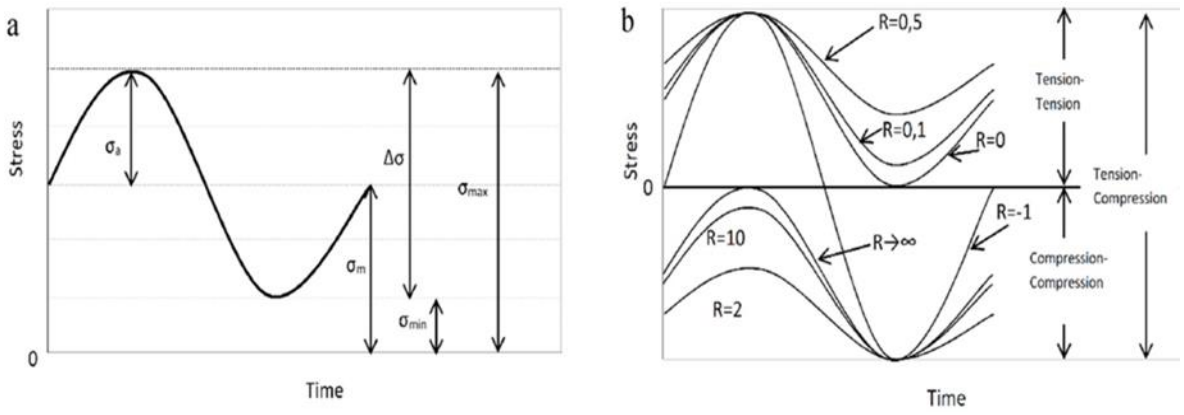

Figure 2. Schematic illustration of a) stress types b) different R ratios on spectrum [18].

Stress amplitude, σ_a is found by:

$$\sigma_a = \frac{\sigma_{max} - \sigma_{min}}{2} \tag{2}$$

Mean stress, σ_m is found by:

$$\sigma_m = \frac{\sigma_{max} + \sigma_{min}}{2} \tag{3}$$

Two of the most common fatigue tests are rotating beam and uniaxial (or axial). These tests are shown in Figure 3. Note that in rotating beam fatigue tests, R=-1 and stress distribution along the cross-section of the specimen is not uniform, with maximum stresses achieved at the surface. In axial tests, however, stresses are uniform over the cross-section of the specimen and R can be adjusted to levels shown in Figure 2. The rotating beam test has been widely used because data can be obtained much more rapidly due to the frequency levels around 20 Hz compared to the typical frequency in axial testing of 3-5 Hz.

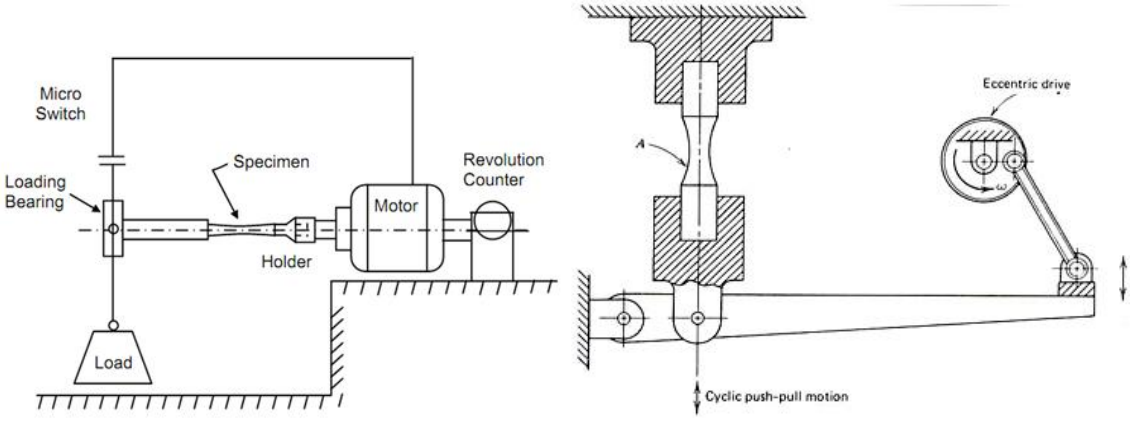

(a) (b)

Figure 3. Schematic illustration of two common fatigue tests: a) rotating beam [21], and b) axial [22].

Total fatigue life of components consists of three stages: (1) crack initiation, (2) crack propagation, and (3) final rupture. Crack initiation can represent a large majority (up to 70%) of total fatigue life in parts with high structural quality, it takes many cycles for a propagating crack to form. In parts with low structural quality, i.e., with many structural defects such as pores, crack initiation stage may be very small, and even nonexistent. In such cases, total fatigue life is essentially equal to crack propagation stage because final rupture takes only several cycles [6].

2.3. Wöhler (S-N) Diagram

Stress amplitude and corresponding cycles to failure (N_f) results in fatigue test are presented in the Wöhler diagram [23] in double-log or semi-log scale. A typical Wöhler diagram can be seen in Figure 4. Note that 1045 steel, there is a horizontal asymptote that starts at approximately 10^6 cycles, known as the endurance limit. Such a limit is usually not observed in aluminum alloys, such as the 2024-T6 alloy. Because there is no endurance limit in aluminum alloys, usually fatigue strength, σ_f, determined at 10^6-10^7 cycles is reported instead of endurance limit.

The change in fatigue life, N_f, with stress amplitude, σ_a, is known to follow the Basquin law [24]:

$$\sigma_a=\sigma_f^{'}N_f^{b} \tag{4}$$

where, $\sigma_f^{'}$ is fatigue strength coefficient and b is the Basquin exponent (also known as elastic exponent). The Basquin law has been used to express the high cycle fatigue (HCF) behavior of metals. Both Basquin parameters are strongly affected by the material [25], specimen geometry [26] as well as the type of test conducted [7]. The S-N curves for 4130

steel obtained with rotating beam and axial (R=-1) fatigue tests are presented in Figure 5. For the same stress amplitude, rotating beam test yields a higher fatigue life (cycles to failure).

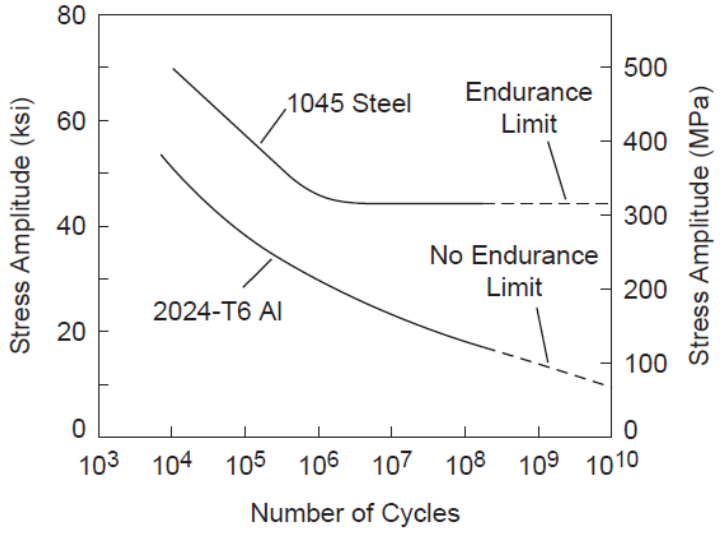

Figure 4. Typical Wöhler diagrams for 1045 steel and 2024 aluminum alloy. Note that there is no endurance limit for 2024 [27].

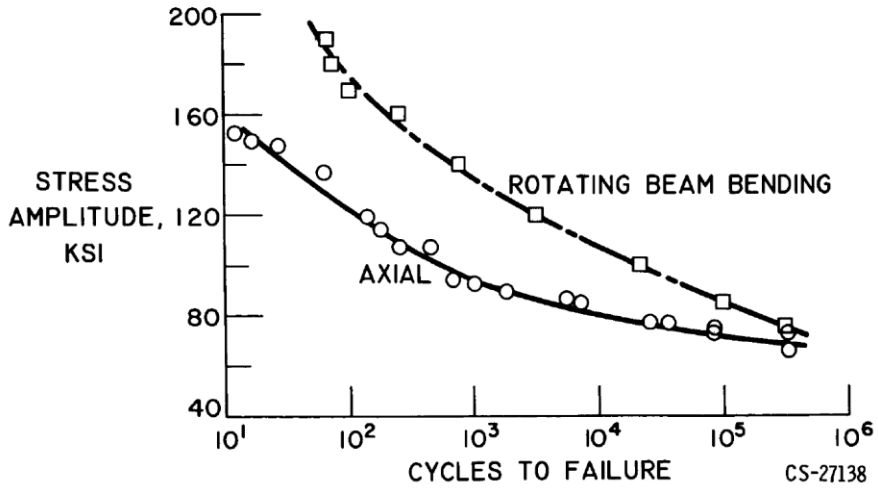

Figure 5. Wöhler diagrams for 4130 steel obtained in axial and rotating beam fatigue testing [7]. Note that R = -1 in both cases.

2.4. The Effect of Mean Stress on S-N Curve

Mean stress, and naturally stress ratio, has a significant effect on the HCF behavior [15, 17]. The effect of mean stress on the S-N curve is shown schematically in Figure 6. When the mean stress is compressive, fatigue life is longest for the same level of alternating stress. When mean stress is tension, fatigue life is lowest. For zero mean stress (R=-1), fatigue life is between the two other S-N curves [13].

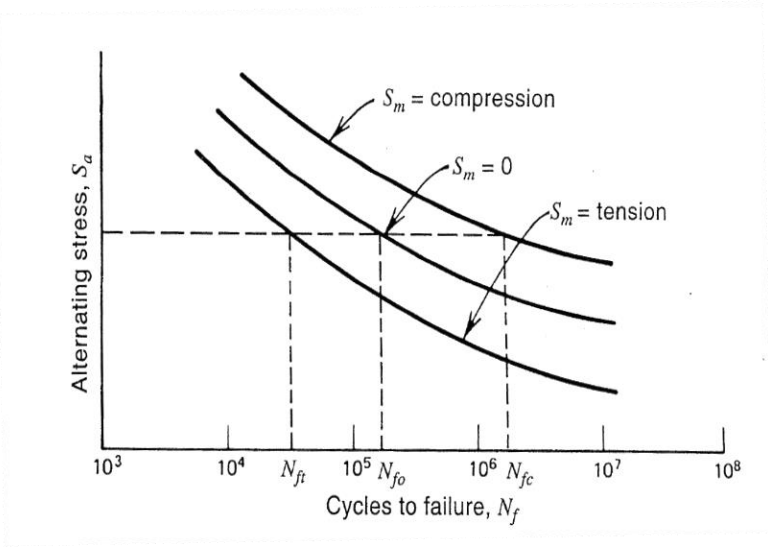

Figure 6. The effect of mean stress on the S-N curve shown schematically [13].

In the literature, numerous correction methods are reported to account for the mean stress effect on fatigue test results. These models have been developed to modify the alternating stress and find the equivalent stress amplitude, σ_{eq}, at R=-1 or zero mean stress. Among those, most widely used ones are those developed by Soderberg [28], Walker [29] and Smith-Watson-Topper (SWT) [20]. Equivalent stress amplitudes for these models are given in Equations (5), (6) and (7), respectively:

$$\frac{\sigma_a}{\sigma_{eq}}+\frac{\sigma_m}{\sigma_y}=1 \tag{5}$$

$$\sigma_{eq}=\sigma_a\left(\frac{2}{1-R}\right)^{\gamma} \tag{6}$$

$$\sigma_{eq}=\sqrt{\sigma_a(\sigma_a+\sigma_m)}=\sigma_a\sqrt{\frac{2}{1-R}} \tag{7}$$

where γ is the Walker parameter, which is an empirical parameter that yields the best fit. The maximum stress versus fatigue life data for 6061-T6 aluminum alloy obtained at different R ratios is presented in Figure 7, along with fits obtained with γ=0.63 [30].

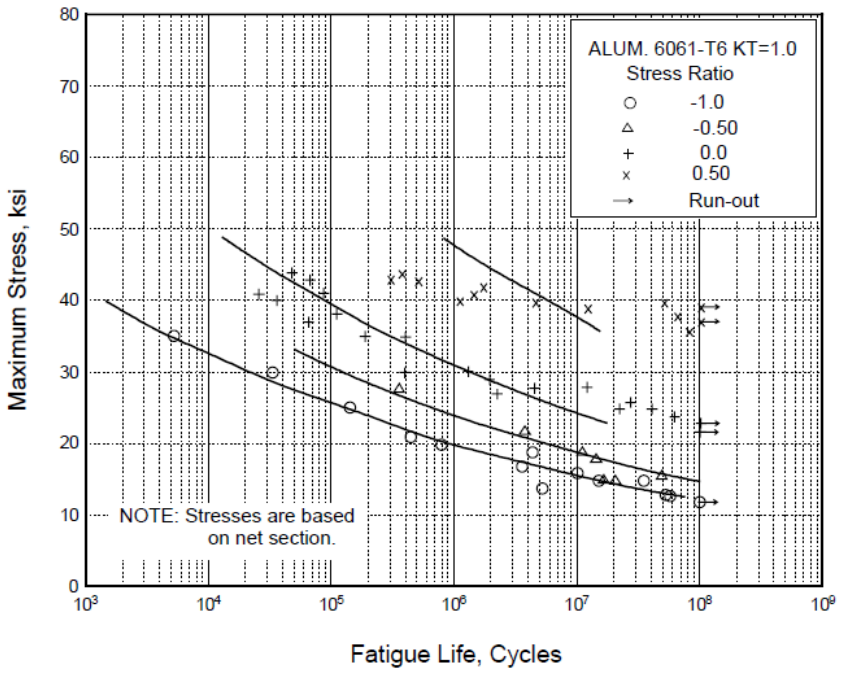

Figure 7. The effect of stress ratio, R, on Wöhler curves in axial fatigue results of 6061-T6 aluminum alloy [30].

Dowling [14] compared widely used methods and reported that the equation developed by Smith, Watson and Topper, Equation (7), was the most accurate for aluminum alloys.

However, there is no study in the literature, to the author's knowledge, that was conducted to determine the value of the Walker parameter for cast aluminum alloys.

2.5. Casting Defects and their Effect on Fatigue and Tensile Performance

In aluminum castings, structural defects, namely oxide bifilms (folded oxide films entrained into the melt during the casting of the metal) and pores, are common as a result of poor melt quality and/or mold filling system design [31]. These structural defects have a deleterious effect on tensile strength and elongation [32, 33], as well as fatigue life [34-37]. A pore that initiated a fatigue crack in a 319-aluminum alloy casting is presented in Figure 8. Similarly, a pore and a folded-over surface oxide film (bifilm) found on the fracture surface of an A356 aluminum alloy casting are shown in Figure 9.

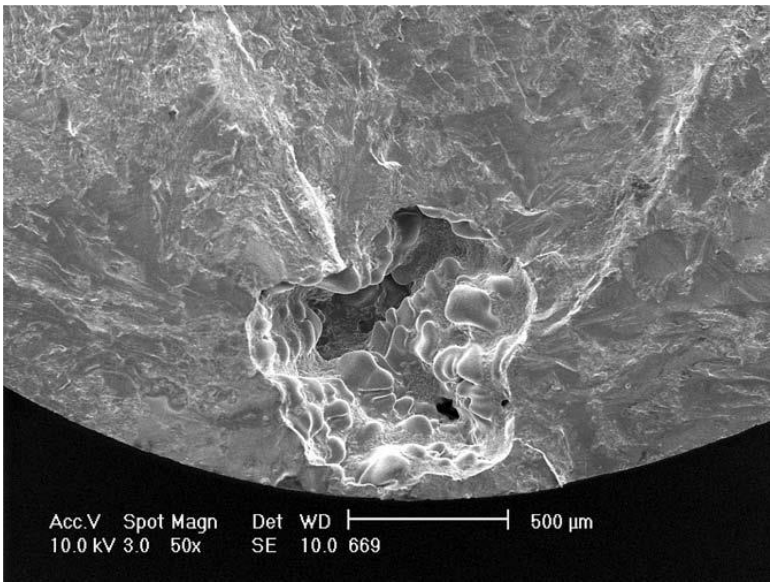

Figure 8. Fatigue crack initiating pore near surface of a 319 aluminum alloy casting [38].

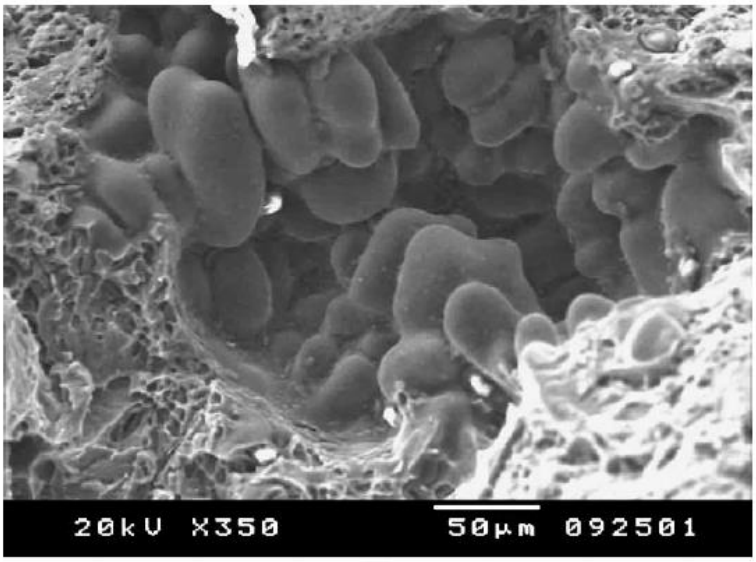

(a)

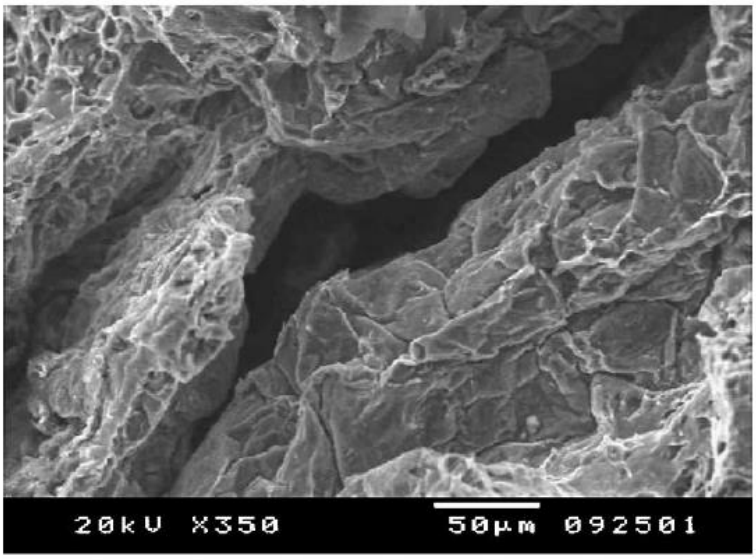

(b)

Figure 9. Structural defects found on the fracture surface of an A356 alloy casting broken in tensile testing [32].

The effect of area fraction of pores, determined by metallographic analysis, on the elongation of A356-T6 alloy castings with a yield strength of 250 MPa is presented in Figure 10. Note that 1% area fraction of porosity is sufficient to reduce elongation by 50%.

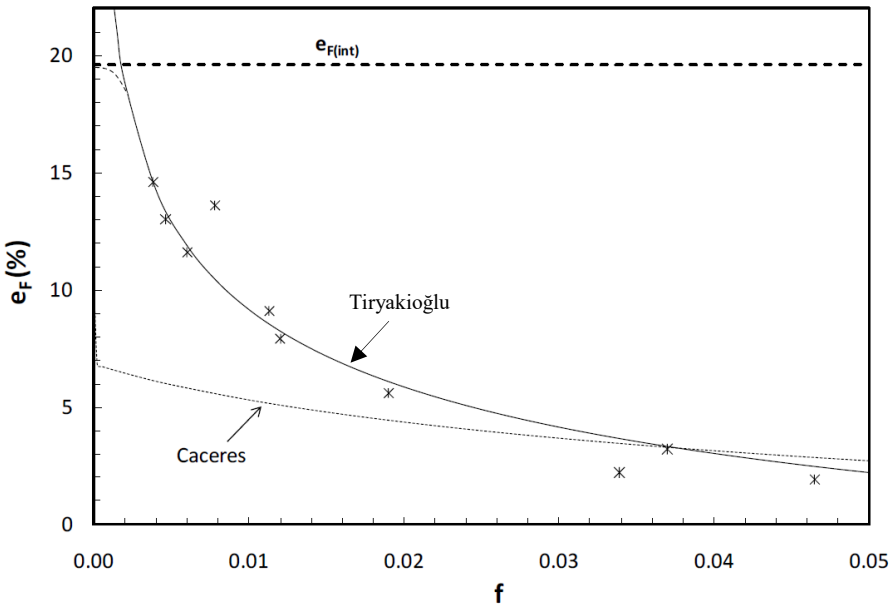

Figure 10. The effect of area fraction of pores (f) on elongation of A356 castings. The expected defect-free elongation ($e_{F(int)}$), as well as fits from two different models are also indicated [33].

One of the earliest studies on the effect of structural quality on the fatigue performance of cast aluminum alloys was conducted by Promisel [39] who characterized the degree of porosity in 295 alloy castings and determined eight distinct quality levels, with 1 as best structural quality and 8 as the worst. The S-N curves for each quality level are presented in Figure 11, which shows that (a) S-N curves are shifted down with decreasing structural quality, (b) the Basquin exponent, b, is affected by the structural quality, and (c) fatigue strength at 10^7 cycles is strongly influenced by porosity level. Wang et al. [40] showed that there is a strong relationship between σ_f at 10^7 cycles and the size of the largest pore in various Al-Si-Mg-(Cu) alloy castings, as presented in Figure 12. Murakami [41-43] developed a model to predict fatigue strength, σ_f, based on the size of inclusions and Vickers hardness, H_v, of the steel:

$$\sigma_f = 1.41 \frac{120 + H_v}{\left(\sqrt{A_i}\right)^{1/6}} \tag{8}$$

Kobayashi and Matsui [44] showed that Murakami method can be used to predict fatigue strength of A356 aluminum alloy castings.

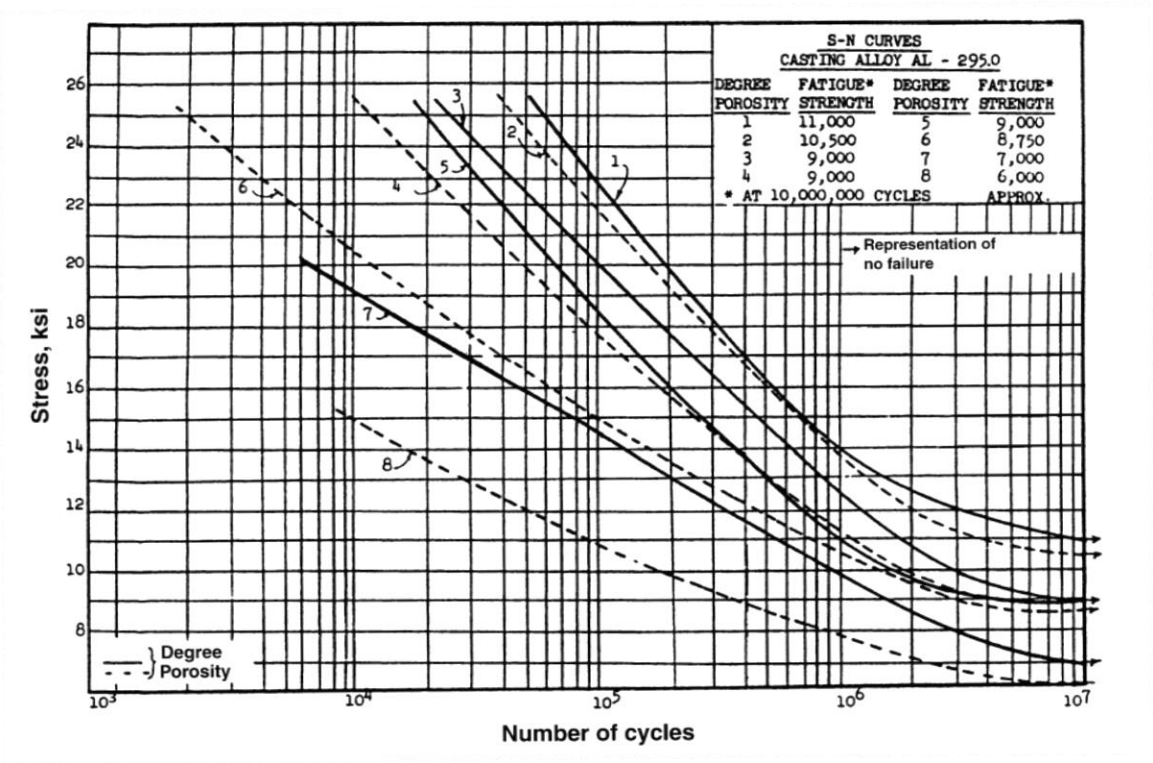

Figure 11. The effect structural quality on the S-N curves of 295 alloy castings [39].

As the size of the structural defects get larger, fatigue strength is reduced. As can be expected, fatigue life at a given alternating stress level is also negatively affected by the area of the largest structural defect, as presented in Figure 13.

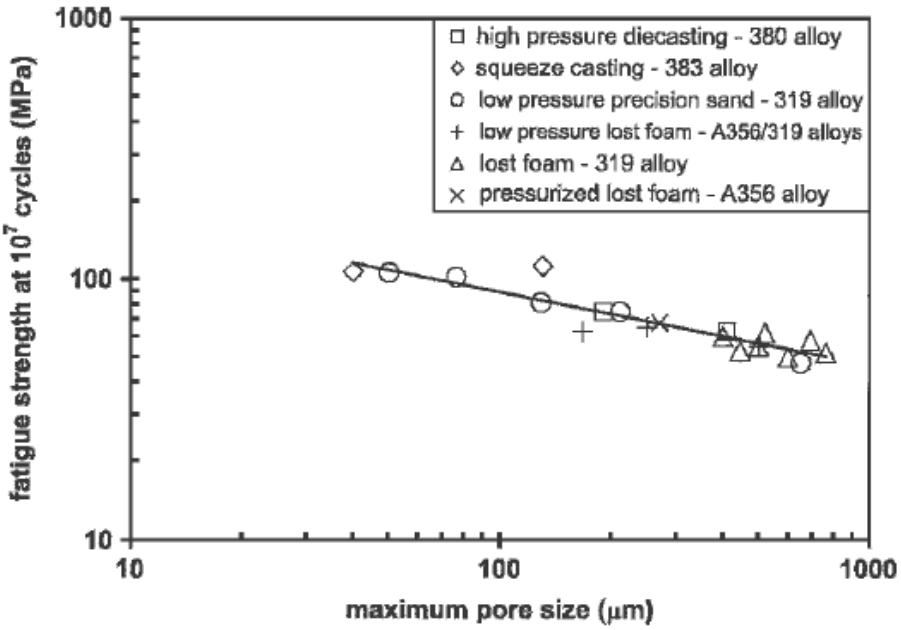

Figure 12. The relationship between maximum pore size and fatigue strength at 10^7 cycles determined in various Al-Si-Mg-(Cu) aluminum alloy castings [40].

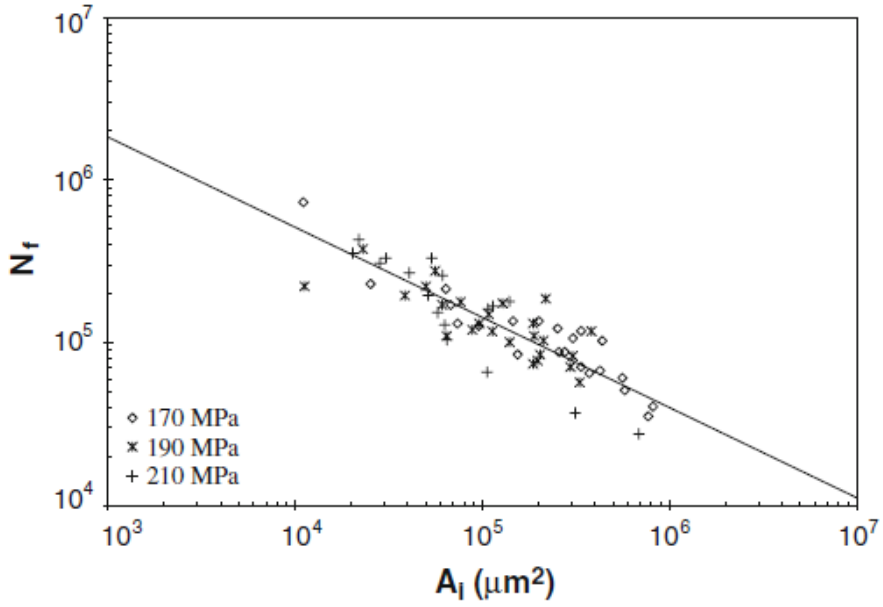

Figure 13. The change in fatigue life with area of the largest pore in A356 castings, obtained originally at three different alternating stress levels, later transformed to the same alternating stress [45].

The stress ratio of the fatigue test was also found to have an effect on the sensitivity of the fatigue strength at 10^7 cycles to the largest pore size in A356 alloy castings [46]. The interaction between the stress ratio and maximum pore size is shown in Figure 14. When R=-1 (where, minimum stress is in compression maximum stress is in tension and they are equal), fatigue strength is not affected by maximum pore sizes smaller than 400 μm. With increasing maximum pore size after 400 μm, however, there is a sharp decrease in the fatigue strength. At R=0 (where, minimum stress is zero and maximum stress is in tension), the sensitivity of fatigue strength to maximum pore size is starting at almost 50 μm. At pores sizes, larger than 400 μm, fatigue strength is not affected by maximum pore size. Hence the behavior is completely opposite of each other at the two stress ratios. This difference may be explained by the effect of the stress ratio at the driving force for crack propagation, as observed by Gall et al. [47] who conducted FEM analysis of fatigue behavior in the presence of pores and hard inclusions embedded in the metal matrix. At R=-1, the contributions of pores and hard inclusions to driving force for crack propagation were identical. At higher R ratios (tensile mean stress), however, the contribution of inclusions was twice of that of pores. Therefore, there is evidence in the literature that fatigue behavior in the presence of structural defects, such as pores, is determined by the stress ratio. Consequently, the assumption made in correction models for mean stress that fatigue behavior is the same regardless of R, is not valid for parts with low structural quality, such as castings.

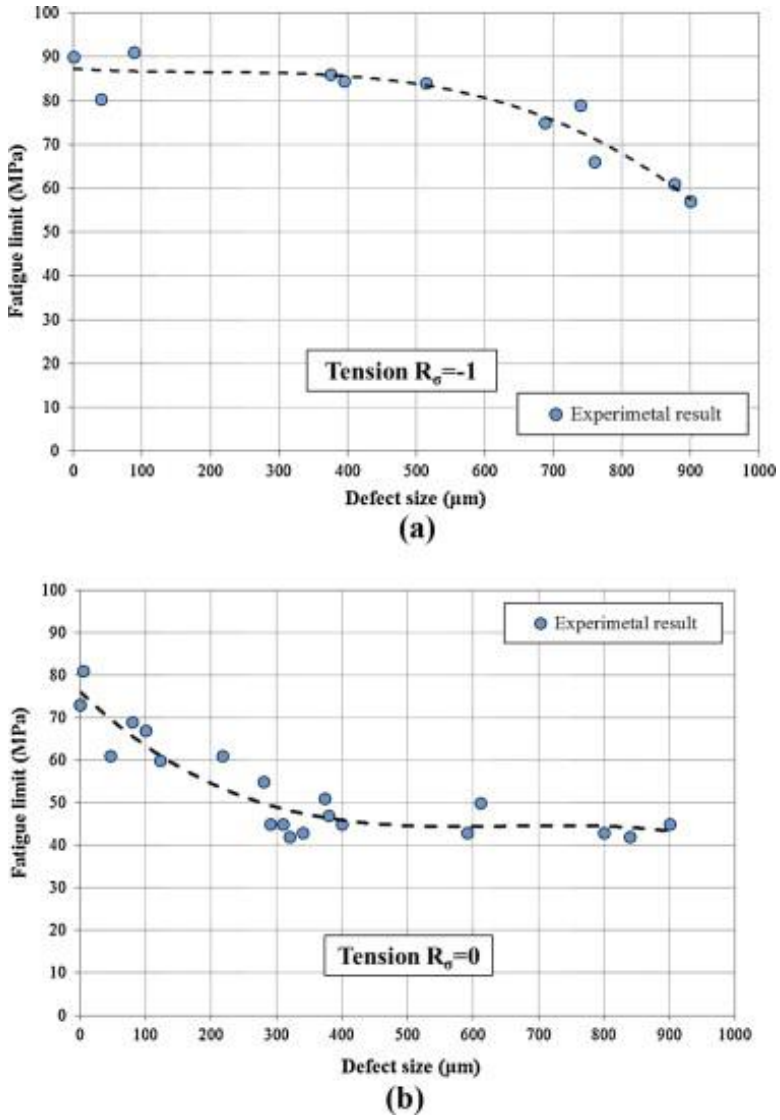

Figure 14. The dependence of fatigue strength at 10^7 cycles on the largest defects size at two R ratios in A356 alloy castings: (a) R=-1, and (b) R=0 [46].

To fully understand how structural defects affect fatigue life and tensile properties especially elongation, it is important to understand the level of stress concentration that they cause. Wicke et al. [48] used micro-computed tomography technique to determine the three dimensional geometry of two pores in an Al-13%Si-1.5%Cu-0.7%Mg alloy castings. The geometry of one of the pores is given in Figure 15. The geometries of the

pores were then used as an input to a finite element model (FEM) in which the stresses generated at the extremities were measured and stress concentration factor, K_t, was determined at each location. Some of the K_t values are also reported in Figure 15. Note that all reported stress concentration factors are above 7 and mostly around 10. K_t values exceeding 7 were reported by Nicoletto et al. in a similar study [49]. These results indicate that although bulk stress may be below the yield strength, local stresses near the pore can easily exceed yield stress and even fracture stress, leading to the formation of a crack that propagates and leads to a premature final fracture.

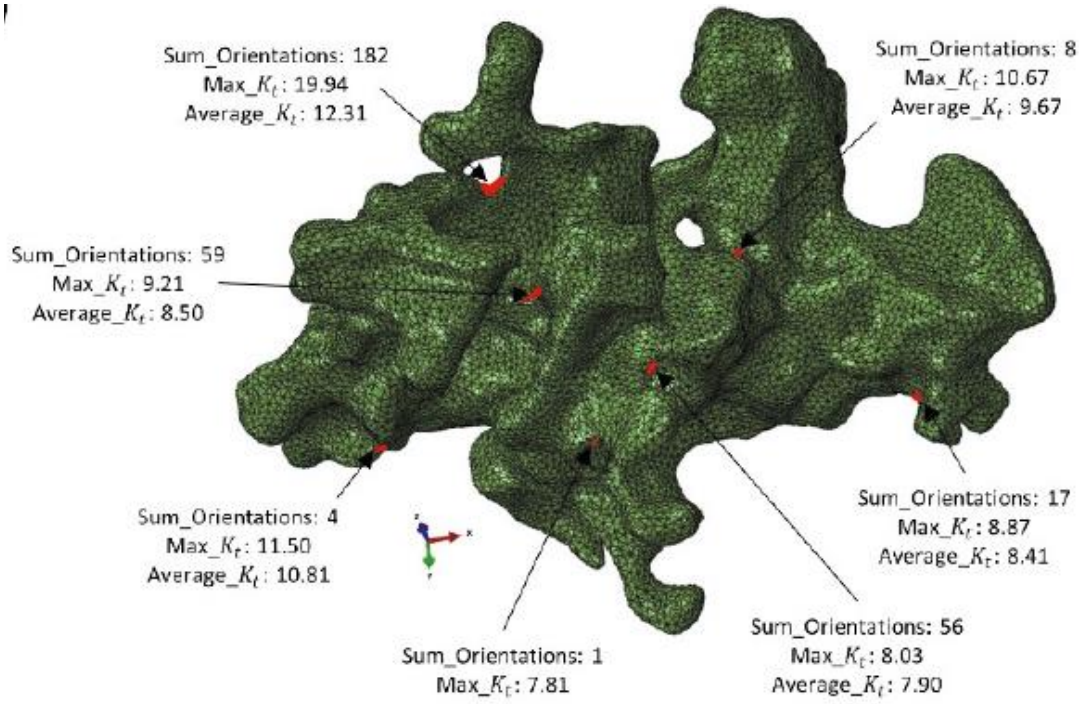

Figure 15. FEM results showing stress concentration factors, K_t, around a pore in an aluminum casting [48].

The areas near the stress concentrators experience a cyclic stress-strain hysteresis in each fatigue cycle, such as the ones shown schematically in Figure 16, which shows three

different curves at R=-1. The area inside the hysteresis is the plastic energy absorbed by the material subjected to this condition. Strong and brittle metals do not absorb much plastic energy per cycle. Weak and ductile metals absorb more energy but undergo heavy deformation which lead to opening of the crack (propagation) after several cycles. Most plastic energy is absorbed by "tough" metals which show a good combination of strength and ductility. The level of the energy absorption is of significant importance and will be addressed in more detail in the following section.

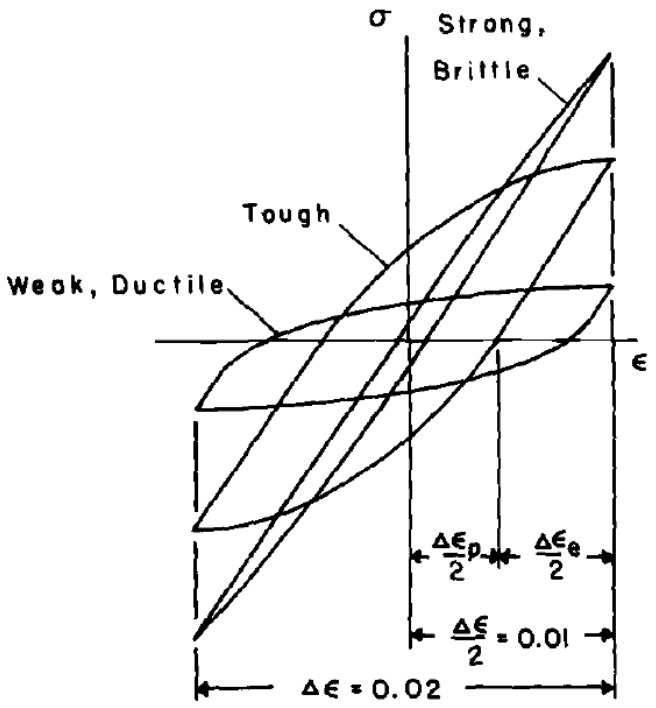

Figure 16. Schematic illustration of the cyclic stress-strain hysteresis for three metals: (1) strong and brittle, (2) weak and ductile, and (3) tough [50].

The cyclic stress-strain hysteresis at different points on the S-N curve are presented schematically in Figure 17. At point 1, the material undergoes heavy local plastic deformation, leading to high energy absorption. At point 2, the local stresses are lower due

the reduced alternation stress, and therefore, the hysteresis is not as wide. At point 3, which is at the endurance limit, there is still small local plastic deformations, which lead to fatigue fracture. At point 4, all deformation is elastic and therefore no propagating crack is formed, at least not before gigacycle fatigue lives are reached [51].

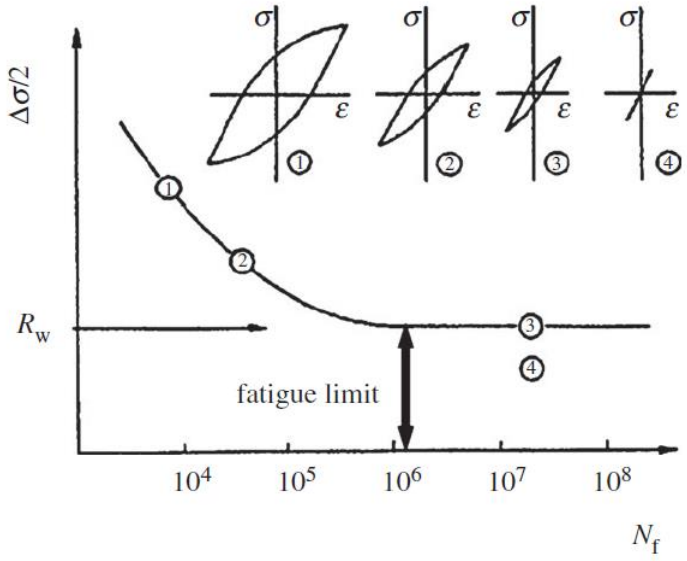

Figure 17. Schematic illustration of the Wöhler curve and the stress-strain hysteresis that take place around casting defects that lead to fatigue failure [52].

2.6. Energy Absorption in Fracture

Failure in metals is the outcome of two competing modes: plastic deformation and fracture [53]. If the stress necessary for permanent deformation is lower than the stress necessary to permanently separate atoms, plastic flow occurs instead of fracture. Tiryakioğlu et al. [54] stated, that from the point of view of maximizing resistance to failure, plastic deformation is a more preferable "failure" mode, since plastic flow preceding fracture markedly increases the energy accompanying the fracture.

The energy absorbed per volume by a specimen, W, (also referred to as the strain energy density) can be found by the area under the true stress-true strain curve:

$$W = \int_{\varepsilon=0}^{\varepsilon_f} \sigma . d\varepsilon \tag{9}$$

Alexopoulos and Tiryakioğlu [55] analyzed true stress-true strain curves in A357 alloy castings and showed that elongation to fracture is an excellent of the strain energy density, as shown in Figure 18. Similar results were reported for A206 aluminum alloy castings [56]. The cyclic stress-strain behavior is usually different from the one obtained in a tensile test [50]. However, the strain energy associated with the area under the tensile true stress-strain curve and the area with the hysteresis during fatigue testing is the same material property [57]. Moreover, it was shown that the strain energy absorbed in tensile testing is the same as the one in fatigue testing [58-62]. Based on this principle, Esin and Jones [61] showed that fatigue life can be estimated by:

$$N_f = \frac{W}{w_p} \tag{10}$$

where w_p is the micro-strain energy per cycle absorbed by the elements subjected to higher stresses, such as near pores. The model was applied with great accuracy to predict the S-N curve for a number of metals [59-61], including the En32b steel shown in Figure 19.

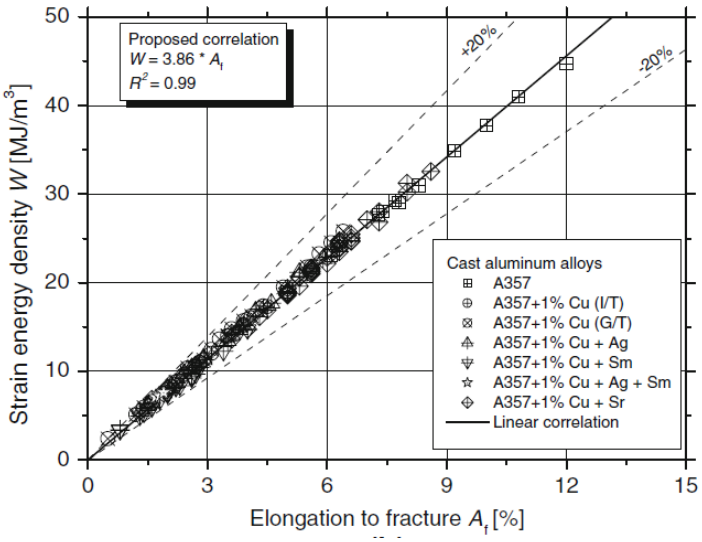

Figure 18. The relationship between elongation-to-fracture and strain energy density in A357 alloy castings [55].

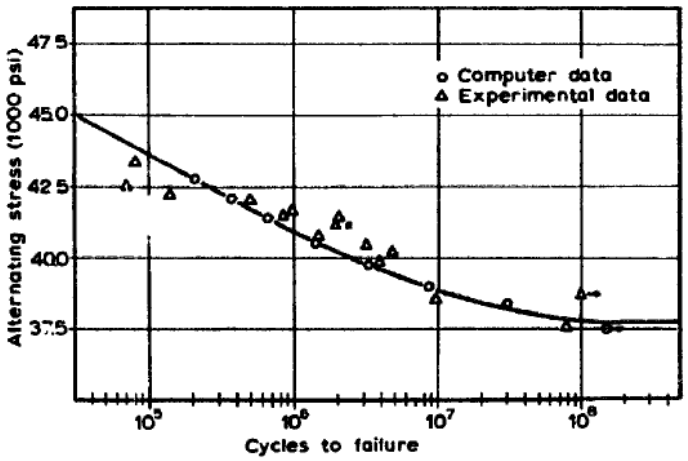

Figure 19. The fatigue data for En32b steel and the model prediction [61].

The discussion above suggests that structural defects that reduce elongation (Figure 10), also reduce the strain energy available to be absorbed during fatigue testing, resulting in lower fatigue life, which is consistent with the findings in the literature (Figure 11 and

Figure 13). More will be built on this point after the introduction of a metric to quantify the structural quality of aluminum castings.

2.7. Concept of Ductility Potential and Quality Index, Q_T

Tiryakioğlu and coworkers collected hundreds of data points from the aerospace and premium castings literature for Al-7Si-Mg, A206 and A201 [63-65] and plotted elongation versus yield strength, which is minimally affected by structural defects. The σ_y-e_F plot for cast Al-7%Si-Mg alloys is presented in Figure 20 [64, 66].

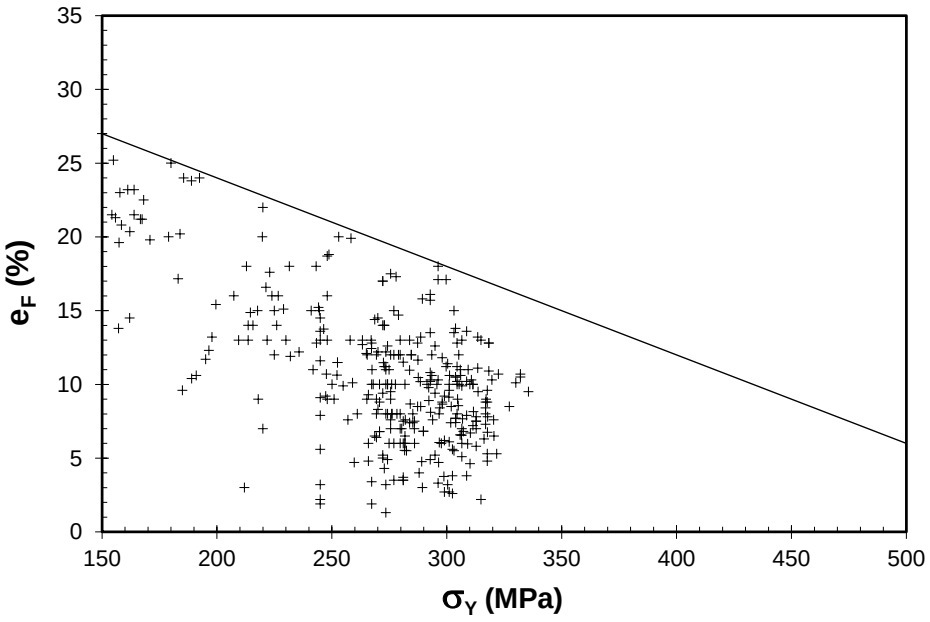

Figure 20. Elongation plotted versus yield strength for cast Al-7%Si-Mg alloys [64]

The highest elongation points form a linear trend, which can be written as:

$$e_{F(max)}=\beta_0-\beta_1\sigma_Y \quad (11)$$

where β_0 and β_1 are alloy-dependent coefficients. For Al-Si-Mg cast alloys, β_0 and β_1 are reported as 36.0 and 0.064 MPa^{-1}, respectively. Equation (11) can be used to estimate the ductility potential of aluminum and magnesium alloy castings [64-69].

The ductility potential was proposed [64, 66, 69] as a metric to determine structural quality. The quality index, Q_T, can then be found by:

$$Q_T = \frac{e_F}{e_{F(max)}} = \frac{e_F}{\beta_0 - \beta_1 \sigma_Y} \tag{12}$$

The application of Q_T to determine structural quality is shown schematically in Figure 21.

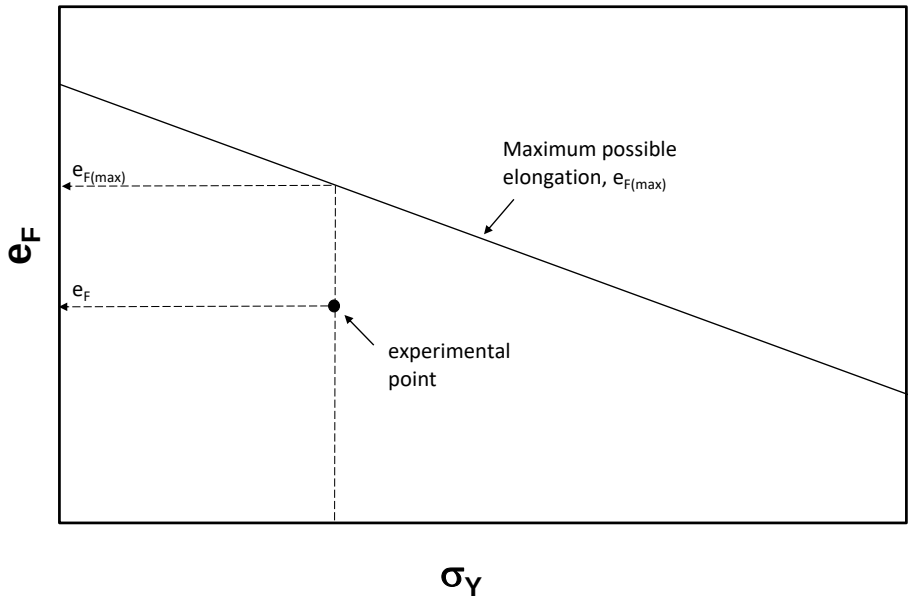

Figure 21. Schematic illustration of the use of Q_T to determine structural quality [64].

Tiryakioğlu and Campbell [64] stated that there are three Q_T regions: "(1) $Q_T < 0.25$, (2) $0.25 \leq Q_T < 0.70$, and (3) $Q_T \geq 0.70$. Region 1, premature fracture is due to "old", coarse oxide bifilms, i.e., the surface of re-melted castings, foundry returns and/or ingot. In this region, tensile specimens do not neck and fatigue failure starts from defects on or close to the specimen surface. Region 2 ($0.25 \leq Q_T < 0.70$) represents castings that are free from major "old" oxides but there is still a considerable density of "young" oxides, entrained into the casting during melt transfers and/or filling of the mold. Tensile specimens may

show some necking and there will be occasional fatigue failures initiating from internal defects with facets around them [36]. In Region 3 ($0.70 \leq Q_T \leq 1.0$), tensile specimens are expected to neck and deform significantly beyond ultimate tensile strength [70]. Moreover, fatigue fracture is predominantly due to internal defects, exhibiting facets on fracture surfaces."

In cast Al-7%Si-Mg alloys, Tiryakioğlu et al. [66] noticed that the tensile strength of maximum points in Figure 20 increases linearly with yield strength. Based on this observation, they proposed that maximum tensile strength, $S_{T(max)}$ can be estimated by:

$$S_{T(max)} = 185.7 + 0.558\sigma_Y \quad (13)$$

2.8. The Relationship between Tensile Properties and Fatigue Characteristics

Wöhler was the first to report that the ratio of fatigue strength to ultimate tensile strength ranged between 0.4 and 0.5 [23]. Recently, it was shown that σ_f / S_T is not constant but is a linear function of S_T [71, 72]. Pang et al. [71] also reported a linear relationship between fatigue strength and yield strength as well as strain energy density.

Recently, Tiryakioğlu [73] analyzed the elongation and fatigue life data of A206-T7 aluminum alloy castings obtained at R=0.1. To normalize for yield strength differences between datasets, Tiryakioğlu converted elongation to Q_T and determined the average of Q_T and N_f distributions. The relationship between average Q_T and N_f in A206 castings is presented in Figure 22. The relationship is linear between Q_T and $\log(N_f)$ and can be written as:

$$\log \overline{N_f} = 3.087 Q_T + 4.73 \quad (14)$$

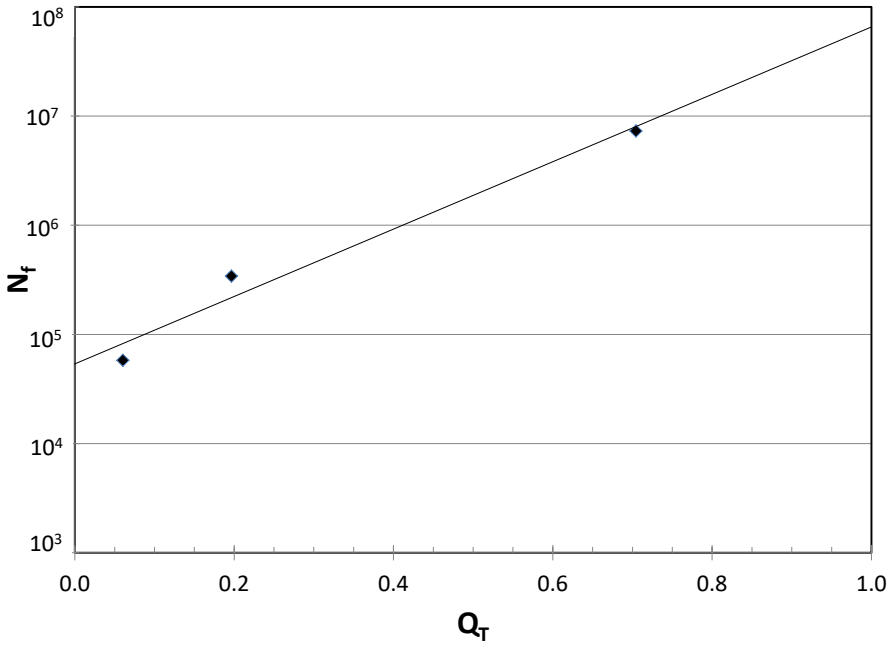

Figure 22. The relationship between structural quality and expected (mean) fatigue life in A206 castings [73].

Extrapolation of Q_T to 1 yields $10^{7.82}$, or 66 million cycles at a maximum stress that corresponds to 58% of yield strength of the alloy.

Based on these results, Tiryakioğlu concluded that the elongation specifications, such as the ones in MIL-A-21180 D [5] can be interpreted as *de facto* fatigue life specifications.

2.9. Fatigue Life Prediction Models from Tensile Results

Most models in the literature are built on the strain-based fatigue life. Equation (4) can be rewritten in terms of strain by dividing both sides of the equation with modulus of elasticity, E:

$$\frac{\Delta\varepsilon_e}{2}=\frac{\Delta\sigma}{2E}=\frac{\sigma_f^{'}}{E}N_f^{b} \tag{15}$$

where, $\Delta\varepsilon_e$ is the elastic strain range. The plastic strain amplitude can be found by the Coffin-Manson relationship [74, 75]:

$$\frac{\Delta\varepsilon_p}{2}=\varepsilon_f^{'}N_f^{c} \tag{16}$$

where $\Delta\varepsilon_p$ is the plastic strain range, $\varepsilon_f^{'}$ is fatigue ductility coefficient and c is plastic exponent. Equations (15) and (16) can be combined to find the total strain equation:

$$\frac{\Delta\varepsilon}{2}=\frac{\Delta\varepsilon_e}{2}+\frac{\Delta\varepsilon_p}{2}=\frac{\sigma_f^{'}}{E}N_f^{b}+\varepsilon_f^{'}N_f^{c} \tag{17}$$

Equation (17) is plotted schematically for SAE 4340 steel in Figure 23. In Figure 23.a, cyclic stress-strain hysteresis at different points on the curve are also indicated, as in Figure 17.

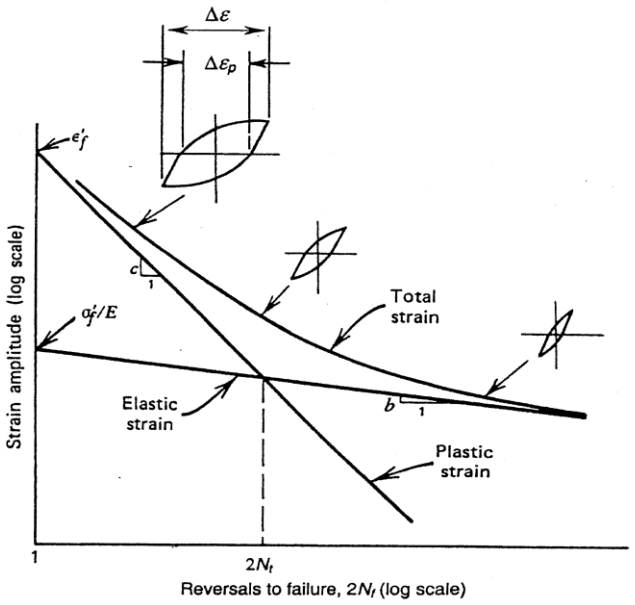

(a)

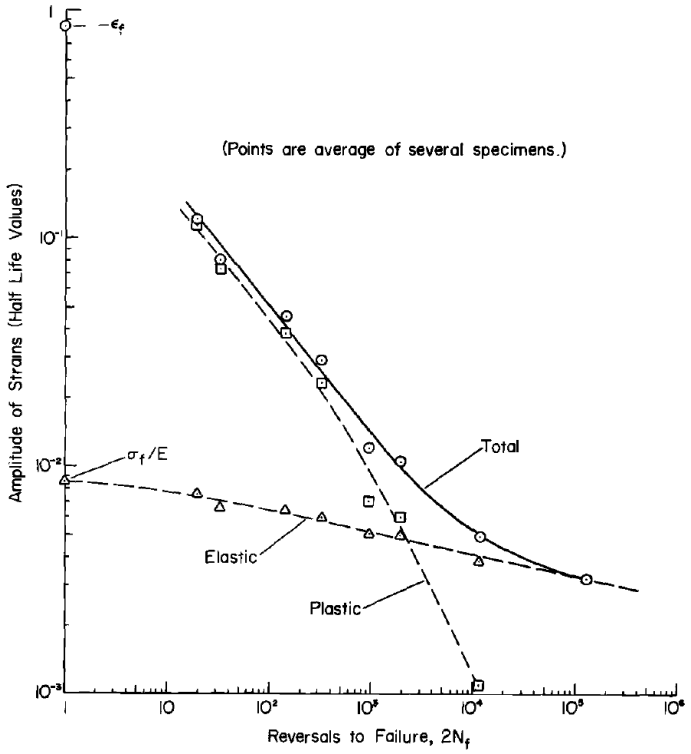

(b)

Figure 23. The two components of the total strain-life curve: (a) schematics, and (b) experimental data for SAE 4340 steel [50]. Note that 2 reversals = 1 cycle.

Manson [7] developed two different methods in 1965 by using data from sixty nine different alloys including steel and aluminum alloys. The first one, known as "universal slope method", assumes the slopes of elastic and plastic lines to be -0.12 and -0.6, respectively. This method is referred to as "Method 1" in the present study. The second one, known as "four-point correlation method", estimates two points on both elastic and plastic lines. This method is referred to as "Method 2". Both methods are based on the use of tensile strength and reduction in areas. These methods are summarized in Figure 24.

Manson and Muralidharan [8] in 1988, revised the "universal-slope method" by changing the assumed elastic and plastic exponents to -0.09 and -0.56 after including more alloys. They also added the ratio of tensile strength to elastic modulus as a new parameter to determine fatigue strength and ductility coefficients. This method is referred to as "Method 3".

After observing significantly different slopes for different alloys, Baumel and Seeger [9] introduced two different methods to correlate monotonic and cyclic properties. They assumed a constant value of fatigue ductility coefficient along with constant elastic and plastic exponents for aluminum and titanium alloys. Only that for aluminum alloys is considered in the present study, and will be referred to as "Method 4".

Meggiolaro and Castro [10], studied available methods statistically and provided the median values for the estimation methods as a new model (Method 5). The summary for the HCF part of these estimation methods is given in Table 1. For simplification, the reduction in area included in the original versions of these models was replaced by e_F based on the observation by McLellan [76] that there is no evidence of necking for either A356-T6 or A356-T7 alloy aerospace castings.

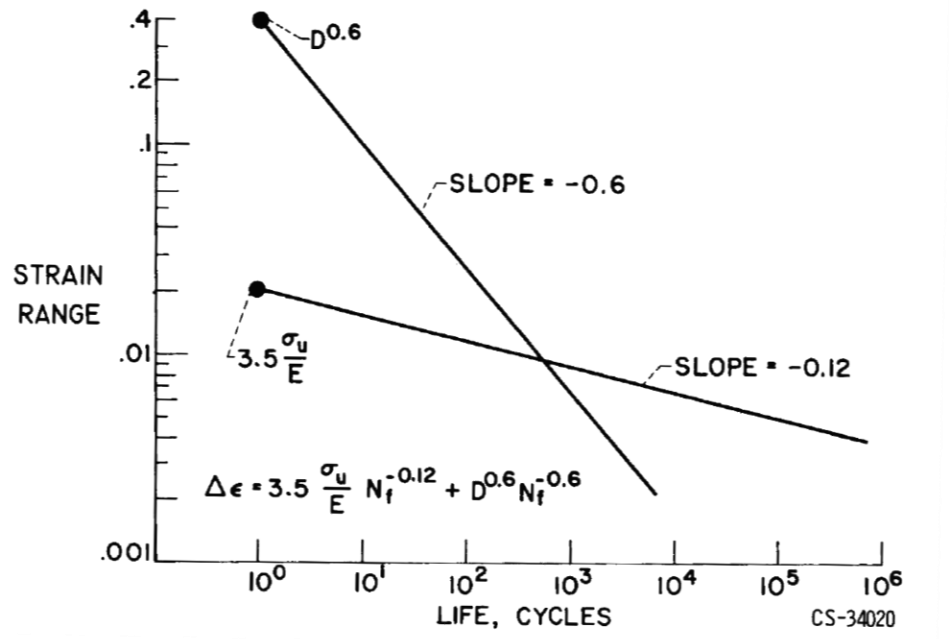

(a)

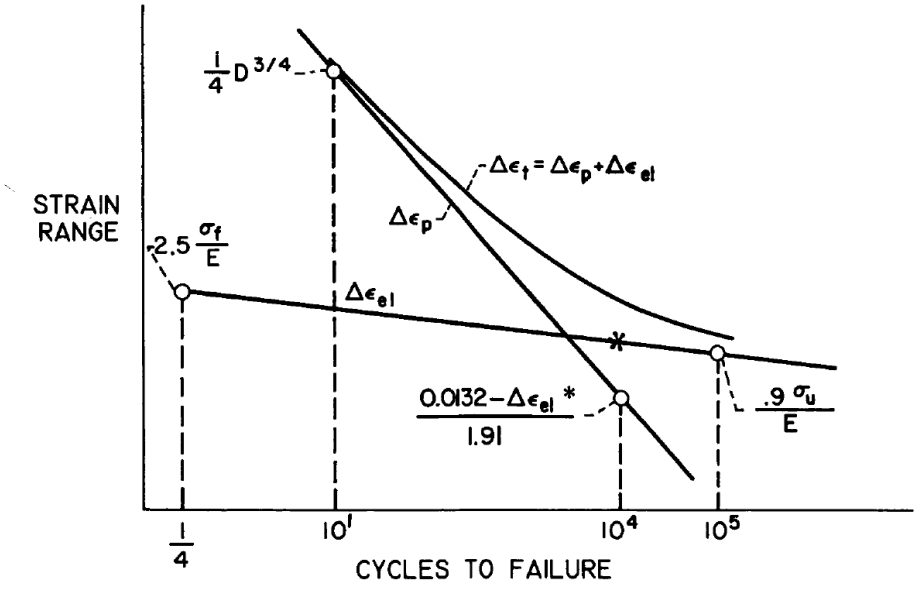

(b)

Figure 24. Methods of estimating total fatigue curves from tensile behavior, introduced by Manson [7]: (a) universal slopes, and (b) four points.

Table 1. Estimation methods for HCF properties.

Method	Reference	σ_f'	b
1	[7]	$1.9S_T$	-0.12
2	[7]	$1.25S_T(1+\ln(1+e_F))2^b$	$\frac{\log(0.36/(1+\ln(1+e_F))}{5.6}$
3	[8]	$0.623E\left(\frac{S_T}{E}\right)^{0.832}$	-0.09
4	[9]	$1.67S_T$	-0.095
5	[10]	$1.9S_T$	-0.11

Heywood [12] suggested a general formula (referred to as Method 6) based on the observation that tensile strength is related to fatigue strength:

$$\frac{\sigma_a}{S_T}=\frac{1+\dfrac{0.0031\left(\frac{1}{b}\log\left(\frac{\sigma_a}{\sigma_f'}\right)\right)^4}{1+0.0065S_T}}{1+0.0031\left(\frac{1}{b}\log\left(\frac{\sigma_a}{\sigma_f'}\right)\right)^4} \tag{18}$$

Even though his equation is valid for plain aluminum alloy specimens made from extruded sections and bars, it is still included in the present study for comparison purposes.

2.10. Estimating uniaxial fatigue behavior by rotating bending fatigue testing

As presented in Figure 5, the S-N curves differ significantly even for the same material when data are obtained in different types of fatigue testing. The stresses developed in uniaxial and rotating beam fatigue tests are quite different; in uniaxial testing, stresses are mostly homogeneous across the cross-section of the specimen. In rotating beam fatigue tests, stress is zero in the midpoint of the specimen and changes linearly from center to surface, where it reaches the maximum stress.

It has been of interest to estimate the uniaxial fatigue performance from rotating beam fatigue tests. Sors [77] indicated that the ratio of fatigue strengths in uniaxial to rotating bending fatigue tests is 0.59, supported by data from literature on various steels.

Manson and Muralidharan [78] developed a methodology by taking the plastic flow into account and based on some material constants, suggested closed form equations to identify the true bending stresses in terms of axial stresses. Their model is described below.

For Equation (17), fatigue life at the intersection point of the two lines N_T (also known as transition life) as indicated in Figure 23, is given by:

$$N_T = \left(\frac{E\varepsilon_f'}{\sigma_f'}\right)^{1/(b-c)} \tag{19}$$

For practical approach, the "universal-slope" method by Manson [7], which proposes elastic and plastic exponent values of -0.12 and -0.6, respectively, can be used to calculate, N_T:

$$N_T = 0.0735 \left(\frac{S_T}{E}\right)^{-2.083} e_F{}^{1.25} \tag{20}$$

Instead of using the known bending moment to calculate the strain, Manson and Muralidharan used strain to calculate required bending moment. Consequently, they provided a correction factor between bending stress amplitude, $\sigma_{a\,|\,rb}$, and axial stress amplitude, $\sigma_{a\,|\,ax}$:

$$\sigma_{a\,|\,ax}=\sigma_{a\,|\,rb}\left(\frac{1+2\left(\frac{N_f}{N_T}\right)^{(c-b)}+\left(\frac{N_f}{N_T}\right)^{2(c-b)}}{1+f_1\left(\frac{N_f}{N_T}\right)^{(c-b)}+f_2\left(\frac{N_f}{N_T}\right)^{2(c-b)}}\right) \tag{21}$$

where,

$$f_1=\frac{1+0.8432\frac{c}{b}}{0.6849+0.255\frac{c}{b}} \tag{22}$$

$$f_2=\frac{2.6188\frac{c}{b}}{1+1.5411\frac{c}{b}} \tag{23}$$

Note that f_1 and f_2 depend on the geometry of the cross-section and are given here only for circular cross-sections. Their results are in good agreement with the calculations made in the low-cyclic region. In the elastic region where volumetric effect plays an important role, Manson and Muralidharan noticed some discrepancy between bending and axial type fatigue stresses.

Esin [79] studied micro-plasticity taking place due to stress distributions across the cross-section of specimens. By taking the volumetric effect into account, and using the macro-micro element concept, Esin provided a model that could successfully correlate uniaxial and rotating beam fatigue testing results in the high-cyclic region in steels. According to Esin, the axial equivalent stress for a rotating beam is given by:

$$\sigma_{a\,|\,ax} = \frac{2\sigma_{a\,|\,rb}}{3}\left(\frac{1-k^3}{1-k^2}\right) \tag{24}$$

where,

$$k = \frac{d}{D} \tag{25}$$

D is the specimen diameter, and d is the diameter of the section of the specimen inside which stresses are lower than the endurance limit. Esin also provided a correction factor for fatigue life:

$$F = \frac{D^2}{\left(D^2 - d^2\right)} \tag{26}$$

$$N_{f\,|\,rb} = N_{f\,|\,ax}.F \tag{27}$$

Even though the true elastic limit of steels was found to be below endurance limit [80], Esin suggested simply using the endurance limit as the true elastic limit for a practical approach.

2.11. Statistics for Fracture Properties

Because mechanical properties that involve fracture can be directly linked to casting defects, the Weibull distribution [81-83] based on the "weakest link" theory [84], has been used to characterize these properties. For the Weibull distribution, the cumulative probability function is expressed as:

$$P = 1 - \exp\left[-V\left(\frac{\sigma-\sigma_T}{\sigma_0}\right)^m\right] \tag{28}$$

where, P is the probability of failure at a given stress (or fatigue life) or lower, V is volume of the specimen subjected to stress, σ_T is the threshold value below which no failure is expected, σ_0 is the scale parameter and m is the shape parameter, alternatively known as the Weibull modulus. Note that when $\sigma_T = 0$, Equation (28) reduces to the 2-parameter Weibull distribution. The mean of the Weibull distribution is found by:

$$\overline{\sigma}=\sigma_T+\sigma_0'\Gamma\left(1+\frac{1}{m}\right) \tag{29}$$

where, $\sigma_0' = \sigma_0 / V^{1/m}$ and Γ is the gamma function. The probability density function, f, for the Weibull distribution is expressed as:

$$f=\frac{m}{\sigma_0'}\left(\frac{\sigma-\sigma_T}{\sigma_0'}\right)^{m-1} \exp\left[-\left(\frac{\sigma-\sigma_T}{\sigma_T'}\right)^{m}\right] \tag{30}$$

When data come from more than one Weibull distribution, such as failure data due to different types of defects, Weibull mixtures are used. The most common and applicable mixing technique for the Weibull distributions [85, 86] is:

$$f=pf_L+(1-p)f_U \tag{31}$$

where p is the fraction of the lower distribution and subscripts L and U refer to lower and upper distributions, respectively. The cumulative probability, P, is expressed as [85]:

$$P=pP_L+(1-p)P_U \tag{32}$$

2.12. Research Questions

Based on the discussion presented above, the following questions will be addressed in this study:

1. How well do Soderberg, Smith Watson Topper and Walker equations perform in cast aluminum alloys, especially in datasets with various levels of structural quality? Is the Walker parameter a function of structural quality?
2. Tiryakioğlu used only three data points in Figure 22 to reach the conclusion that (a) there is a strong correlation between $\log(N_f)$ and Q_T, and (b) elongation specification in industrial standards are de facto fatigue life specifications. Is there more evidence for this from the aerospace and automotive castings literature?
3. How do methods to estimate HCF perform with aluminum castings? If they do not perform well, can a new model for aluminum castings be developed?
4. What is the fatigue performance of an A356-T6 casting in rotating beam and axial fatigue testing? Can axial fatigue be predicted from rotating beam fatigue test data? If so, what model among the existing ones provides the best fit?

The first three questions will be answered by using data from the literature and questions 4, by analyzing data collected in this study.

3. Details and Results of the Analysis of Data from Literature

3.1. Evaluation of Mean Stress Correction Models [19]

The effectiveness of the mean stress correction equations by Soderberg, Smith-Watson-Topper (SWT) and Walker (Equations 5-7) is investigated in this section. Note that there are other mean stress correction equations in the literature that involve ultimate tensile strength, such as the one by Goodman [87]. These equations were found to be ineffective previously [17]. Consequently, those equations that use ultimate tensile strength are not addressed here.

Data from six studies [34, 88-92] involving seven datasets of cast Al7%Si-Mg alloys published in the literature with various R ratios have been reanalyzed [19]. The datasets used in this analysis are as follows:

- Wang *et al*. [34] used Sr-modified A356 casting alloy in T6 heat treatment condition to study the influence of casting defects on the room temperature fatigue performance by using unnotched polished cylindrical specimens. R ratio of 0.1 and -1 have been included in the study.
- Jana *et al*. [88] studied cast F357 (Be-free variant of A357) plates of ~3.3mm thickness to investigate the effect of friction stir processing (FSP) on fatigue life of sand castings. Fatigue tests were run at stress ratio of R=0 and R=-1. The FSP dataset has a total number of seventeen fatigue life data with one run-out.
- Oswalt [89] investigated unchilled test bars of 357-T6 alloy to determine the notched fatigue strength. R ratios of 0.2 and -1 were used in the study.

- Koutiri *et al*. [90] studied the high-cycle fatigue behavior of cast hypo-eutectic Al-Si alloy to investigate the fatigue damage mechanisms under complex loading conditions with different load ratios.
- Mu *et al*. [91] used AS7G06 (A357) cast aluminum alloy in T6 heat treatment condition for two different R ratios to analyze types of defects at the origin of the failure.
- Munoz [92] focused on A357-T6 cast aluminum alloy to investigate the effect of the material microstructural parameters that affect the small fatigue cracks. R ratio of 0.1 and -1 have been included in the study.

The analysis conducted in this study [19]incorporated a maximum likelihood (ML) method developed by Sarkani *et al.* [93] and censored Weibull analysis. The details of the model by Sarkani *et al.* are summarized in Appendix. To the author's knowledge, such a study with the correct treatment of survival data has not been conducted before.

The sequence of steps taken in the analyses are presented in the flowchart in Figure 25. For the datasets, which include run-outs, Basquin parameters were estimated by the ML method. Linear fits were obtained to log (N_f) vs. log(σ_{eq}) data to estimate $\sigma_f^{`}$ and b in the Basquin equation and the coefficient of determination, R^2, was calculated for each linear fit. Since the SWT and Walker equations give identical results with $\gamma = 0.5$, the initial estimate of adjustable constant was taken as 0.5 and the value of γ that yields the highest R^2 was determined for each dataset [19]. The equivalent fatigue life, N_{eq}, at R=-1 and σ_a=100 MPa was found by:

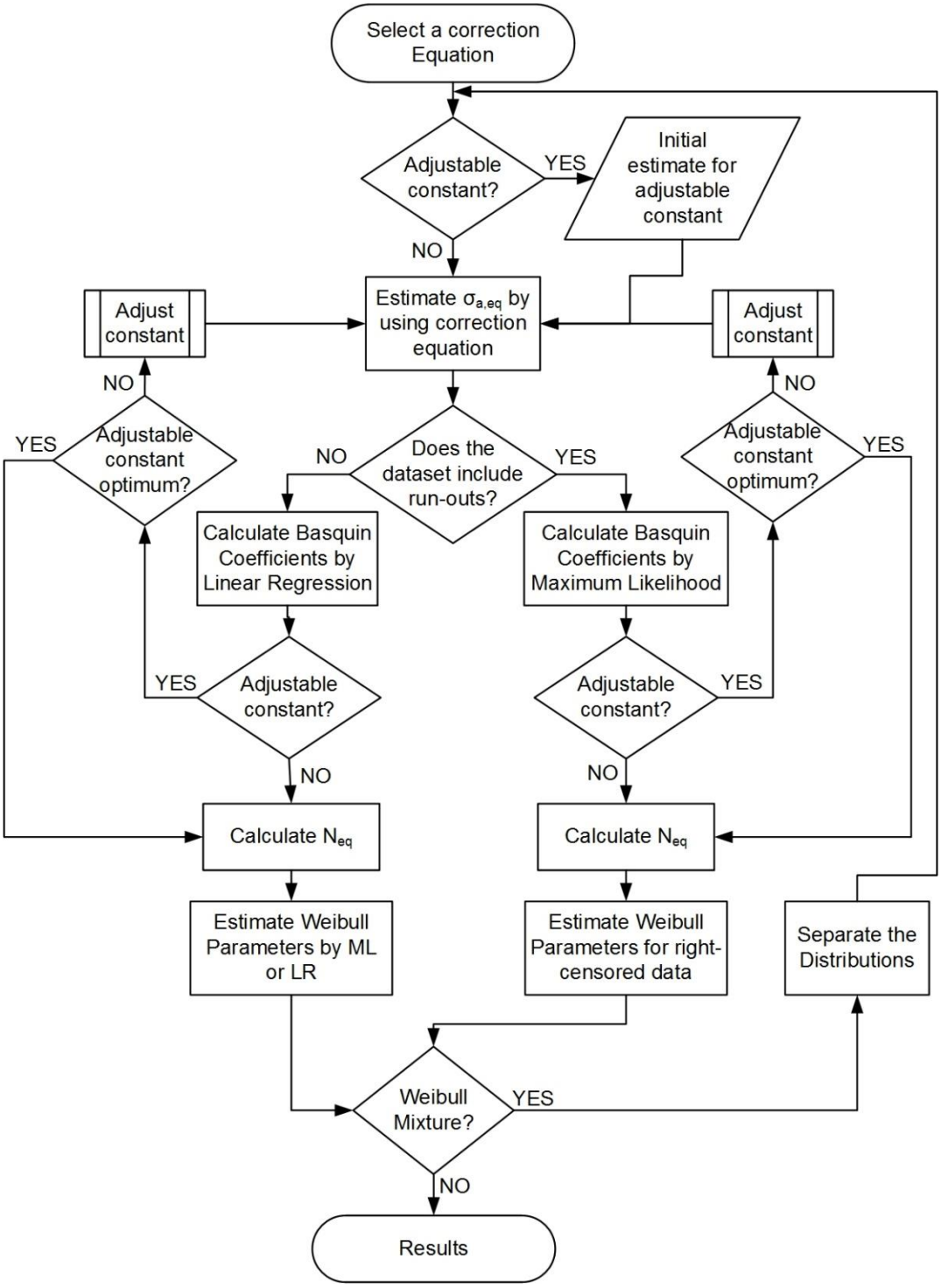

Figure 25. The flowchart of the analysis conducted for mean stress correction [19].

$$N_{eq}=N_f\left(\frac{\sigma_a}{\sigma_{eq}}\right)^{-1/b} \quad (33)$$

Weibull probability plots of N_{eq} were analyzed and interpreted based on guidelines recommended by Tiryakioğlu and Campbell [86].

Estimated Basquin parameters and associated R^2 values, the value of the Walker parameter as well as the estimated Weibull parameters for N_{eq} are provided in Table 2.

Table 2. Estimated parameters and additional information about datasets.

Alloy	Ref.	Correction Equation	γ	Basquin		R^2	Weibull		
				σ'_f (MPa)	b		σ_T	σ_0	m
A356	[34]	Soderberg		1,697.5	-0.232	0.509	2,220	1,915,4	0.33
		SWT		602	-0.120	0.605	2,801	2,167,0	0.31
		Walker	0.501	601	-0.120	**0.606**	2,818	2,174,5	0.31
F357 (FSP)	[88]	Soderberg		1,764	-0.212	0.962	506,481	322,914	1.38
		SWT		1,512	-0.199	0.984	572,960	290,993	2.15
		Walker	0.530	1,529	-0.201	**0.985**	479,778	352,628	2.75
F357 (Sand Cast)		Soderberg		2,472	-0.229	0.932	0	1,415,4	3.58
		SWT		2,006	-0.213	0.967	0	1,572,8	5.06
		Walker	0.380	1,877	-0.205	**0.986**	0	316,093	0.80
357 (aerospace)	[89]	Soderberg		1,735	-0.261	0.801	7,161	72,381	0.70
		SWT		975	-0.213	0.858	9,994	51,467	0.91
		Walker	0.476	989	-0.213	**0.860**	11,233	52,813	0.91
A356 +0.5Cu	[90]	Soderberg		595	-0.12	0.131	40,192	5,499,9	0.47
		SWT		1,109	-0.185	0.787	236,288	206,760	0.68
		Walker	0.481	1,061	-0.180	**0.791**	262,063	258,195	0.72
A357	[91]	Soderberg		648	-0.126	0.639	0	3,843,4	1.71
		SWT		481	-0.105	0.654	0	4,827,7	1.51
		Walker	0.473	480	-0.104	**0.657**	0	5,222,4	1.55
A357	[92]	Soderberg		1,298	-0.215	0.589	0	2,040,0	1.31
		SWT		741	-0.140	0.752	0	2,469,4	1.39
		Walker	0.461	768	-0.141	**0.770**	0	2,822,5	1.41

The results show that the Walker method provides better fits [19], as indicated by higher R^2 values, than the Soderberg and SWT methods. This result can be attributed to its adjustable constant, γ.

The S-N curves for the sand-cast F357, friction stir-processed F357 and A357 after Walker corrections are presented in Figure 26. For all three datasets, fatigue life data, originally obtained at R=0, are corrected, and subsequently lie almost perfectly on the Basquin curves for R=-1.

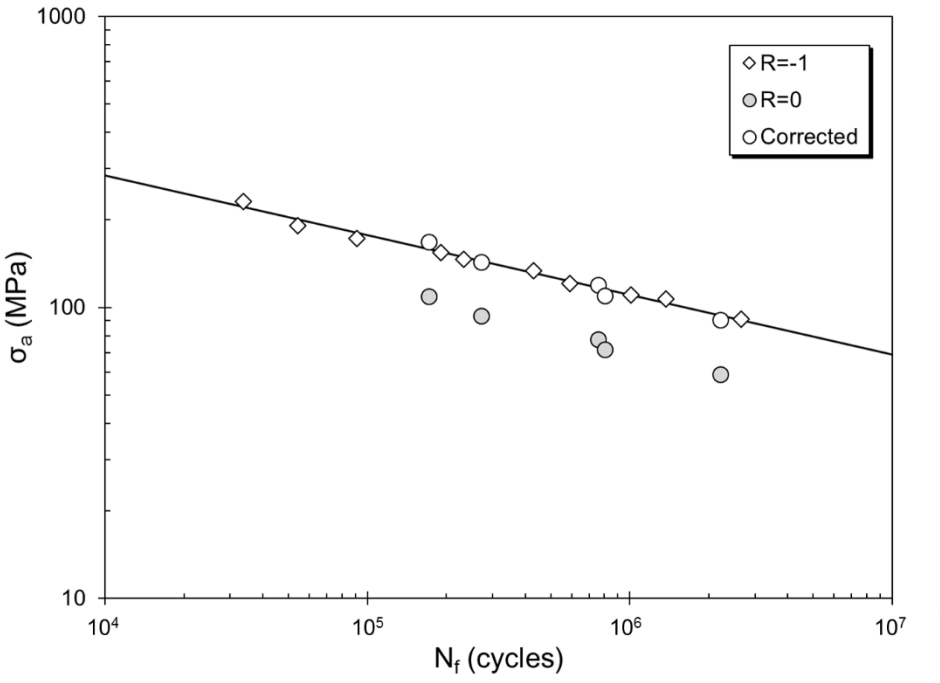

(a)

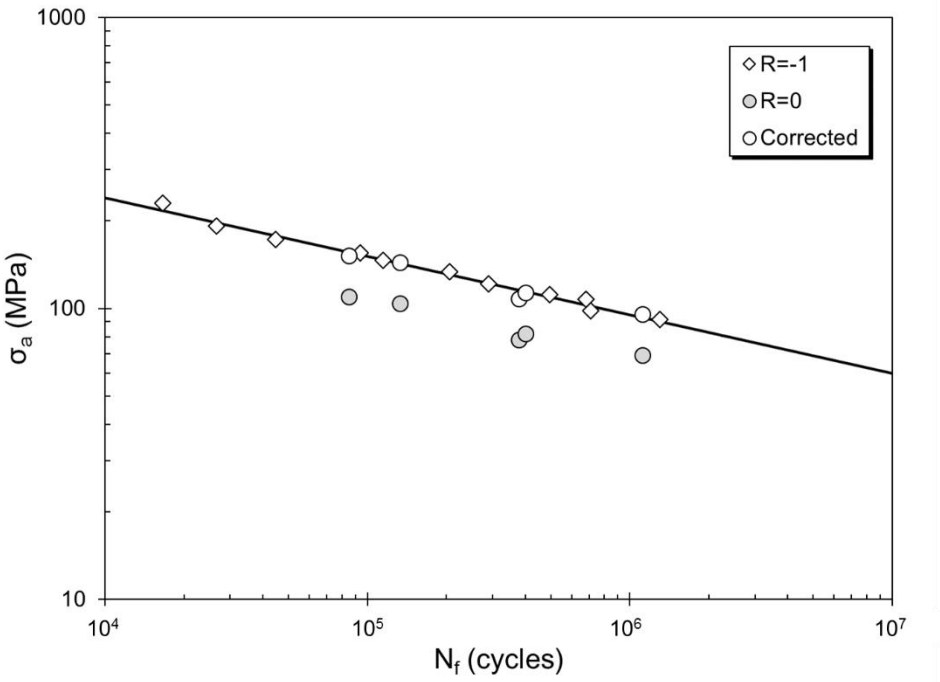

(b)

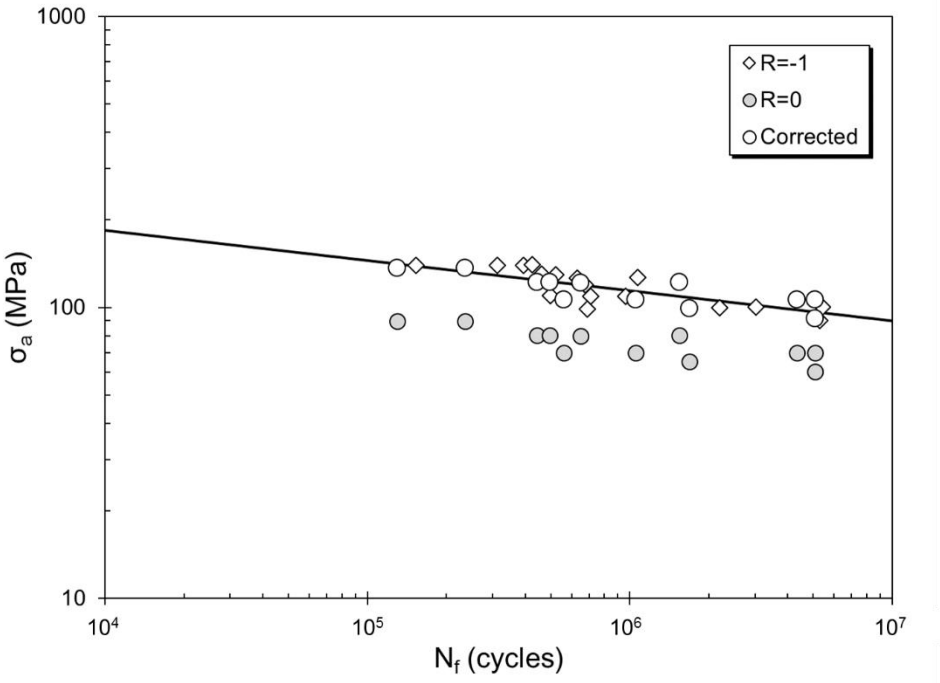

(c)

Figure 26. The S-N curves at R=-1 after Walker mean stress correction for (a) sand cast F357 by Jana *et al.*, (b) A357 by Mu *et al.*, and (c) friction stir processed F357 by Jana *et al*. The original data for R=0 as well as their correction are also indicated.

The probability density functions of the Weibull distributions corresponding to the three mean stress correction methods for friction stir processed F357 and aerospace 357 castings are results are presented in Figure 27 for the four datasets. Note that the total area under each curve is 1.0 although areas look different in size because of the use of logarithmic scale for the x-axis. It is significant in Figure 27 that the distribution is affected to a great extent by the selection of the mean stress correction method. This is especially the case for the friction stir processed F357; in Figure 27.a, the shape of the distribution for the Soderberg correction is significantly different from the other two distributions for the same dataset. In Figure 27.b, although the distributions look similar, the threshold values (vertical lines) are strongly affected by the mean stress correction method [19].

To determine whether the value of γ is affected by the structural quality of the castings, tensile properties from each dataset were collected. The reported tensile properties and the Q_T values calculated for each dataset are given in Table 3. The Q_T versus γ plots is presented in Figure 28. Note that there is strong evidence that the Walker parameter is affected by the structural quality of aluminum castings. The best fit curve indicated in Figure 28 is expressed as:

$$\gamma=0.540+0.1272.\log\left(Q_T\right) \tag{34}$$

with a $R^2=0.965$. In the literature, the Walker parameter is regarded as a material property. However, the effect of Q_T on the Walker parameter found in this study indicates that γ, at least, includes the quality of the material and therefore has an extrinsic component.

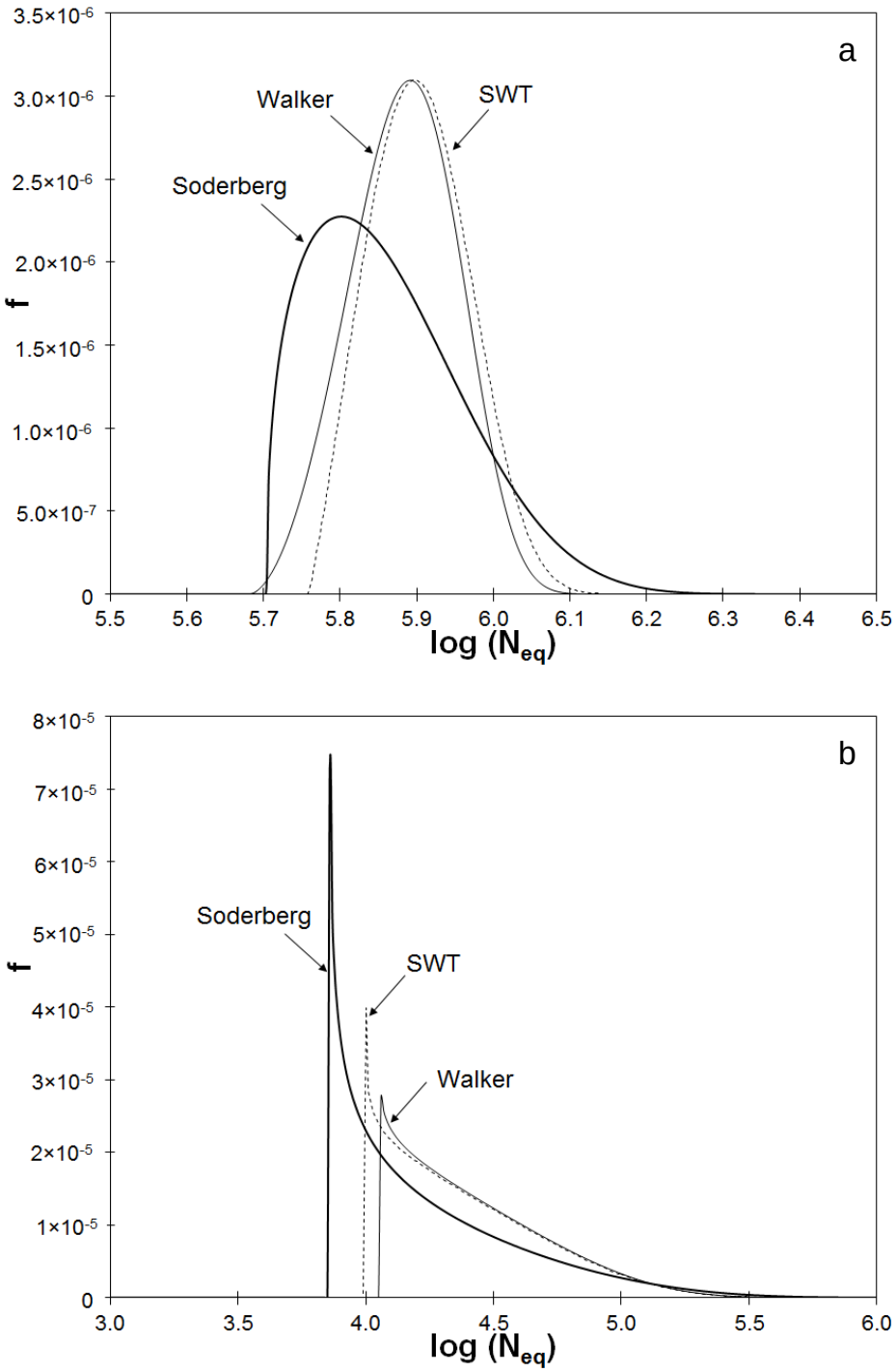

Figure 27. Probability density functions for N_{eq} obtained after mean stress correction by the three models for (a) friction-stir processed F357-T6, (b) 357-T6 aerospace alloy datasets [19].

Table 3. Tensile properties and structural quality, Q_T (calculated by using Eq. (12) , for each dataset.

	Ref.	σ_y (MPa)	S_T (MPa)	e_F (%)	Q_T
A356	[34]	240	300	10.0	0.485
F357 (FSP)	[88]	290	330	15.0	0.860
F357 (Sand Cast)		290	300	1.0	0.057
357 (aerospace)	[89]	303	351	4.8	0.289
A356+0.5Cu	[90]	250	330	5.7	0.285
A357	[91]	275	335	5.0	0.272
A357	[92]	275	335	6.0	0.326

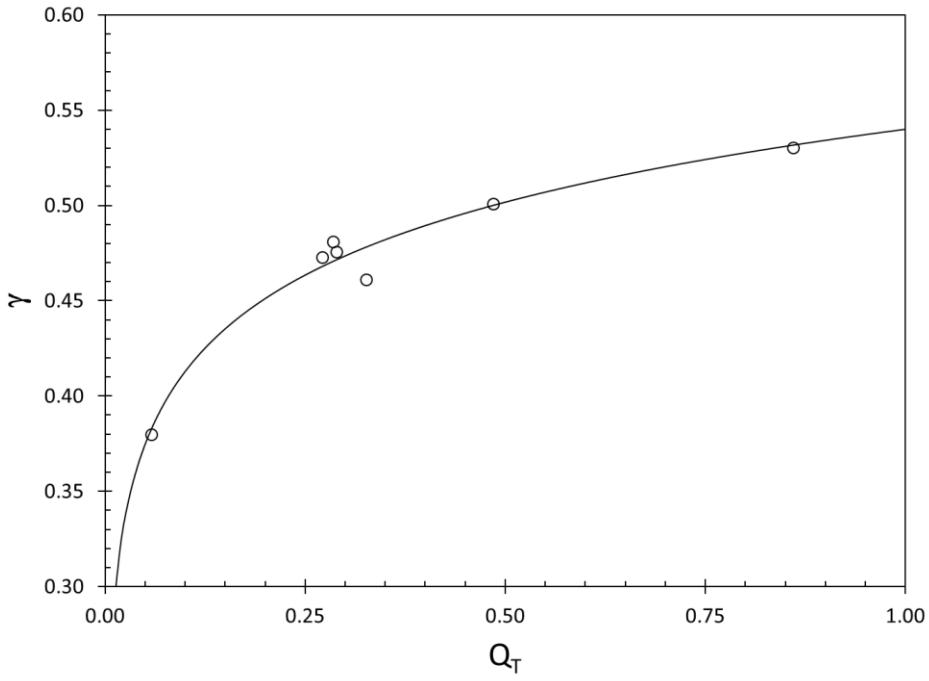

Figure 28. The change in γ as a function of Q_T.

That structural quality affects the Walker parameter has implications for aluminum castings with low quality levels, which are a vast majority of castings in service [66]. Equation (6) can be rewritten as:

$$\frac{\sigma_{eq}}{\sigma_{max}} = \left(\frac{1\text{-}R}{2}\right)^{\gamma} \tag{35}$$

The plot of Equation (35) with γ calculated from Equation (34) for three R ratios and Q_T levels between 0 and 1 is presented in Figure 29. Note that with decreasing quality level, the equivalent alternating stress approaches σ_{max} regardless of the stress ratio. Moreover, the fatigue properties of low quality castings are less sensitive to the stress ratio of the fatigue test. That is why the tensile test results of aluminum castings should be reported along with fatigue performance in all studies for better interpretation of the experimental data.

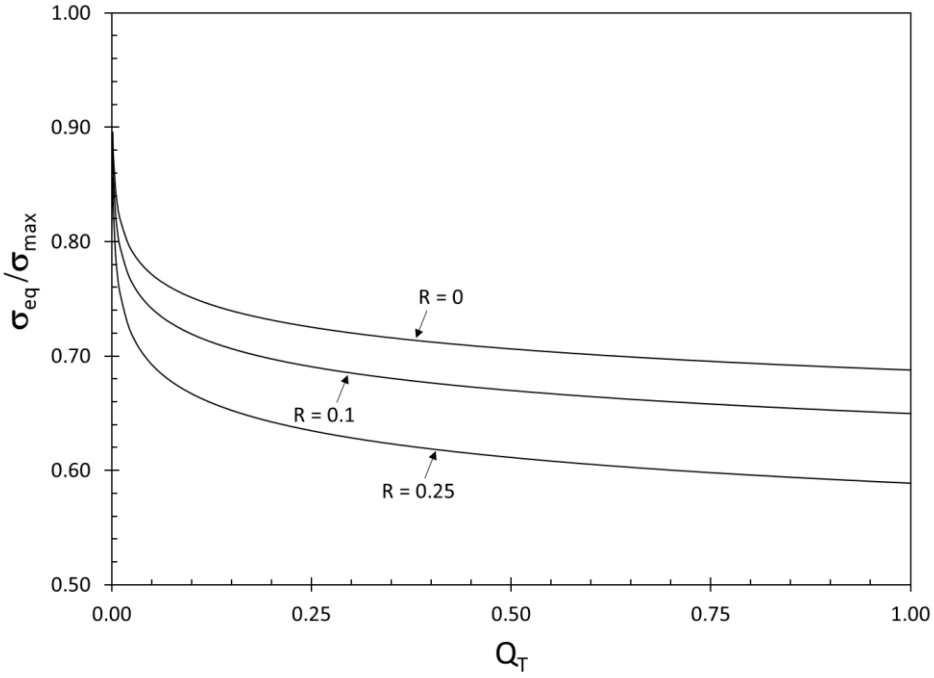

Figure 29. The effect of quality index and R-ratio on the equivalent stress-to-maximum stress ratio.

3.2. Relationships between Q_T and N_f distributions

To determine whether there is more evidence for a relationship between Q_T and N_f distributions, data from four studies on the 319 alloy, used heavily in automotive applications, and data from one study on B201 and D357 alloys, used in aerospace applications have been reanalyzed.

3.2.1. 319 Aluminum Alloy Castings

The details of the datasets reanalyzed in this study are as follows:

- Boileau [94] conducted experiments to determine the effects of solidification time and heat treatment on tensile and fatigue properties of W319 type cast aluminum alloys. Dendrite arm spacing (DAS) was used as a measure of solidification time and ranged between 10-100 μm in wedge-shaped casting. Three groups of rectangular blanks taken from various locations of the castings which were subsequently heat treated to T6 or T7 tempers. At least four tensile specimens were tested for each DAS and heat treatment combination. Fatigue tests were conducted at R = -1, at stress amplitude (σ_a) levels ranging from 31.0 to 180.5 MPa. A total of 280 fatigue test results were provided in the original study. The fatigue life data from hot iso-statically pressed (HIP) specimens were not included in the present study because (i) those datasets had a low number of test results so that methodology followed in this study could not be applied, and (ii) there was evidence that HIP resulted in mixed distributions, which is consistent with results from previous studies on fatigue life of cast aluminum alloys [64, 85]. Therefore, only 174 of the results were used in the present study.

- Byczynski [95] produced sand castings with and without a ceramic foam filter in the filling system to determine the effects of surface oxide bifilms entrained into the casting during mold filling on fatigue life. Fifty-eight fatigue tests were performed at room temperature at an R ratio of 0.1, with a stress amplitude of 67.5 MPa. Byczynski also determined the tensile properties in these two conditions by testing 25 specimens for each dataset.
- Chaudhury *et al.* [96] used 319 aluminum alloy heat treated to T5, T6 and T7. Seven datasets were produced by altering the hold time and furnace type. Eighty-nine fatigue tests were performed at R = -1 with stress amplitude levels ranging from 70.0 to 180.0 MPa. For each condition, one tensile test result was provided [97].
- Zhu [98] used commercially available E319 type aluminum alloy heat treated to T7 and conducted 94 fatigue tests at R = -1, with stress amplitude levels ranging from 70.0 to 160.0 MPa at temperatures of 20, 150 and 250^{o}C. Only the thirty-eight fatigue test results obtained at 20^{o}C have been included in the present study due to effects of temperature [99].

Details for heat treatment conditions from different studies are summarized in Table 4.

The strength coefficients and Basquin exponents estimated by using the methodology developed by Sarkani *et al.* are provided in Table 5. The *b* values in Table 5 are consistent with those provided in the literature for cast Al-Si-Mg alloys [100]. The S-N curves for three datasets, namely '70μm DAS, T7B' [94], 'R' [96] and 'T7' [98] are provided in Figure 30, with runouts indicated with arrows. Note that the estimated σ_f' and *b* values provided respectable fits to the experimental data.

Table 4. Summary of heat treatment sequences for specimens in the four studies.

Ref.	Temper	Solution Treatment	Quench	Aging Treatment
[94]	T6	8 hours at 495°C	BWQ	5 hours at 190°C
	T7	8 hours at 495°C	BWQ	4 hours at 260°C
[95]	T6	4.5 hours at 500°C	CWQ	19 hours hold at RT + 4 hours at 260°C
[96]	T7 (Group A)	2 hours at 498°C	FB (RT)	4 hours at 240°C
	T6 (Group B)	2 hours at 498°C	FB (RT)	4 hours at 210°C
	T7 (Group C)	2 hours at 498°C	FB (RT)	1.5 hours at 250°C (FB)
	T7 (Group D)	8 hours at 498°C	FB (RT)	1.5 hours at 250°C (FB)
	T6 (Group E)	2 hours at 498°C	FB (RT)	1.5 hours at 230°C (FB)
	T6 (Group F)	8 hours at 498°C	FB (RT)	1.5 hours at 230°C (FB)
	T5 (Group R)	††	††	4 hours at 210°C
[98]	T7	8 hours at 495°C	BWQ	4 hours at 260°C

BWQ: boiling water quench, CWQ: cold water quench, FB: fluidized bed, RT: room temperature

All fatigue life data used in this study were transformed by using Eq. (33) to an equivalent fatigue life at a stress level amplitude of 100 MPa and R =-1. For fatigue life data with runouts, the Weibull distribution parameters have been estimated by using the linear regression technique and the plotting position formula developed by Kaplan and Meier [101] for censored samples.

Table 5. Relevant information and estimated Basquin coefficients for all datasets.

Dataset	Ref.	Group	# of data points	# of runouts	σ_f' (MPa)	b
Boileau	[94]	23μm DAS, T6	25	11	460.8	-0.087
		70μm DAS, T6	23	2	1092.9	-0.199
		100μm DAS, T6	29	5	770.2	-0.178
		23μm DAS, T7	25	3	427.6	-0.099
		60μm DAS, T7	17	3	419.5	-0.118
		70μm DAS, T7	27	5	412.0	-0.123
		100μm DAS, T7	28	2	360.6	-0.131
Byczynski	[95]	Filtered	31	1	†	†
		Unfiltered	27	1	†	†
Chaudhury	[96]	A	17	3	425.4	-0.099
		B	17	3	570.8	-0.117
		C	10	3	469.2	-0.112
		D	10	2	497.4	-0.116
		E	10	3	465.9	-0.109
		F	9	1	728.6	-0.136
		R	16	2	548.8	-0.125
Zhu	[98]	T7	28	4	412.6	-0.102

† Fatigue tests were conducted at constant stress amplitude level. Therefore, coefficients of Basquin could not be estimated.

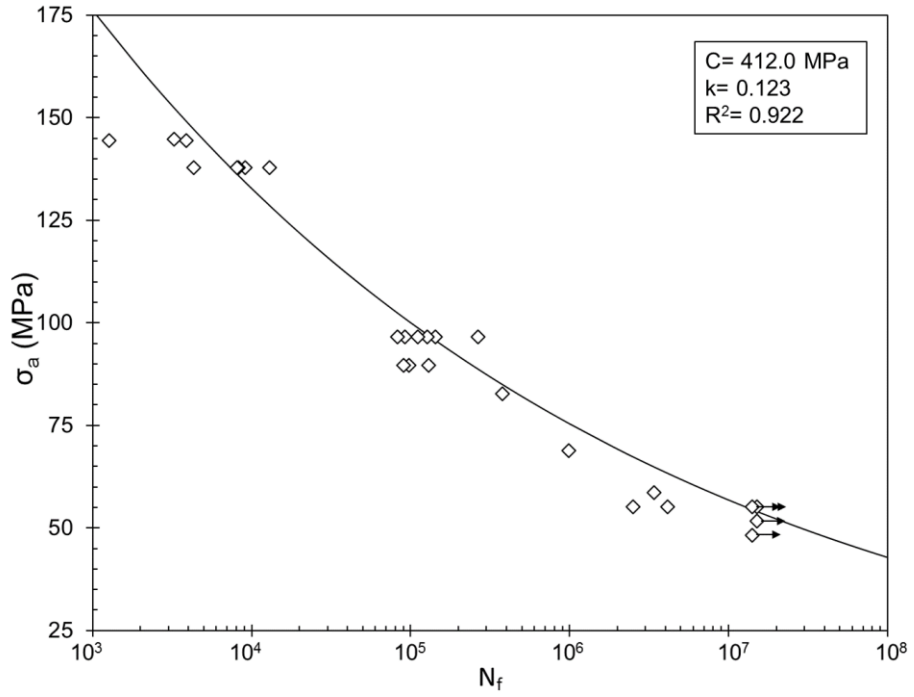
C= 412.0 MPa
k= 0.123
R²= 0.922
σa (MPa)
Nf
175
150
125
100
75
50
25
10³
10⁴
10⁵
10⁶
10⁷
10⁸

(a)

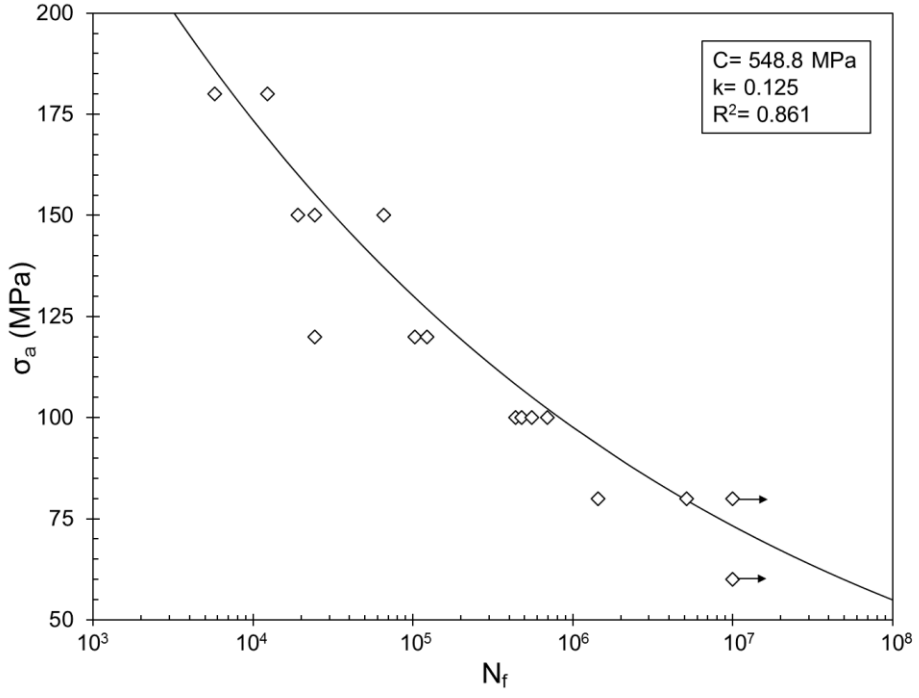
C= 548.8 MPa
k= 0.125
R²= 0.861
σa (MPa)
Nf
200
175
150
125
100
75
50
10³
10⁴
10⁵
10⁶
10⁷
10⁸

(b)

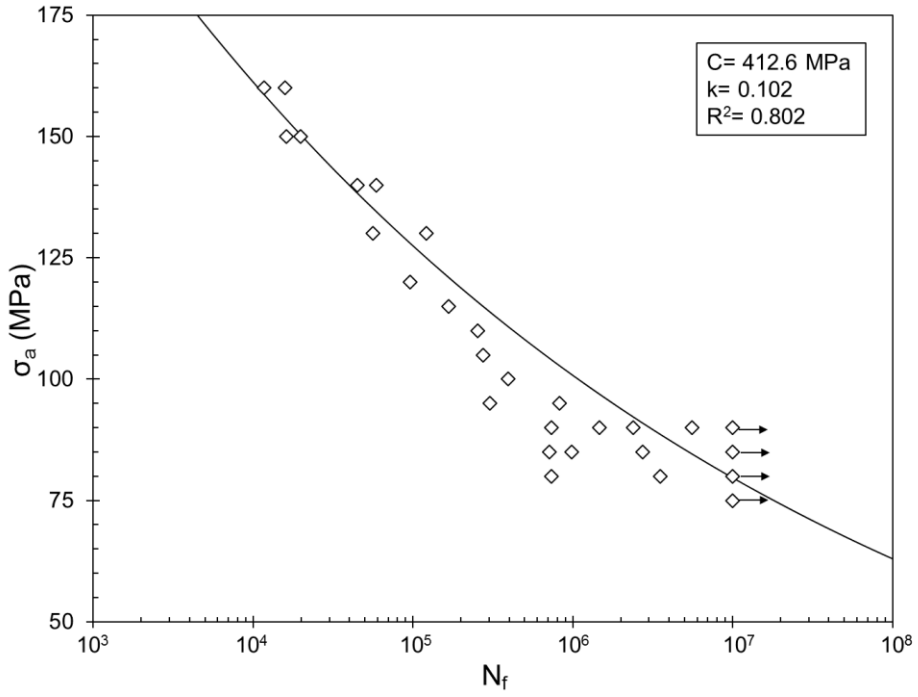

(c)

Figure 30. S-N curve of (a) 70µm DAS, T7 [94], (b) R, T5 [96], (c) T7 [98] datasets.

Estimated Weibull parameters for all fatigue life datasets are given in Table 6. The coefficient of determination for all fits obtained by the linear regression model exceed the critical R^2 values for respective sample sizes [102]. Therefore, Weibull fits cannot be rejected. The Weibull probability plots for the T6 and T7 datasets from Boileau are provided in Figure 31. Note that the Weibull fits are excellent to the experimental data as well as the runouts, which are not indicated in Figure 31.

Table 6. Estimated Weibull parameters for all datasets.

Dataset	Ref.	Group	m	$N_0/V^{1/m}$	$\overline{N_{eq}}$
Boileau	[94]	23µm DAS, T6	0.815	41,690,985	46,632,271
		70µm DAS, T6	1.912	163,933	145,439
		100µm DAS, T6	1.147	94,778	90,273
		23µm DAS, T7	1.138	2,239,343	2,137,868
		60µm DAS, T7	1.306	165,033	152,278
		70µm DAS, T7	2.020	96,051	85,109
		100µm DAS, T7	1.504	17,471	15,767
Byczynski	[95]	Filtered	1.174	611,809	578,914
		Unfiltered	1.539	718,117	646,357
Chaudhury	[96]	A	1.201	2,067,435	1,944,370
		B	1.519	2,692,600	2,427,151
		C	1.281	1,038,128	961,672
		D	1.299	1,045,690	965,926
		E	1.334	1,516,528	1,393,581
		F	2.944	1,998,149	1,782,855
		R	1.731	791,472	705,363
Zhu	[98]	T7	1.376	1,011,639	924,669

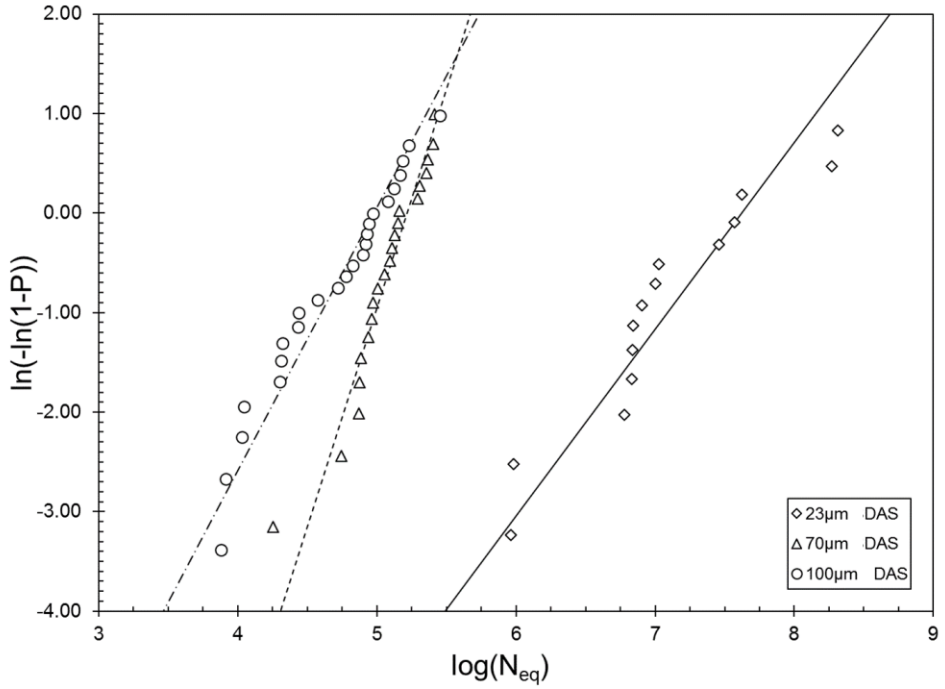

(a)

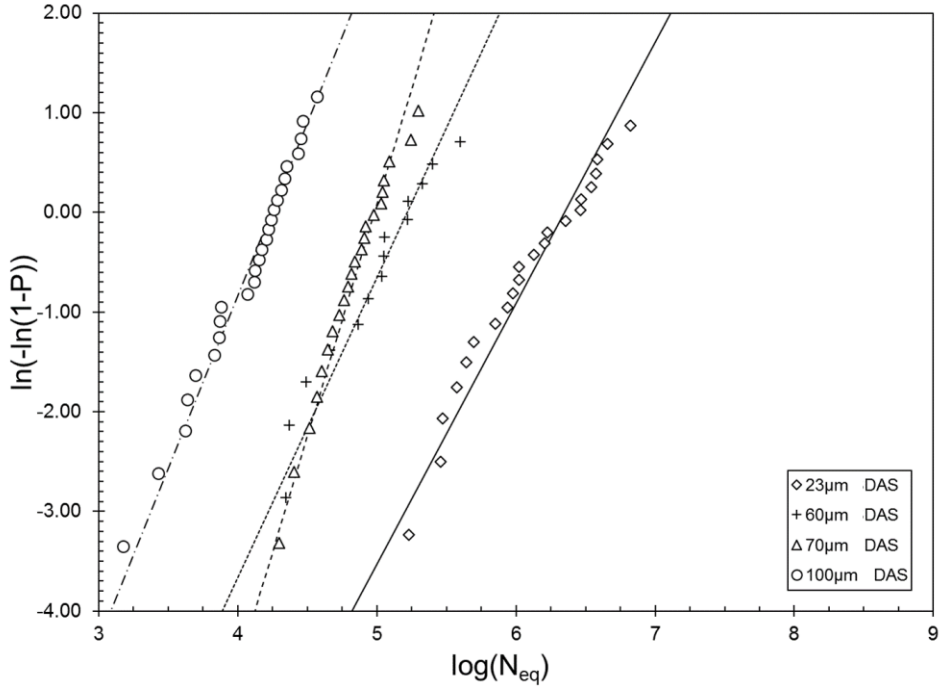

(b)

Figure 31. Weibull probability plots of Boileau's (a) T6 and (b) T7 datasets.

It should be noted that in all datasets except for those of Byczynski, tensile data were provided as either an average or results from only one tensile test were reported in the original studies. Consequently, Weibull distributions could only be fit to quality index data of Byczynski. For the filtered and unfiltered castings, the Weibull modulus has been estimated as 6.055 and 5.579, respectively. The mean Q_T for filtered and unfiltered castings are 0.073 and 0.068, respectively.

Effective volumes of each specimen used in the four studies are provided in the Table 7. Volumetric correction has been made by:

$$\overline{x_1} = \overline{x_2}\left(\frac{V_2}{V_1}\right)^{1/m} \tag{36}$$

for V=308 and 1021 mm^3 as the reference values for fatigue and tensile specimens, respectively, as used by Boileau. For the analysis of tensile data, quality index (Equation 1) was calculated by using β_0 and β_1 of 36 and 0.064 MPa^{-1} [64] respectively, for cast Al-Si-Mg alloys. For correction of Q_T values, it has been assumed that (i) all elongation data follow the Weibull distribution, which is consistent with the literature [86, 103], and (ii) Weibull modulus for all datasets are 5.58, as reported above for unfiltered castings by Byczynski.

The relationship between mean Q_T and mean N_f is given in Figure 32. Data indicate a linear relationship when fatigue life mean is presented logarithmically, similar to what was reported for A206 [73]. The best-fit equation for the relationship is:

$$\log\left(\overline{N_{eq}}\right) = 9.41\overline{Q_T} + 4.93 \tag{37}$$

Table 7. Effective volumes of specimens used in the studies.

Dataset	Ref.	Fatigue Specimen			Tensile Specimen		
		Diameter (mm)	**Gage Length** (mm)	**Eff. Volume** (mm^3)	**Dimension** (mm)	**Gage Length** (mm)	**Eff. Volume** (mm^3)
Boileau	[94]	5.1	15.2	308.1	6.4†	31.8	1,021.4
Byczynski	[95]	5.0	15.0	294.5	12.5†	50.0	6,135.9
Chaudhury	[96]	6.4	12.7	402.2	6.4×5.1††	25.4	819.4
Zhu	[98]	5.0	15.0	294.5	12.5†	50.0	6,135.9

† Diameter
†† Length × Width

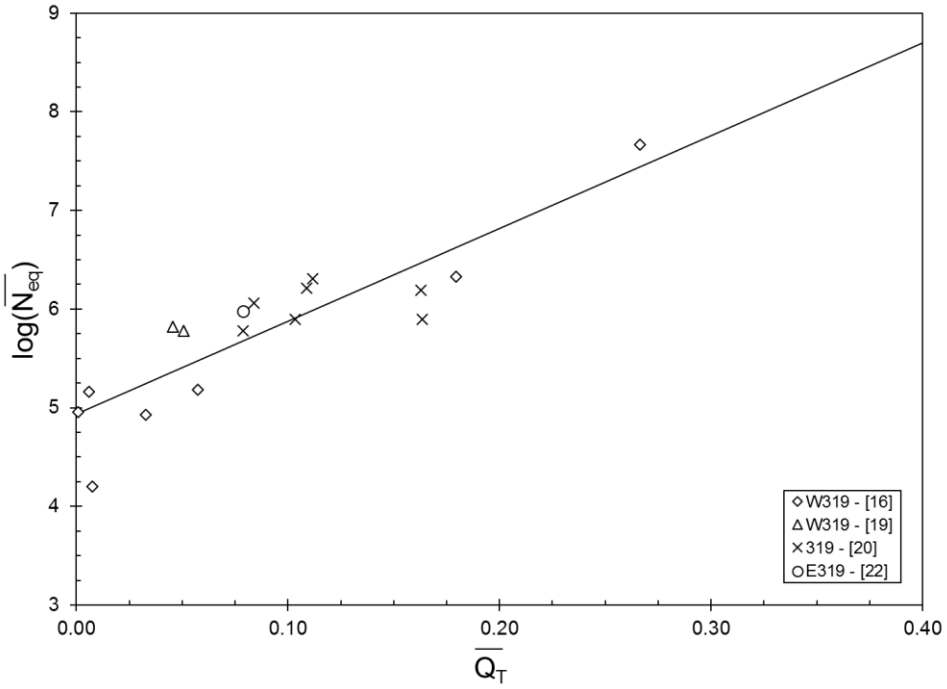

Figure 32. The relationship between expected (mean) quality index and fatigue life.

That a common relationship between quality index and fatigue life in data collected in four independent studies is astonishing. The strong relationship between elongation or Q_T, and fatigue life identified in the study can be interpreted as follows; it is well known that fatigue

life consists of crack initiation (N_i), crack propagation (N_p), and rapid fracture. In many studies on fatigue behavior of cast aluminum alloys, N_i was found to be almost zero [104-107]; cracks started to propagate from casting defects almost immediately after fatigue testing started. Therefore, it is common to assume that $N_i=0$ for aluminum alloy castings [108]. However, Jiang *et al*. [109] found that crack initiation phase can be as high as ~60% of total fatigue life in A356 aluminum alloy castings. They also noted that any improvement in the total fatigue life will most likely be due to longer initiation phase because once the crack reaches a certain size, crack propagation rate was found to be similar in specimens with varying duration of crack initiation phases. Farahmand and Nikbin [110] analyzed how ΔK_{th}, the threshold in crack propagation, increases linearly with elongation in various alloys and found that fatigue initiation value increases with elongation of the alloys. Hence, a specimen with a higher structural quality can be expected to have a longer N_i, as suggested by Jiang *et al*. This is consistent with the results of Han *et al*. [111] who compared the fatigue crack growth rates for A356 at three different elongation (Q_T) levels. With increasing Q_T, they found the ΔK_{th} to increase, as suggested by Farahmand and Nikbin. They also showed that crack propagation rate is slightly slower in the specimen with a higher Q_T. Rading *et al*. [106] observed that fatigue cracks in 206 aluminum alloy castings propagated much more rapidly when they encountered oxide bifilms. Therefore, a lower number of oxide bifilms (higher structural quality) should result in a lower crack propagation rate.

It should be noted that Equation (37) can be used to estimate fatigue life at R=-1 and σ_a=100 MPa for $Q_T \leq 0.30$. For extrapolation to larger Q_T values, Equation (37) will overestimate the expected fatigue life. This can be explained as follows. At low structural quality values,

failure will be initiated by a defect that is connected to the surface. With increasing structural quality (i.e., smaller defect density and smaller defect size), the probability that fatigue failure is initiated by a defect that is subsurface, rather than on surface, increases [73]. Recent studies [112-118] have shown that there are different S-N curves for fracture initiation from defects on the surface and subsurface. Consequently, the extrapolation of N_f on higher values of Q_T must be up to a certain quality level, after which a different mode of failure is expected, such as fatigue crack initiation in subsurface defects. Nevertheless, at Q_T=1, it can be argued that specimens will have no surface or subsurface defects, leading to an expected fatigue life of at least 2.2×10^{14}, which, in practice, can be considered infinite fatigue life. More research on fatigue performance of 319 alloy specimens with high structural quality levels is needed.

Kun *et al.* [25] investigated the physical meaning of the Basquin exponent and concluded that it is a measure of the degradation taking place at the micro-level. Therefore, a higher structural quality would result in lower degradation with cycles, leading to a higher *b* value, which is consistent with experimental results reported for cast Al-Si-Mg alloys [119].

3.2.2. D357 and B201 Aluminum Alloy Castings [1, 120]

Four datasets reported by Ozelton *et al*. [121] who investigated the durability and damage tolerance for D357-T6 and B201-T7 cast aluminum alloys were reanalyzed in this study. For both alloys, two solidification rates based on the pour temperature and the chill material were used. The experimental details for "slow" and "fast" cooled specimens are given in Table 8.

Table 8. Experimental design used by Ozelton et al. for D357 and B201 castings.

	D357-T6		**B201-T7**	
Solidification Rate	Slow	Fast	Slow	Fast
Pouring T (ºC)	782	748	787	732
Chill Material	Iron	Copper	Iron	Copper

Ozelton *et al.* performed tensile and fatigue tests in accordance with the ASTM B557 and ASTM E466, respectively. The geometry of the fatigue specimen was carefully selected to mimic aircraft components with holes where fatigue cracks are usually initiated due to stress concentrations. In total, 170 fatigue life and 165 tensile test results obtained by Ozelton *et al.* have been re-evaluated in the investigation [1, 120]. It is significant that there were no fatigue run-outs in the datasets.

The dot-plot for elongation data for D357-T6 and B201-T7 castings is presented in Figure 33. Note in Figure 33.a that the highest data for "fast" solidification is higher than in "slow" solidification, although minimum data in both datasets are similar. Hence the scatter is higher in "fast" solidification D357 castings. In Figure 33.b, the elongation data for "fast" B201-T7 castings are only slightly higher than in "slow" castings. Moreover, there is an apparent gap in both datasets, as indicated in Figure 33.b.

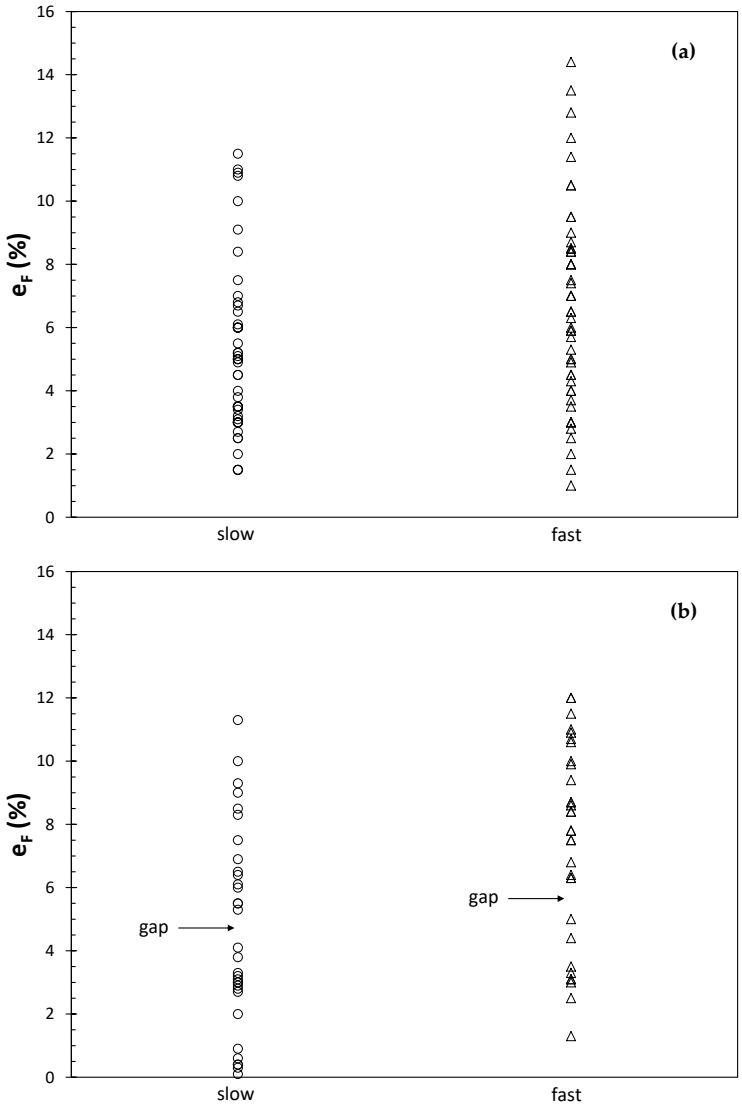

Figure 33. Dot-plot for elongation data of "slow" and "fast" specimens for (a) D357-T6 and (b) B201-T7 aluminum alloy castings [1, 120].

The fatigue life data for the two aluminum alloy castings are presented in Figure 34. For D357, minimum data are almost identical for "slow" and "fast" castings, Figure 34.a. However longest fatigue life is significantly higher for "fast" castings. As in elongation, fatigue life data in B201 aluminum alloy castings have a significant gap, as shown in Figure 34.b. The gaps in datasets are an indication that data have been collected from two distinct

distributions. Hence, there is evidence that there is a mixture of at least two distributions in elongation and fatigue life data for B201-T7 aluminum alloy castings [1, 120].

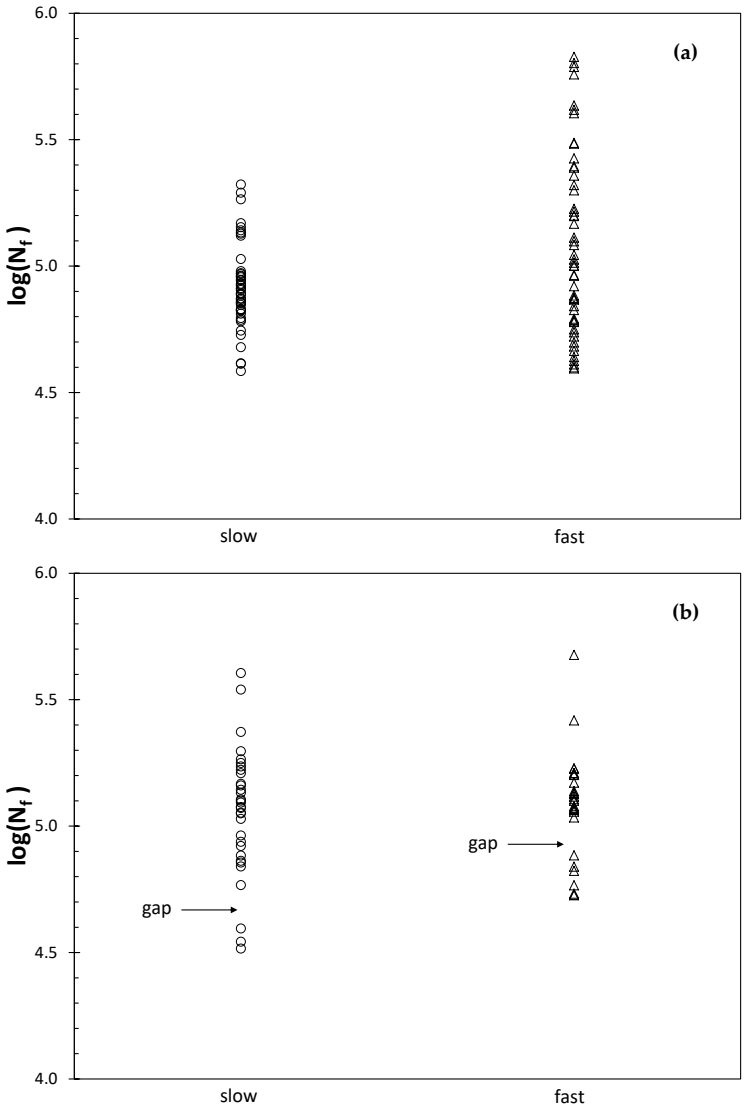

Figure 34. Dot-plot for fatigue life of "slow" and "fast" specimens for (a) D357-T6 and (b) B201-T7 aluminum alloy castings [1, 120].

Tensile data were transformed to Q_T by using the β_0 and β_1 of 36 and 0.064MPa^{-1} for D357 [64] and 34.5 and 0.047MPa^{-1} for B201 [67], respectively. Weibull distributions with both two and three parameters have been fitted to the tensile and fatigue life data by

using the maximum likelihood method. Estimated Weibull parameters for each dataset are given in Table 9. Note that for B201, fatigue life and quality index data were found to have Weibull mixtures, as indicated in Table 9.

Table 9. Estimated Weibull parameters for Q_T and N_f for D357 and B201 castings.

Alloy	**Solid. Rate**	**Distribution Tag**		**Weibull parameters**			
				p	**σ_T**	**σ_0**	**m**
D357-T6	Slow	Q_T			0.077	0.239	1.52
		N_f			37,291	57,340	1.43
	Fast	Q_T			0.010	0.433	2.27
		N_f			38,688	120,966	0.74
B201-T7	Slow	Q_T	Lower	0.250	0	0.066	1.13
			Upper		0.179	0.234	1.34
		N_f	Lower	0.114	26,351	16,963	1.62
			Upper		67,720	90,284	0.82
	Fast	Q_T	Lower	0.188	0	0.200	4.79
			Upper		0	0.623	6.26
		N_f	Lower	0.281	51,372	18,730	0.95
			Upper		113,610	58,081	0.57

The Weibull probability plots for Q_T and N_f for D357-T6 aluminum alloy castings are presented in Figure 35. Fits indicated by the two curves in Figure 35 are in close agreement with the data. The goodness-of-fit of the estimated parameters was tested by using the Anderson-Darling statistic [122]. In all cases, the hypothesis that the data come from the fitted Weibull distributions could not be rejected. Note in Figure 35.a that the Q_T data for fast-cooled castings fall on almost a straight line, which indicates that the threshold is close to zero (0.010), Table 9. The data for slow-cooled castings indicate a curve relationship which is indicative of a positive threshold. Moreover, both fatigue life distributions have almost the same threshold. Because lowest fatigue life in a distribution is determined by the largest defects possible in specimens [86], the size of the largest

defects is almost the same in “fast” and “slow” datasets, regardless of how fast the metal solidified [1, 120].

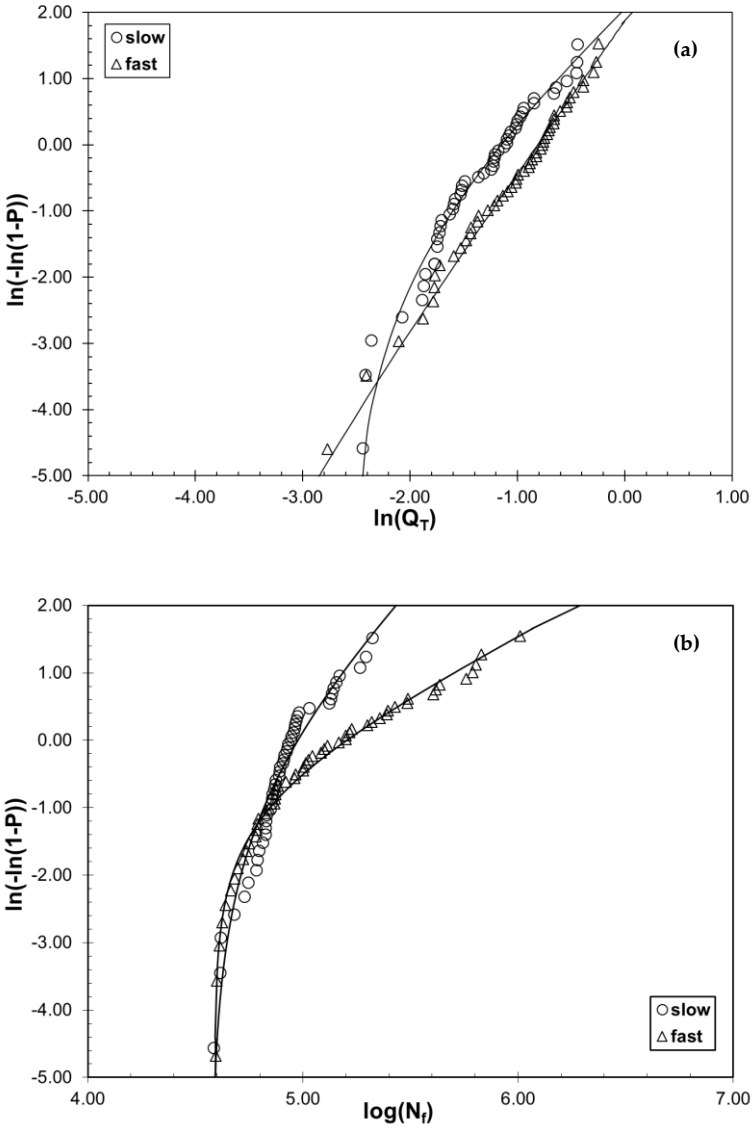

Figure 35. Weibull probability plots of (a) Q_T and (b) N_f in D357-T6 aluminum alloy castings [1, 120].

The Weibull probability plots for Q_T and N_f for B201-T7 aluminum alloy castings are provided in Figure 36. Note that for both Q_T and N_f, there are inflection points in the probability plots which are indicative of Weibull mixtures [85, 86, 123]. Consequently, lower and upper Weibull distributions were fitted separately and mixed by using Equation (32).

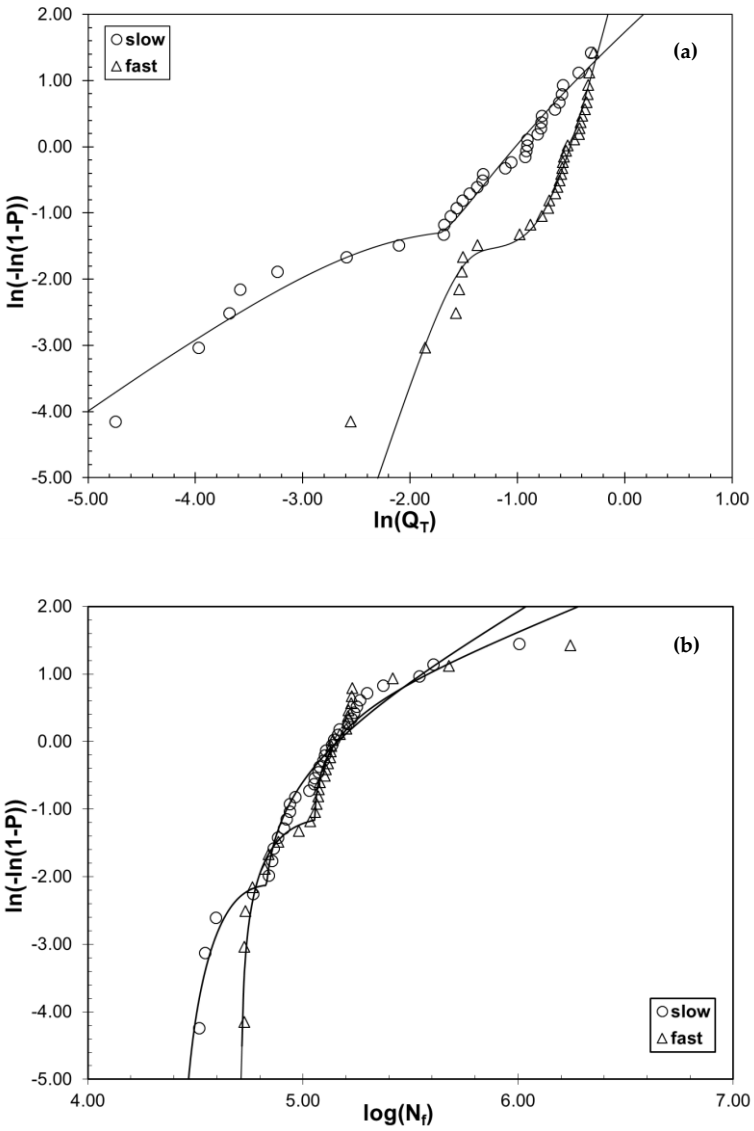

Figure 36. Weibull probability plots for (a) Q_T and (b) N_f in B201-T7 aluminum alloy castings [1, 120].

That both Q_T and N_f data for B201 aluminum alloy castings showed Weibull mixtures is noteworthy. Analysis of fracture surfaces in A206-T7 aluminum alloy castings showed [73, 124, 125] that the lower distribution for elongation was attributed to the "old", coarse oxide bifilms that were generated during previous melt processing or were on the skin of the ingots. For fatigue life, the lower distribution is due to the fatigue crack initiation at surface defects. The two lower distributions are linked because the probability that a defect will be on the surface of the fatigue specimen increases with its size and number density [73]. Hence, premature fracture in fatigue must be accompanied by low elongation, or alternatively, Q_T. As expected, increased solidification rate has a positive effect on both Q_T and N_f. It is also noteworthy that the improvement is most significant in the lower distributions. Moreover, the lower distributions remain significantly separated from the upper distributions [1, 120], showing that chilling is a much less effective way to improve properties than eliminating structural defects, mainly bifilms and pores. It has been only recently understood [31, 126] that the degradation of and variability in the mechanical properties of castings are related to these very defects that are incorporated into the bulk of the liquid by an entrainment process, in which the surface oxide folds over itself. In most steel castings, the oxide has a significantly lower density than the metal, and therefore floats to the surface quickly, leaving the metal relatively free of defects. In aluminum alloys, the folded oxide has practically neutral buoyancy, so that defects tend to remain in suspension. The layer of air in the folded oxide can (i) grow into a pore as a result of the negative pressure due to contraction of the solidifying metal and/or rejection of gases, originally dissolved in liquid metal, upon solidification, or (ii) remain as an un-bonded

surface, like a crack, in the solidified alloy, which usually serves as heterogeneous nucleation sites for intermetallic.

Prior studies [34, 35, 40, 103, 127, 128] have shown that there are multiple types of defects in castings, including bifilms and pores associated with bifilms. From a process viewpoint, it is not surprising to find Weibull plots for tensile data that reveal at least two populations of defects [86]:

1. the original rather fine scattering of defects remaining in suspension in the original poured liquid from the crucible or ladle (prior damage). These "old" bifilms have a typical minimum thickness of approximately 10 μm and show only coarse wrinkles.
2. the large new bifilms (new damage) that would have been produced during the melt transfer and/or pouring and filling if the filling system was not designed properly. These "young" oxides have a minimum thickness of tens of nanometers or less and show fine wrinkles on fracture surfaces of castings.

The probability density functions for Q_T and corresponding N_f distributions are presented in Figure 37. The different shapes of N_f distributions are a product of the use of the 3-parameter version of the Weibull distribution and the value of the shape parameter; when $m \leq 1$, the shape of the 3-parameter Weibull distribution resembles that of an exponential decay curve [1, 120].

The expected (mean) values for all six distributions were calculated by using Equation (29) and the estimated Weibull parameters in Table 9. As stated above, the lower distributions in Q_T and N_f in B201 were associated with each other. The relationship between expected Q_T and N_f values is presented in Figure 38.

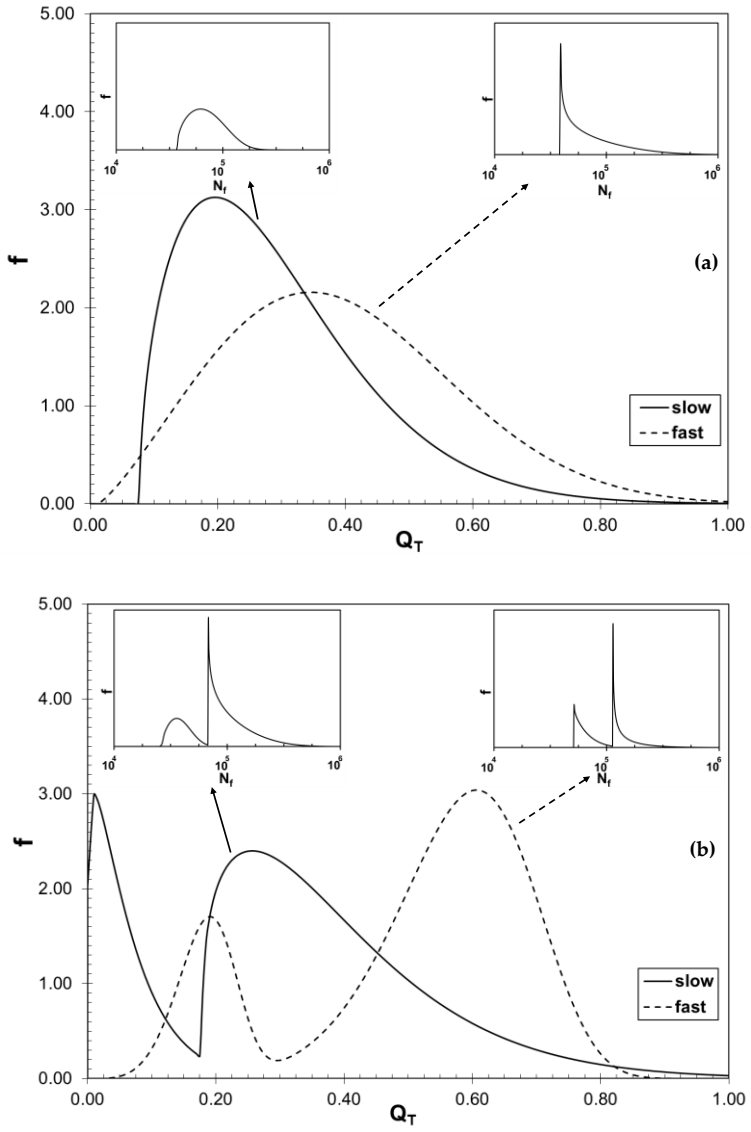

Figure 37. Probability density functions for Q_T and corresponding probability density functions for N_f for (a) D357 and (b) B201 aluminum alloy castings [1, 120].

Similar to what was reported for A206-T7 aluminum alloy castings [73] and the results for 319 reported above, a linear relationship was observed between expected Q_T and the logarithm of expected fatigue life. The best fit line indicated with dashed lines in Figure 38 has the following equation:

$$\log(\overline{N}_f) = 4.57 + 1.46\overline{Q}_T \quad (38)$$

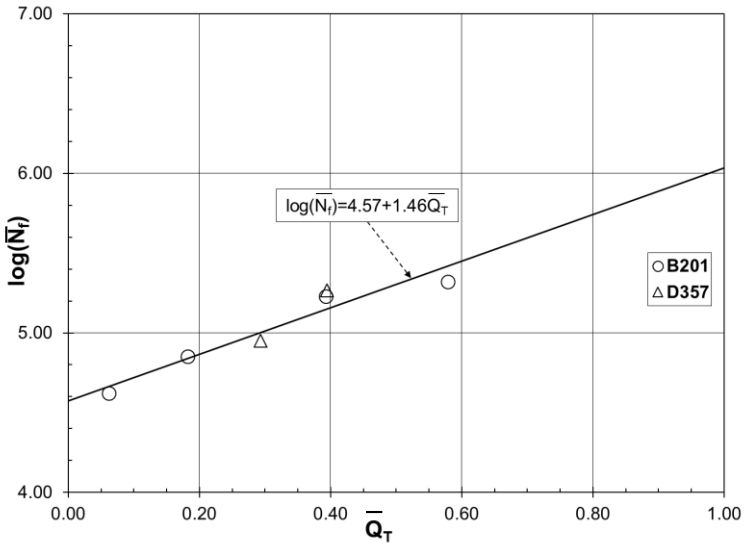

Figure 38. Relationship between the means of Q_T and N_f distributions [1, 120].

Note that the best fit equation estimates approximately 10^6 cycles when the specimen could reach the maximum quality (defect free condition). Therefore, fatigue life of aerospace castings can be extended by at least six times if structural defects are eliminated. It is also noteworthy that two alloys with different microstructures could follow the same trend; B201 has an aluminum matrix with Cu, Mg and Ag providing the strengthening phase. D357 has 7wt.%Si, resulting in eutectic Si phase, based on which the alloy can be interpreted as an *in-situ* metal matrix composite. Hence it is possible that the difference in trendlines in Figure 32 and Figure 38 is due to different specimen geometries used in these studies. More research is needed to validate this point.

The proportions of the Q_T distributions in all three regions as well as the probability of survival after 10^5 cycles were calculated by using estimated Weibull parameters in Table 9. The results are presented in
Table 10. The proportion of Region 1 ($Q_T \leq 0.25$) versus probability of $N_f > 10^5$ is plotted in Figure 39.a. Clearly, probability of survival after 10^5 cycles decreases significantly with

the proportion of castings in Region 1 [1, 120]. A similarly strong relationship between the probability of survival after 10^5 cycles versus the proportion of castings in Region 3 (Q_T>0.70) is presented in Figure 39.b. As the casting quality is improved, probability of survival also increases, as can be expected. Hence there is strong evidence in Figure 39, as well as in Figure 38, that elongation (quality index) and fatigue performance are related; (i) there is a strong correlation between mean values, and (ii) the probability of survival is directly linked to the proportion of the elongation distribution in Region 1 and Region 3. Therefore, the statement that the elongation requirement in industrial specifications is a *de facto* fatigue life specification is justified.

Table 10. Fraction of distributions for Q_T in each region and probability of survival at 10^5 cycles.

			$P(Q_T \leq 0.25)$	$P(0.25 \leq Q_T < 0.70)$	$P(Q_T \geq 0.70)$	$P(N_f \geq 10^5)$
D357	Slow		0.458	0.529	0.014	0.321
	Fast		0.230	0.713	0.056	0.546
B201	Slow	L	0.989	0.011	0.000	0.000
		U	0.183	0.763	0.054	0.650
	Fast	L	0.946	0.054	0.000	0.084
		U	0.003	0.871	0.126	1.000

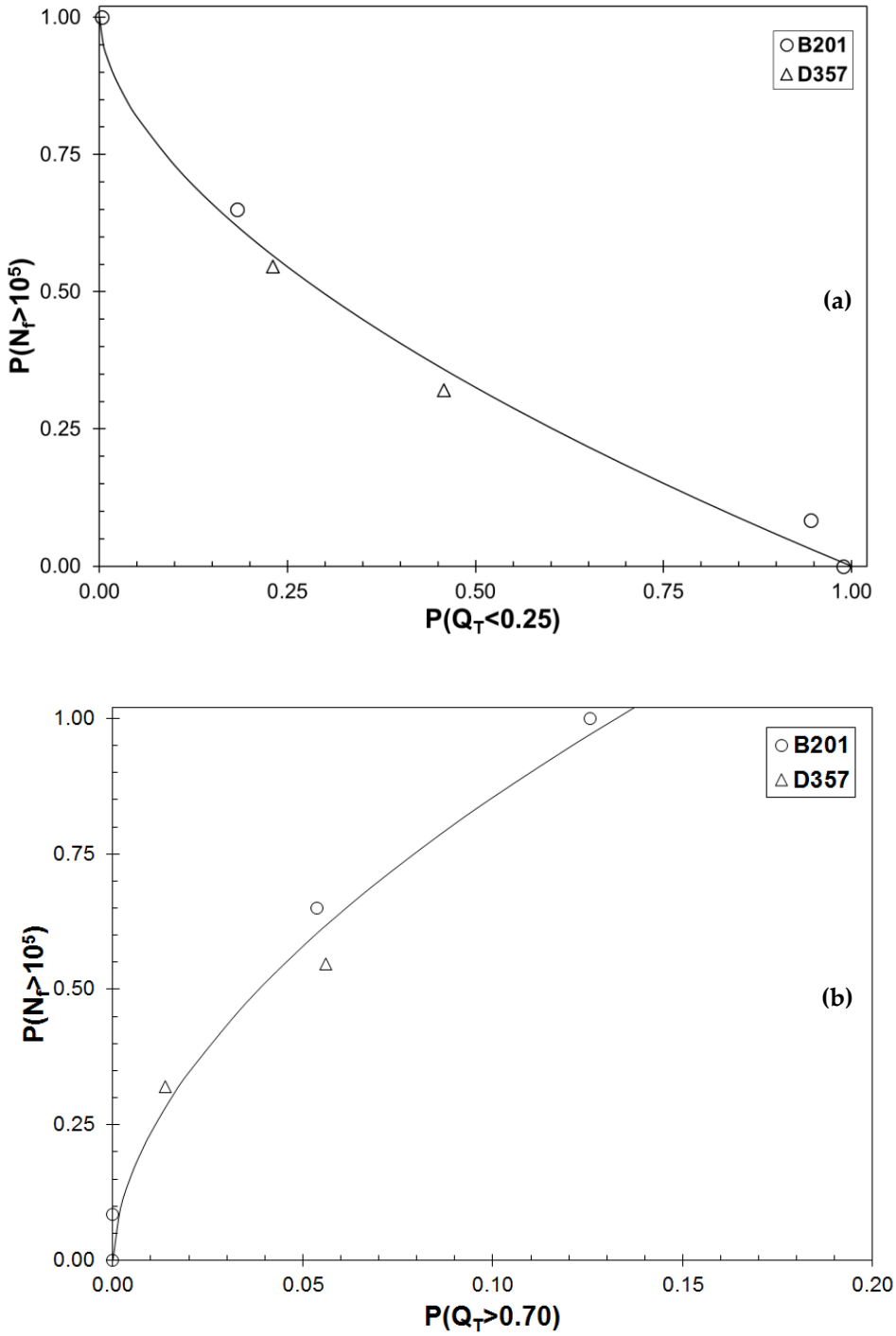

Figure 39. The change in the probability of survival after 10^5 cycles versus the estimated fraction of the Q_T distribution in (a) Region 1 and (b) Region 3 [1, 120].

3.3. The Effectiveness of the Methods used to Predict HCF from Tensile Data

The effectiveness of the six methods outlined in Table 1 and Equation (18) has been investigated by using five datasets from the literature from two independent studies. The details of the two studies are given below.

- Zhu [98] used commercially available E319 type aluminum alloy heat treated to T7 and conducted tensile tests and fatigue tests at R = -1, with stress amplitude levels ranging from 70 to 160 MPa [99].
- Couper *et al*. [129] heat-treated castings of CP601 Australian alloy (A356) to different conditions and conducted tensile and fatigue tests at R = -1. The conditions at which specimens were tested are (i) as cast, (ii) underanged after 1 hour of artificial aging at 155^{o}C (1UA), (iii) under aged after 8 hours of artificial aging at 155^{o}C, (iv) peak-aged (12PA), after 12 hours of artificial aging, and (v) overaged after 200 hours at 155^{o}C. The stress amplitude ranged between 100 and 250 MPa.

Tensile data for all datasets are summarized in Table 11. Note that all tensile properties of 1UA and 8UA are identical. Therefore, data from these two datasets have been combined.

Table 11. Tensile data for the five datasets.

Dataset	Ref.	σ_y (MPa)	S_T (MPa)	e_F (%)	E (GPa)
E319-T7	[98]	199	290	2.0	77.5
As Cast	[129]	120	250	13.0	70.0
1UA & 8UA		220	310	9.0	70.0
12PA		250	320	8.0	70.0
200UA		220	310	7.0	70.0

The Basquin parameters estimated by using the six methods and the tensile data given in Table 11 are presented in Table 12. Note that the parameters for the best fit estimated by the ML method given in the Appendix is also presented. The fits of the methods to the data by Zhu (E319-T7) are indicated in Figure 40. Only the estimate by Method 1 is close to the actual S-N curve. The coefficients of determination, R^2, calculated for all estimates are given in Table 13.

Table 12. Estimated Basquin fits to the five datasets models for each dataset.

Dataset	Parameter	Best fit	Method 1	Method 2	Method 3	Method 4	Method 5	Method 6
E319-T7	σ_f'	403.6	551.0	349.6	461.9	484.3	551.0	388.0
	b	-0.104	-0.120	-0.081	-0.090	-0.095	-0.110	-0.073
As Cast	σ_f'	360.1	475.0	329.9	401.4	417.5	475.0	285.4
	b	-0.072	-0.120	-0.088	-0.090	-0.095	-0.110	-0.057
1UA & 8UA	σ_f'	475.7	589.0	396.6	480.0	517.7	589.0	410.7
	b	-0.089	-0.120	-0.086	-0.090	-0.095	-0.110	-0.074
12PA	σ_f'	776.9	608.0	406.1	492.9	534.4	608.0	445.4
	b	-0.129	-0.120	-0.085	-0.090	-0.095	-0.110	-0.078
200OA	σ_f'	588.6	589.0	390.2	480.0	517.7	589.0	445.5
	b	-0.104	-0.120	-0.084	-0.090	-0.095	-0.110	-0.074

The S-N curves estimated by the six methods to the four datasets by Couper *et al*. are presented in Figure 41. For the "As Cast" dataset, Method 6 seems to provide the best estimate of the fatigue performance, as can be seen in Figure 41.a. For the "1UA & 8UA", dataset in Figure 41.b, there seem to be several good estimates. The R^2 values in Table 13 indicate that Methods 3, 4 and 6 are very close, with Method 3 yielding the highest R^2. For the "12PA" dataset in Figure 41.c, almost all methods give close estimates but Method 5

has the best fit (Table 13). Finally, Figure 41.c shows the estimates for the "200OA" dataset, with Method 4 giving the best estimate.

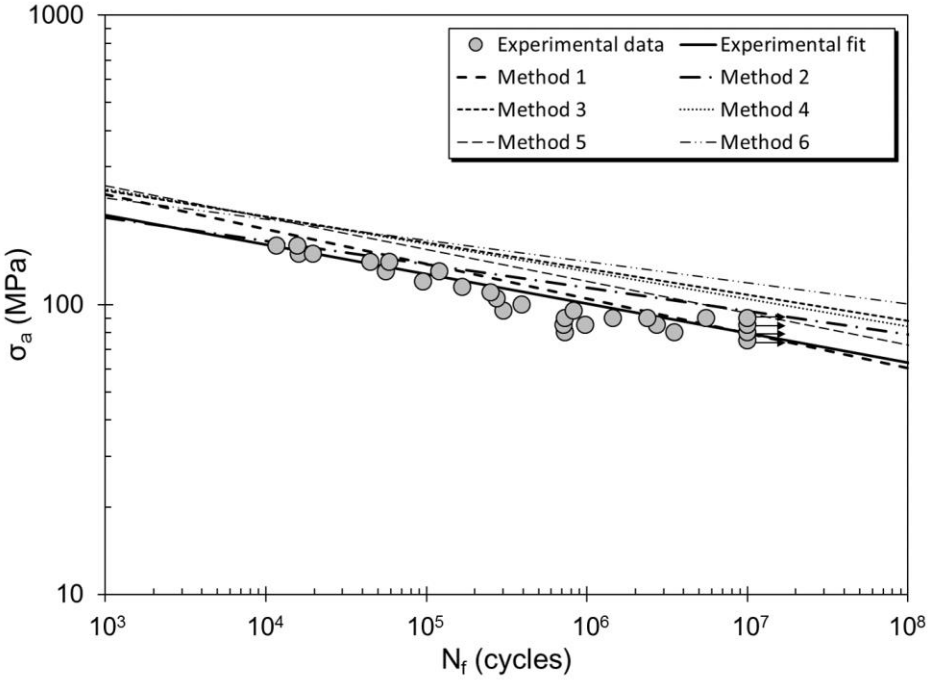

Figure 40. The application of the six methods to the E319 dataset by Zhu.

Table 13. Coefficient of determination, R^2 values for the six models for each dataset. Best estimate for each dataset is given in bold.

Dataset	Method 1	Method 2	Method 3	Method 4	Method 5	Method 6
E319-T7	**0.640**	0.352	< 0	< 0	< 0	< 0
As Cast	< 0	< 0	< 0	< 0	< 0	**0.577**
1UA & 8UA	0.119	0.375	**0.771**	0.767	0.683	0.756
12PA	0.761	0.730	0.838	0.841	**0.916**	0.734
200OA	< 0	< 0	0.645	**0.685**	0.470	0.681

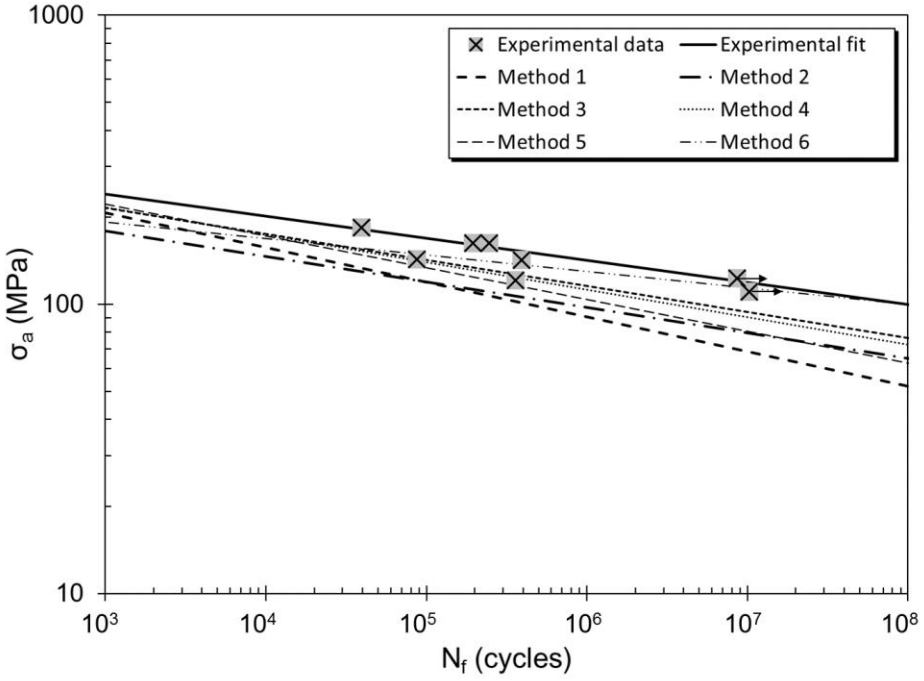
1000
100
10
σa (MPa)
10³
10⁴
10⁵
10⁶
10⁷
10⁸
Nf (cycles)
Experimental data
Experimental fit
Method 1
Method 2
Method 3
Method 4
Method 5
Method 6

(a)

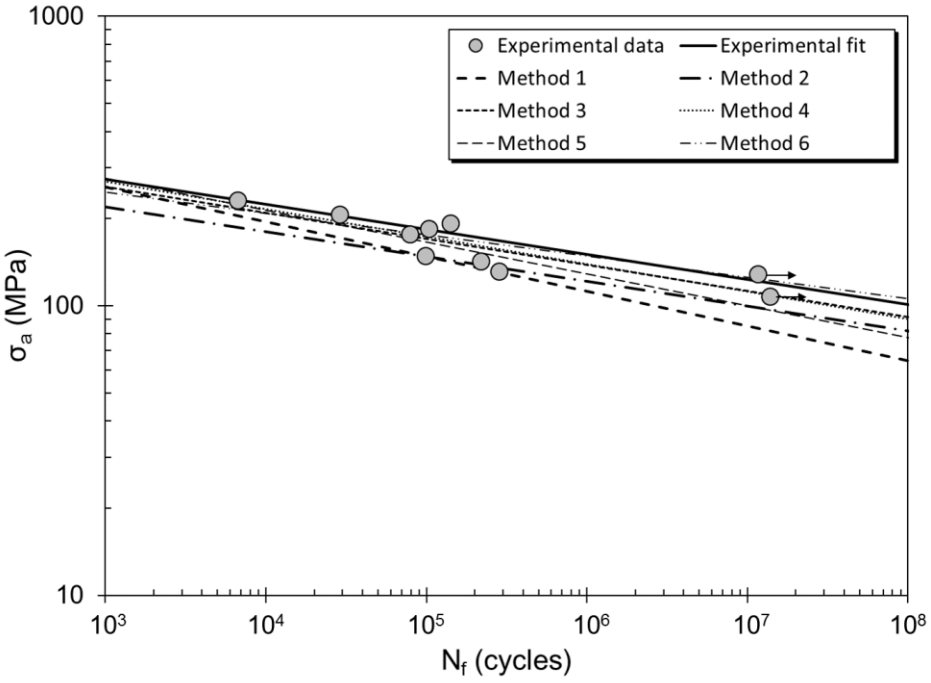
1000
100
10
σa (MPa)
10³
10⁴
10⁵
10⁶
10⁷
10⁸
Nf (cycles)
Experimental data
Experimental fit
Method 1
Method 2
Method 3
Method 4
Method 5
Method 6

(b)

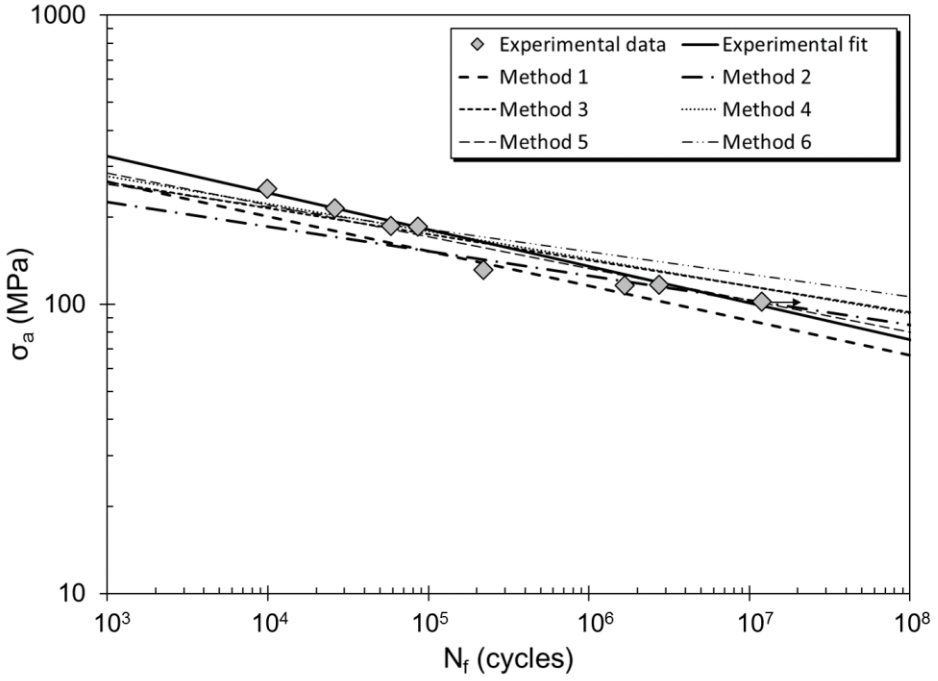

(c)

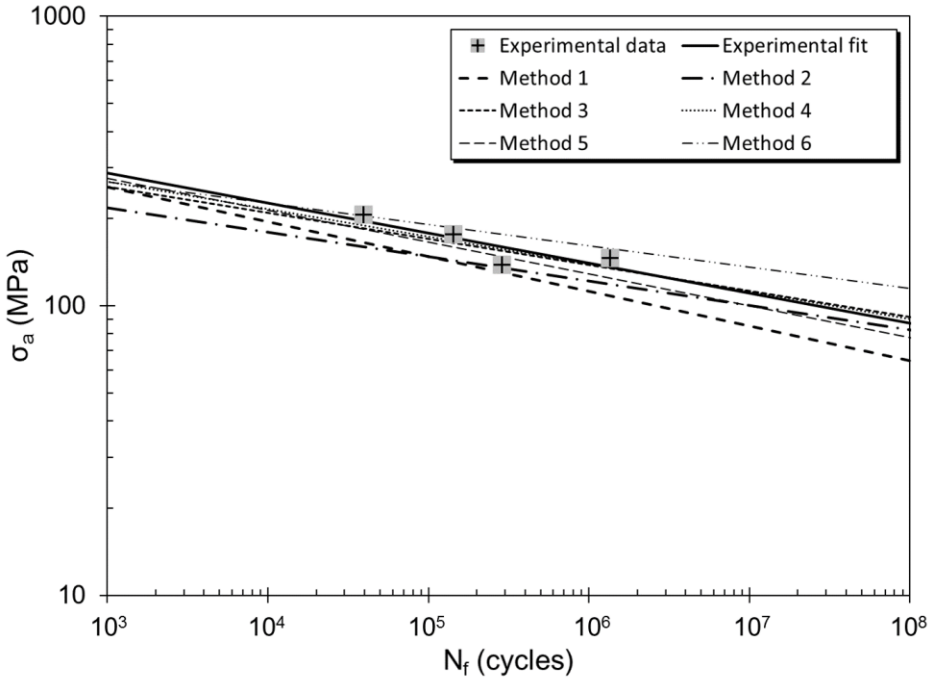

(d)

Figure 41. The application of the six methods to the four datasets by Couper *et al.*: (a) as cast, (b) 1UA & 8UA, (c) 12PA, and (d) 200OA.

The estimates presented above do not provide a clear picture about which among the six methods performs the best for cast aluminum alloys. For all five datasets, the method that provided the best fit is a different one and the only method that failed to give the best fit to any dataset is the "four points" (Method 2). The mixed success of the six methods, unfortunately, make them unreliable for estimating fatigue performance in aluminum castings.

The mixed successes of the six methods may be explained by how they were developed. The datasets most commonly available in the literature are from steels. Most steel have excellent ductility even as castings. The surface oxide films entrained during mold filling or melt preparation in the casting process usually are harmless in steels because the film is also in liquid state and much less dense than liquid steel [31]. Thus, the entrained film quickly floats to the surface, leaving clean metal behind. In aluminum alloys, however, the surface oxide film is solid and has almost the same density as liquid aluminum. Therefore, when entrained, the folded-over film, i.e., bifilm remains suspended in the liquid metal and leads to the formation of pores which are detrimental to mechanical properties, especially elongation and fatigue life. Hence, properties related to fracture are dominated by structural defects (extrinsic) whereas the microstructure seldom affects properties [31]. All six methods evaluated in this study assume that all mechanical data are intrinsic and there is no accommodation for extrinsic factors. Based on this point, it is clear that a new method is needed for estimating the fatigue performance of aluminum castings.

3.4. Development of a New Model to Predict HCF from Tensile Data

Based on the findings of Kun *et al.* [25] that the Basquin exponent, b, is a measure of structural integrity in fibers, it is hypothesized that *b* is affected by structural quality (Q_T) in aluminum alloy castings. To test this hypothesis, data for thirty-six S-N curves for cast Al-Si-Mg alloys and thirty-five S-N curves for cast Al-Si-Mg-Cu alloys were collected from the literature. These datasets came from sixteen independent studies for Al-Si-Mg alloys and fifteen for Al-Si-Mg-Cu alloys. Only studies in which round specimens were used have been included. For some S-N curves, σ_f and b reported originally in the studies have been taken directly into the analysis. However, for a majority of the S-N curves, the stress amplitude-fatigue life raw data have been harvested, reanalyzed and reinterpreted. The details of the datasets used in this section are provided in Table 14.

The Basquin exponents versus structural quality index, Q_T, for Al-Si-Mg and Al-Si-Mg-Cu alloys are presented in Figure 42. Note that b increases with Q_T and the scatter in *b* decreases with Q_T. Hence there is strong evidence in support of the hypothesis stated above that *b* is affected by structural quality, and therefore, has an extrinsic component.

To accommodate the different scatter levels in Figure 42, nominal, as well as upper limit (subscript UL) and lower limit (subscript LL) curves have been fit to the data. The equations for the nominal, upper limit and lower limit are:

$$b = -0.136 \exp(-1.236\, Q_T) \tag{39}$$

$$b_{UL} = -0.101 \exp(-1.150\, Q_T) \tag{40}$$

$$b_{LL} = -0.182 \exp(-1.370\, Q_T) \tag{41}$$

respectively.

Table 14. Summary of the gathered data from the literature.

	Alloy	Ref.	# of S-N curves	Process	Notes
Al-Si-Mg	A356	[130]	4	Sand cast	As reported
	A356	[119]	1	Low-pressure die cast	Reinterpreted
	A356	[131]	1	Low-pressure die cast	As reported
	356	[132]	3	Lost foam	Reinterpreted
	A356	[133]	1	Not specified; HIPed	Reinterpreted
	A356	[134]	4	Not specified	As reported
	A356	[135]	1	Semi-solid	Reinterpreted
	A356	[136]	1	Squeeze cast	Reinterpreted
	357	[137]	1	Semi-solid	Reinterpreted
	A356	[138]	3	Not specified	Reinterpreted
	A356	[139]	4	Investment cast, HIPed	Reinterpreted
	A357	[91]	1	Permanent mold	Reinterpreted
	A356	[140]	1	Permanent mold	Reinterpreted
	A356	[141]	3	High pressure die cast	Reinterpreted
	A356	[142]	5	Not specified; HIPed	Reinterpreted
	A356	[143]	2	High-pressure die cast	As reported
Al-Si-Mg-Cu	Al-7Si-1Cu-0.5Mg	[144]	1	Permanent mold	Reinterpreted
	Al-7Si-1Cu-0.5Mg	[145]	1	Permanent mold	Reinterpreted
	Al-7Si-1Cu-0.5Mg	[146]	3	Not specified	As reported
	C354	[147]	2	Not specified; HIPed	Reinterpreted
	Modified 319	[137]	1	Semi-solid	Reinterpreted
	A319	[148]	1	Not specified	Reinterpreted
	319	[38]	1	Not specified	Reinterpreted
	A319	[149]	2	Not specified	As reported
	W319	[94]	5	Sand casting	Reinterpreted
	319	[96, 97]	7	Not specified	Reinterpreted
	319	[150]	3	Not specified	Reinterpreted
	Al-10Si-2Cu-0.3Mg	[151]	1	Sand casting	Reinterpreted
	333	[152]	1	Not specified	As reported
	Al-7Si-3Cu-0.4Mg	[153]	6	Not specified	Reinterpreted

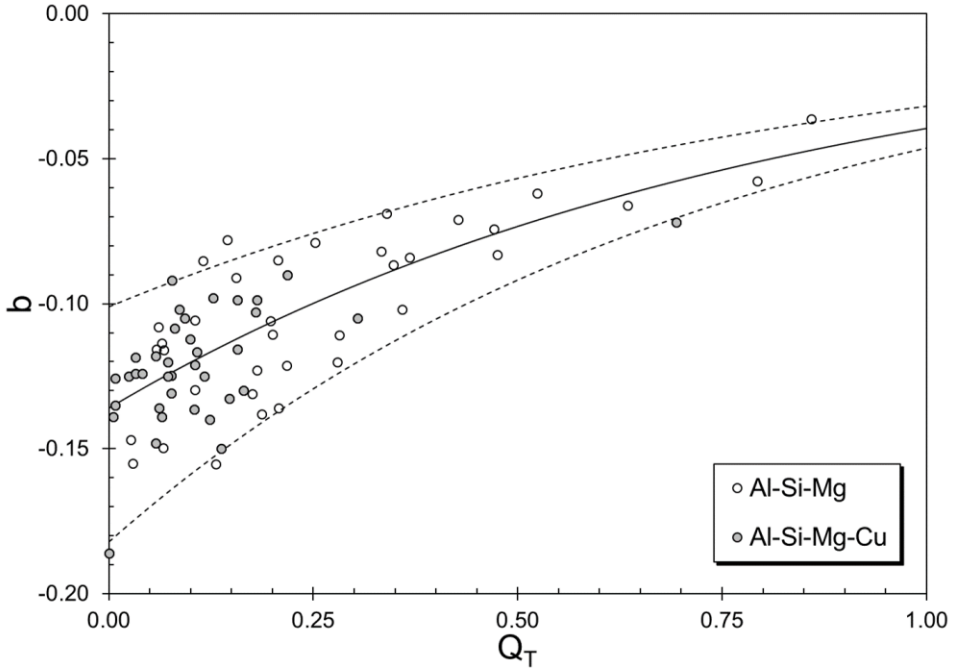

Figure 42. Correlation between quality index and the Basquin exponent.

For each S-N curve analyzed in this study, fatigue strength at 10^6 cycles was determined. The change in σ_f with Q_T is presented in Figure 43, which shows significant scatter around the best fit line. Because fatigue strength is known to be strongly affected by strength [23, 71, 72], how the fatigue strength-to-tensile strength ratio changes with Q_T was analyzed. The results are presented in Figure 44. Although scatter around the best fit line is less than in Figure 43, significant scatter remains.

By definition, ultimate tensile strength is the point on the tensile engineering stress-strain curve where the reduction in area with deformation can no longer be supported by the increase in strength due to work hardening, causing plastic instability. Alternatively, it is the point where Considere criterion is met such that true stress is equal to work hardening rate. In aluminum castings, however, fracture usually takes place before Considere

criterion is met because of major structural defects [56, 154]. Consequently, elongation and tensile strength are determined from the same point on the stress-strain curve. Only in high quality castings, (Q_T>0.70), there is some necking and non-uniform deformation [70]. Because tensile strength is also affected by structural quality, the ratio of fatigue strength-to-maximum tensile strength was used. Maximum tensile strength for each data point was estimated by using Equation (13). Results are presented in Figure 45. The scatter is much reduced compared to Figure 44. The best fit line in Figure 45 is:

$$\frac{\sigma_f}{S_{T(max)}} = 0.405Q_T+0.280 \qquad (42)$$

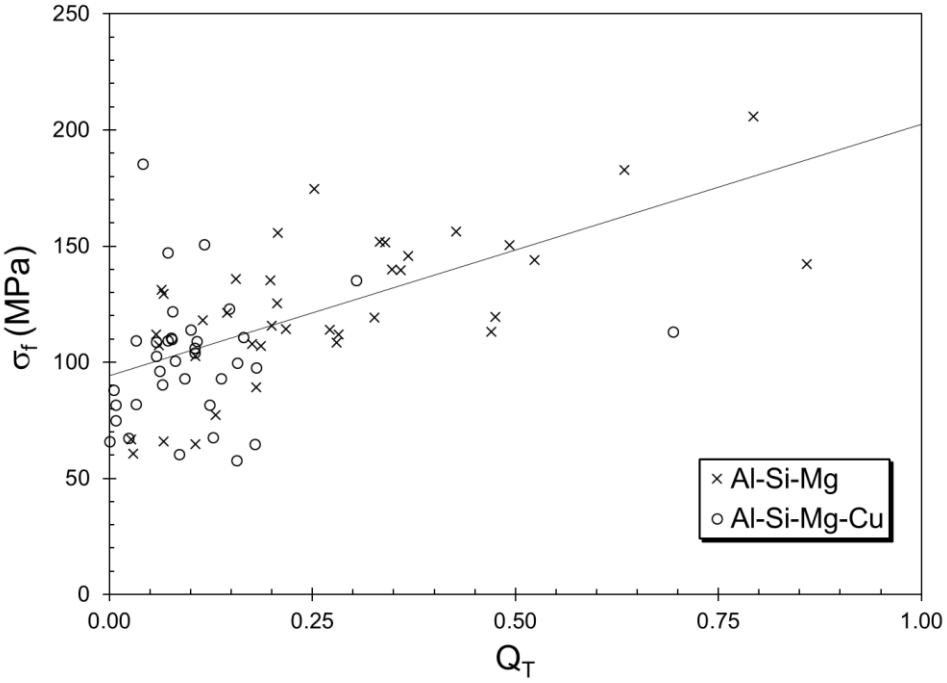

Figure 43. Change in σ_f with Q_T.

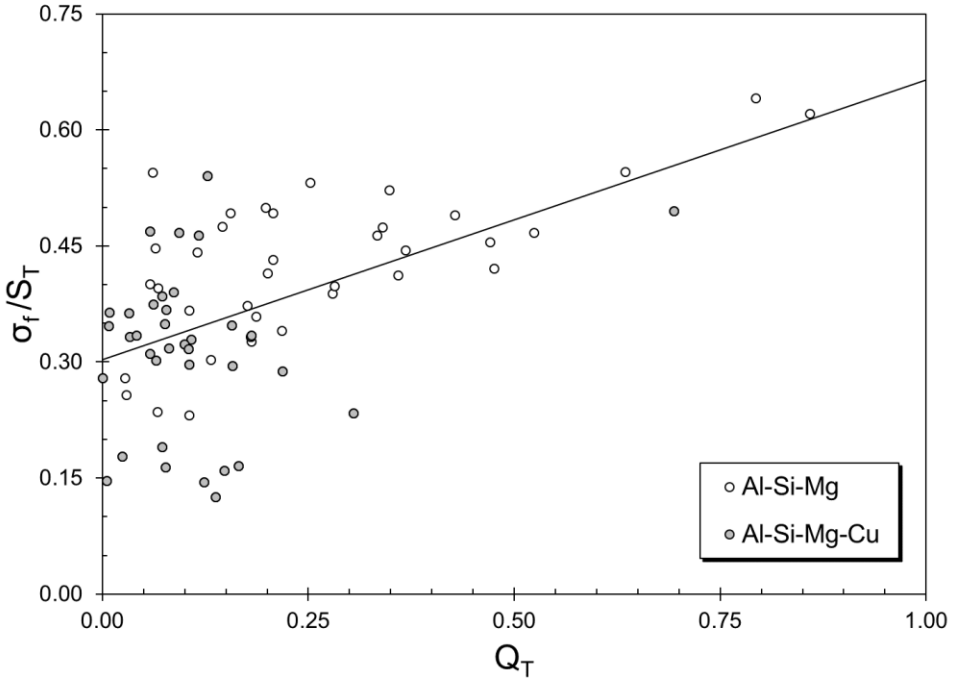

Figure 44. Correlation between Q_T and ratio of fatigue strength to tensile strength.

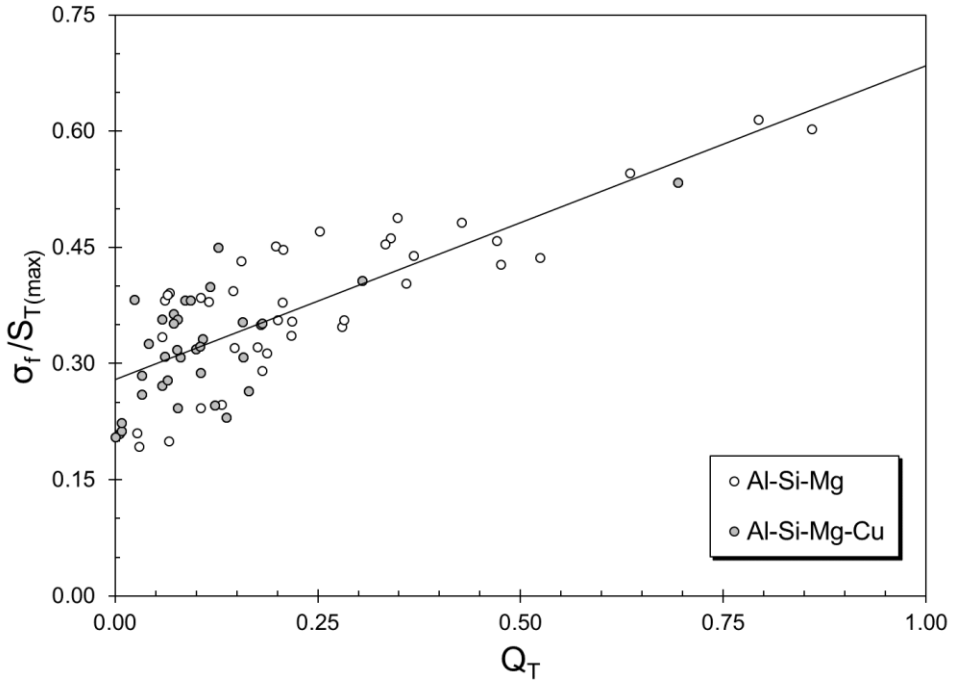

Figure 45. Correlation between quality index and ratio of fatigue strength to maximum tensile strength.

The correlation between Basquin exponent and fatigue strength-to-maximum tensile strength is presented in Figure 45. The scatter is more uniform around the best fit line, which has the form:

$$\frac{\sigma_f}{S_{T(max)}} = 2.977b+0.696 \quad (43)$$

Equations (39) to (41) can be used to estimate the Basquin exponent (and if needed upper and lower limits. Subsequently, Equation (42) or (43) can be used to estimate $\sigma_f / S_{T(max)}$ ratio. By using Equation (13), $S_{T(max)}$ can be found, which leads to the estimate of first σ_f, and finally σ'_f.

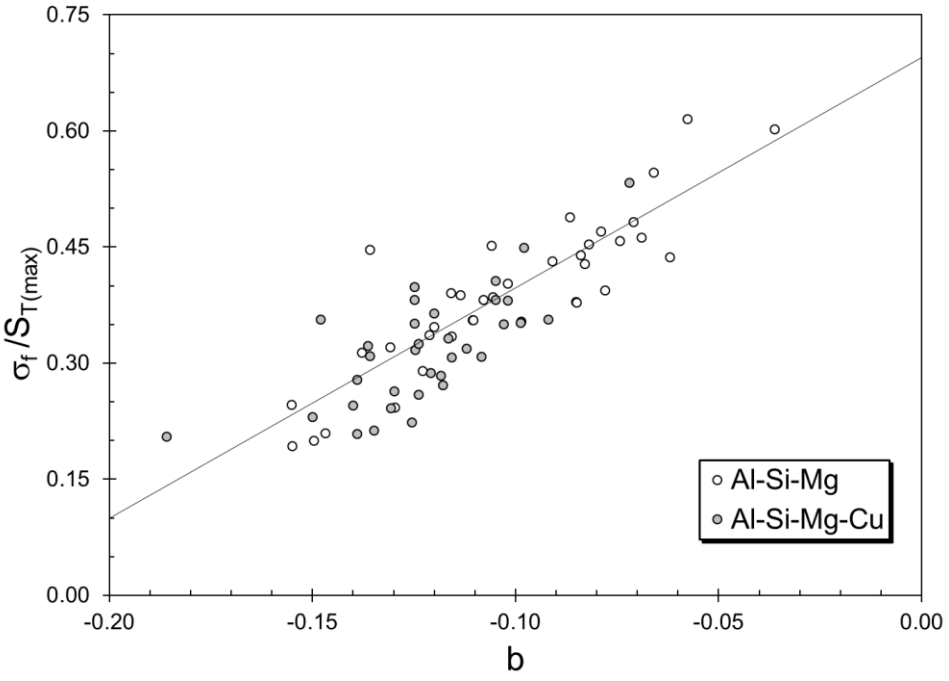

Figure 46. Correlation between Basquin exponent and ratio of fatigue strength to maximum tensile strength.

The application of the model proposed above is first demonstrated on the data by Zhu (E319-T7) and then applied to the four datasets by Couper *et al*.

Step 1: Find Q_T

By using the yield strength and elongation data in Table 11, Q_T is found as:

$$Q_T = \frac{e_F}{e_{F(max)}} = \frac{e_F}{\beta_0 - \beta_1 \sigma_Y}$$

$$Q_T = \frac{2.0}{36.0 - 0.064(199)} = 0.086$$

Step 2: Find b

$$b = -0.136 \exp(-1.236\, Q_T)$$

$$b = -0.136\, exp\left(-1.236(0.086)\right) = -0.122$$

Step 3: Find $\sigma_f / S_{T(max)}$

$$\frac{\sigma_f}{S_{T(max)}} = 0.405 Q_T + 0.280$$

$$\frac{\sigma_f}{S_{T(max)}} = 0.405(0.086) + 0.280 = 0.314$$

Step 4: Find $S_{T(max)}$

$$S_{T(max)} = 185.7 + 0.558 \sigma_Y$$

$$S_{T(max)} = 185.7 + 0.558(199) = 296.7 \text{ MPa}$$

Step 5: Find σ_f

$$\sigma_f = 0.314(296.7) = 93.3 \text{ MPa}$$

Step 6: Find σ'_f

$$\sigma_f' = \frac{93.3}{(10^6)^{-0.122}} = 505.4 \text{ MPa}$$

The estimated S-N curve for the data by Zhu is presented in Figure 47. It is clear that the new model provides an excellent estimate of the HCF behavior for E319-T7 castings by Zhu. The R^2 for this estimate is 0.828 which is higher than that of the only reliable estimate obtained from the six methods (0.640) in section 3.3.

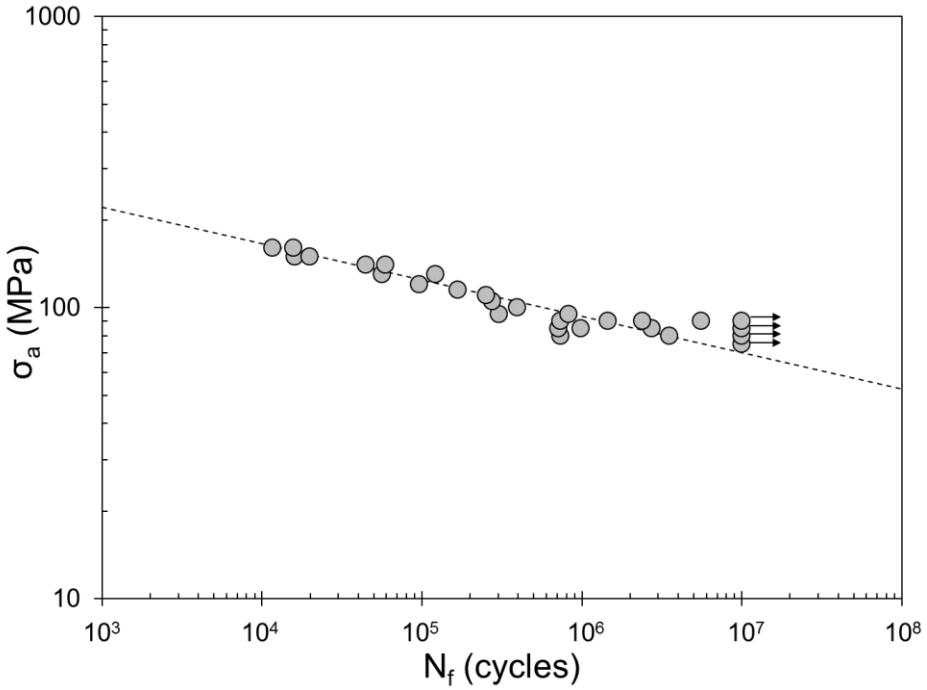

Figure 47. Trend lines of the dataset from Zhu [98].

The new method has also been applied to the four datasets by Couper *et al*. The estimates for each dataset, based on the step-by-step procedure given above, are presented in Table 15, in which R^2 values for each estimate is also provided. The estimated S-N curves are

presented in Figure 48 and Figure 49. Note that the new method provides respectable fits to almost all datasets by Couper *et al*. When compared with the R^2 values given in Table 13 for the six methods, the new method outperforms Methods 1-5 based on the goodness of fits of the estimates. Because none of the estimates of the new method for the five datasets yielded a negative R^2, it can be claimed that the new method is superior to all six.

Table 15. Estimates obtained by the new method to the five datasets.

Dataset	Q_T	$\sigma_f/S_{T(max)}$	$S_{T(max)}$ (MPa)	(MPa)	$\sigma_f^{'}$ (MPa)	b	R^2
E319-T7	0.086	0.314	296.7	93.3	505.4	-0.122	0.828
As Cast	0.459	0.466	252.7	117.6	341.4	-0.077	0.079
1UA&8UA	0.411	0.446	308.5	137.6	426.4	-0.082	0.755
12PA	0.400	0.442	325.2	143.6	451.9	-0.083	0.803
200OA	0.319	0.409	308.5	117.7	447.5	-0.092	0.063

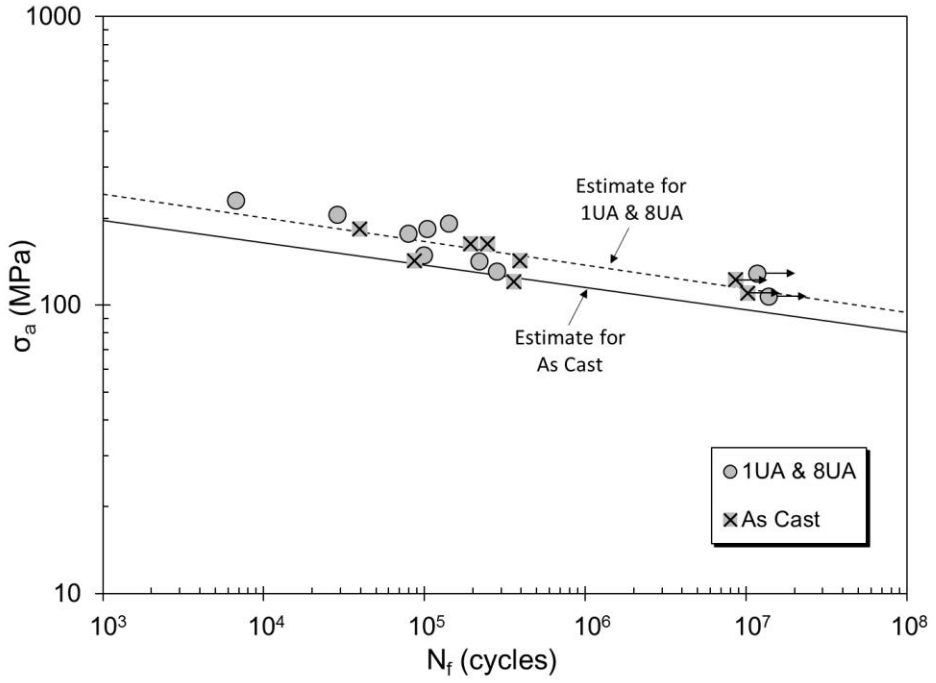

Figure 48. Estimated S-N curves for the As Cast and 1UA & 8UA datasets from Couper *et al*. [129].

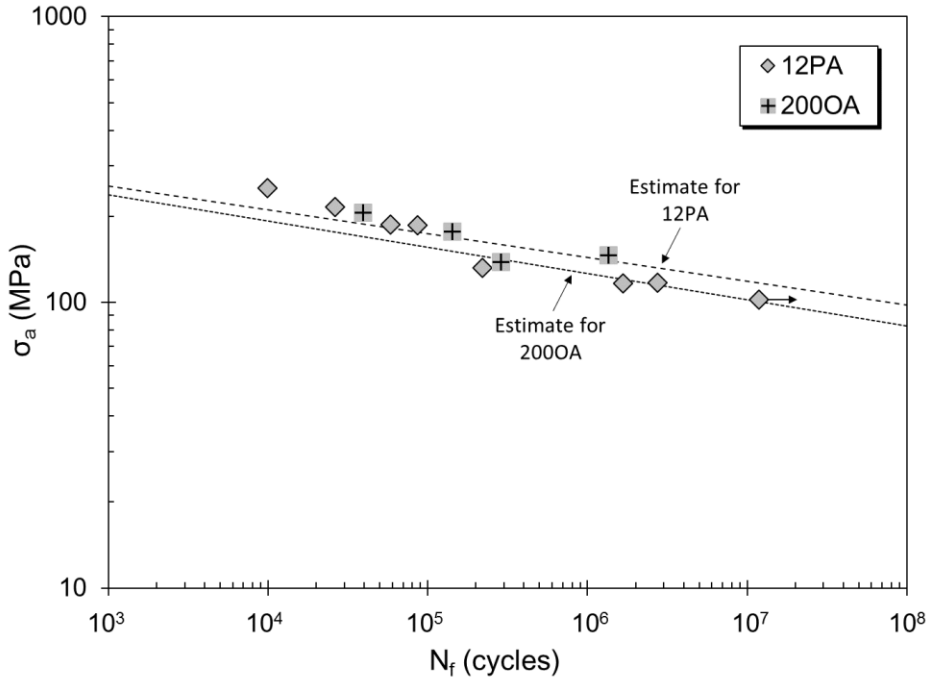

Figure 49. Estimated S-N curves for the 12PA and 200OA datasets from Couper *et al*. [129].

Based on the analysis of data from the literature and interpretation of results, structural quality has a significant effect on several aspects of fatigue performance in cast aluminum alloys, such as the effect of mean stress, reliability of estimates of HCF behavior from tensile data. Based on these findings, experiments were conducted to test some of these findings with in-house data and also determine whether axial HCF performance can be estimated from rotating beam (bending) fatigue data.

4. Experimental Details

4.1. Material

The specimens were excised from an A356 aluminum wheel hub that is commercially available. Typical chemical composition of the A356 alloy is given in Table 16.

Table 16. Chemical composition (wt.%) of A356.

Si	Mg	Fe	Ti	Cu	Sr	Al
7.10	0.33	0.10	0.12	0.006	0.021	Balance

Heat treatment of A356 involves a solution treatment of 8 hours at 540^{o}C, quenching in cold water, natural aging at room temperature for 24 hours, followed by artificial aging of 8 hours at 170^{o}C.

4.1. Mechanical Testing

Five tensile tests were run based on ASTM E8 standard. Tensile specimens had an initial diameter of 8.9 mm and a gage length of 32 mm. Twelve uniaxial fatigue tests were conducted at R=-1 at various alternating stress level on specimens with a diameter of 6.3 mm based on ASTM-E466-15 standard. Tests were stopped after 3×10^{6} cycles. Twelve rotating beam fatigue tests were run using four-point loading machine at various maximum stress levels on specimens with a diameter of 4.8 mm. Rotating beam specimens were machined according to ISO 1143. All mechanical tests were conducted at Westmoreland Mechanical Testing and Research, Inc., Youngstown, PA.

4.2 Fractography

The fracture surfaces of three specimens, one tensile, one uniaxial fatigue and one rotating beam fatigue, were analyzed via scanning electron microscopy. Before fractography, all specimens were cleaned ultrasonically in a methanol solution. Fractographic analysis was conducted at University of Florida, MAIC.

5. Results and Discussion

Results of the tensile tests results are listed in Table 17. Note that elongation values, which typically have the highest scatter among the three tensile properties, are very consistent.

Table 17. Experimental Tensile data for A356 Aluminum Alloy.

σ_y (MPa)	S_T (MPa)	e_F (%)
208.1	243.2	2.9
202.6	230.1	2.1
201.2	235.6	2.1
196.4	226.0	2.1
200.5	228.8	2.1

The data collected in axial fatigue tests are provided in Table 18. There is only one run-out in the dataset.

The results of the rotating beam fatigue tests are presented in Table 19. There is no run-out in the rotating beam fatigue dataset.

The results for axial and rotating beam fatigue tests are shown together in Figure 50. As in Figure 5, results from the rotating beam fatigue tests are higher than those from the axial fatigue for a given alternating stress level. The best fits to the data in Figure 50 were obtained by σ'_f = 491.4 MPa, b = -0.141 for axial, and σ'_f = 1764.6 MPa, b = -0.208 for rotating beam.

Table 18. Experimental Uniaxial Fatigue test data for A356 Aluminum Alloy.

σ_a (MPa)	N_f (cycles)	Status
150	10,120	Failed
135	6,244	Failed
125	45,692	Failed
117	31,662	Failed
110	85,740	Failed
105	125,091	Failed
100	162,875	Failed
90	175,437	Failed
82	467,204	Failed
75	535,990	Failed
60	1,475,511	Failed
52	3,000,000	Run-out

Table 19. Experimental Rotating-bending Fatigue data for A356 Aluminum Alloy.

σ_a (MPa)	N_f (cycles)	Status
220	16,525	Failed
193	35,255	Failed
179	69,186	Failed
165	144,507	Failed
138	390,362	Failed
119	699,383	Failed
109	693,140	Failed
109	813,448	Failed
86	2,984,236	Failed
80	2,554,237	Failed
70	1,006,665	Failed

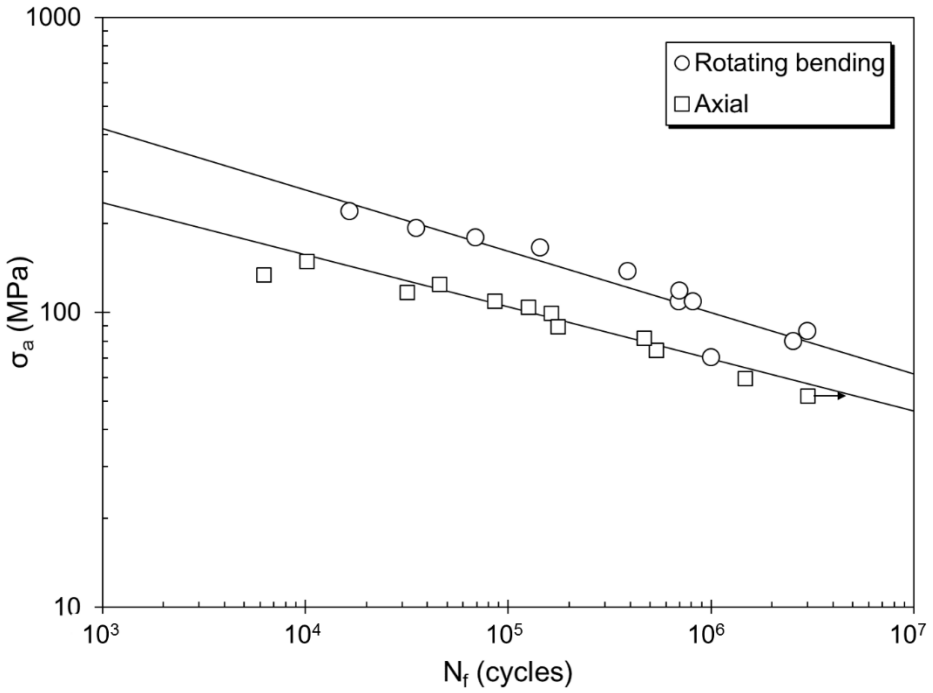

Figure 50. Rotating beam and uniaxial fatigue data for A356 aluminum castings.

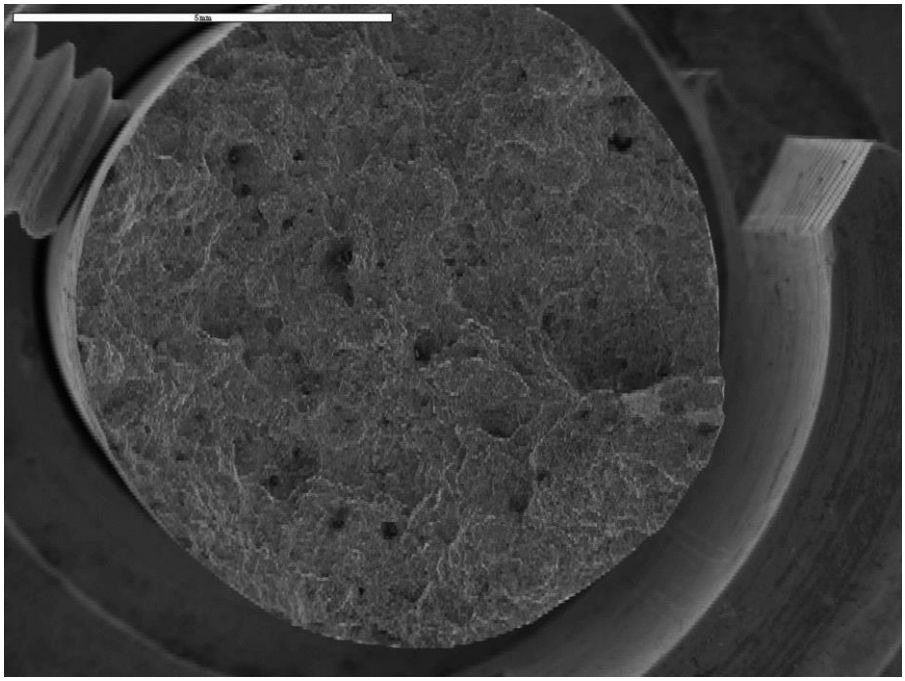

Figure 51. Overall view of the fracture surface of A356 alloy tensile specimen.

Fracture surface of tensile specimen of A356 alloy is presented in Figure 51. Several structural defects are visible across the specimen. A closer view is presented in Figure 52. Pores with dendrite arms are visible on the fracture surface. Note that the shape of the exposed pore is tortuous and has a morphology similar to the pore presented in Figure 15.

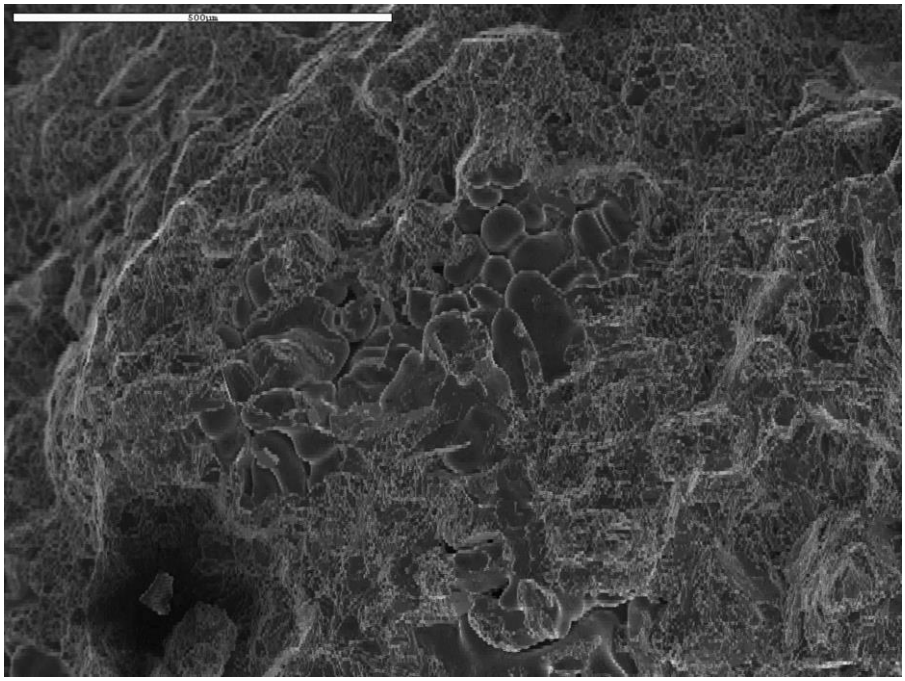

Figure 52. Pores exposed on the fracture surface of the tensile specimen.

Fracture surface of a uniaxial A356 fatigue specimen tested at a stress level of 60 MPa (N_f =1,475,511 cycles) is presented in Figure 53. The overall fracture surface has several visible structural defects. However, the fatigue crack seems to have initiated from a pore on or just below the specimen surface, as indicated with an arrow.

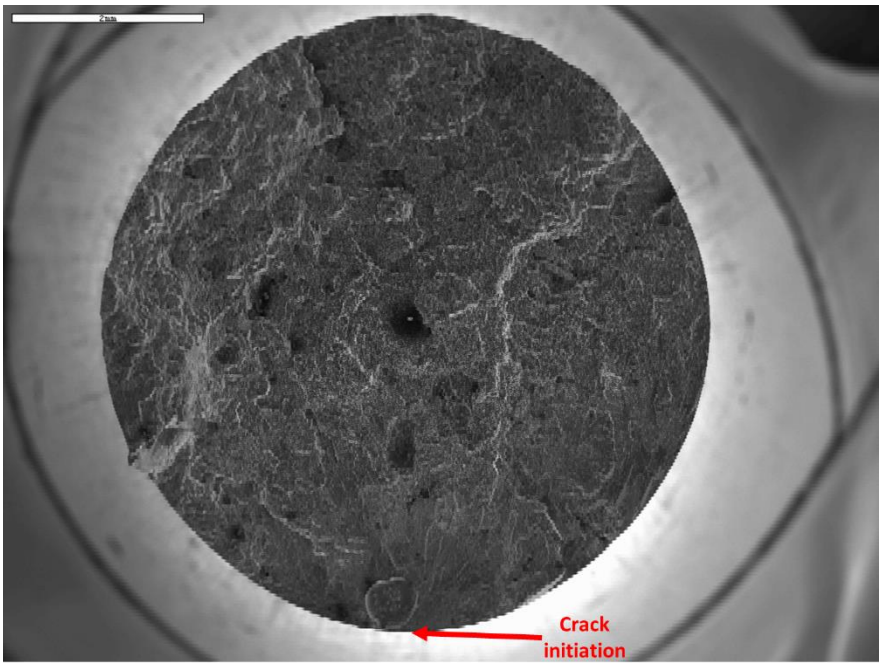

Figure 53. Overall view of the fracture surface of A356 alloy uniaxial specimen.

A closer view of the fatigue crack initiator shown in Figure 53 is provided in Figure 54. As opposed to the pores shown in Figure 8 and Figure 15 with a tortuous shape, this pore is almost perfectly round, which is either due to the high level of dissolved hydrogen in the aluminum melt, making the pore round when hydrogen is rejected by the solidifying aluminum, or the pore is a bubble entrained into the casting during the filling stage [31]. It is the opinion of the author that the pore is a bubble.

The striae showing fatigue crack propagation around the pore are visible in Figure 55. The area for final rupture shows signs of high ductility, as shown in Figure 56.

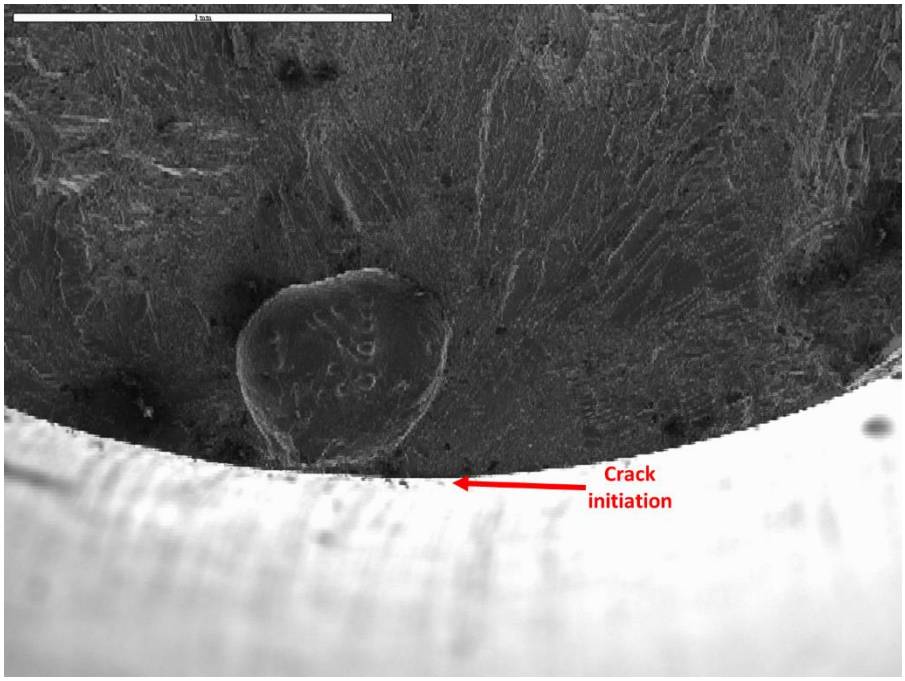

Figure 54. Close-up look at the fatigue initiating pore right below the specimen surface in uniaxial fatigue specimen.

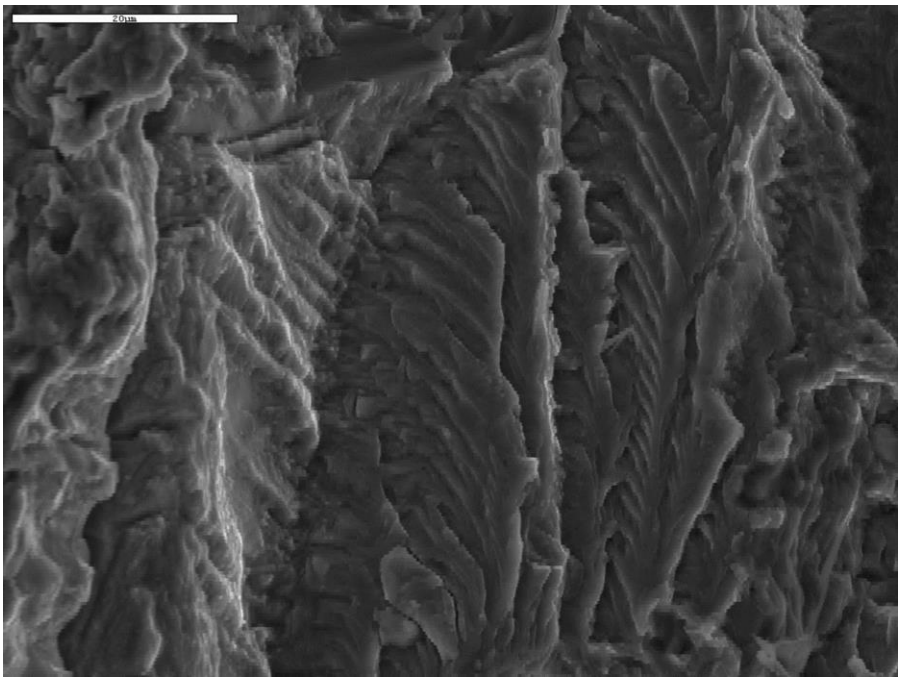

Figure 55. SEM micrograph indicating the fatigue striae of A356 alloy specimen.

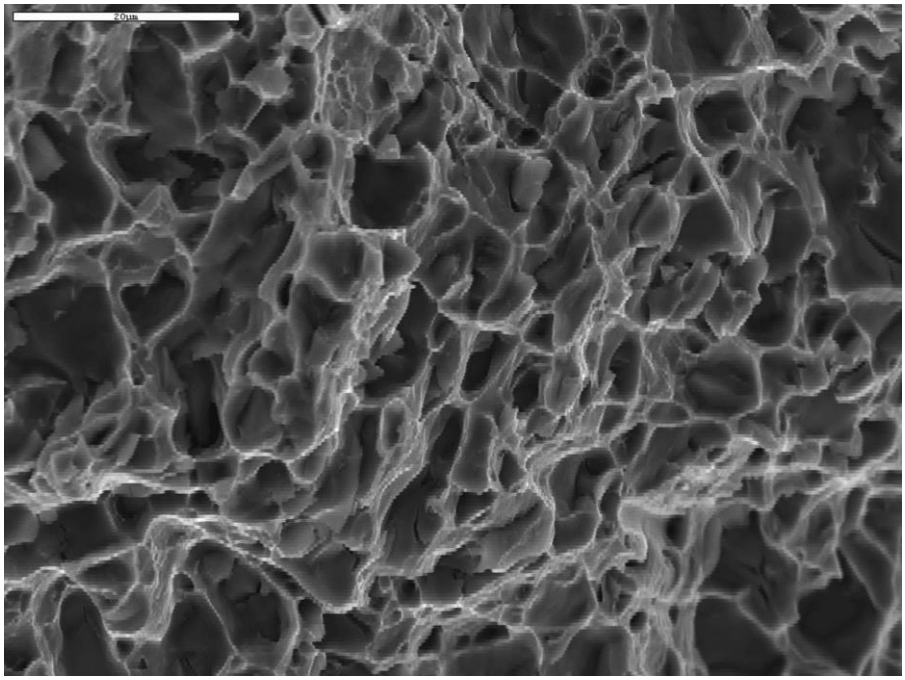

Figure 56. SEM fractograph indicating the ductile fracture for the remaining parts of A356 alloy uniaxial specimen.

Fracture surface of a rotating bending A356 fatigue specimen tested at a stress level of 70 MPa (N_f =1,006,665 cycles) is presented in Figure 57. The overall fracture surface has several visible structural defects.

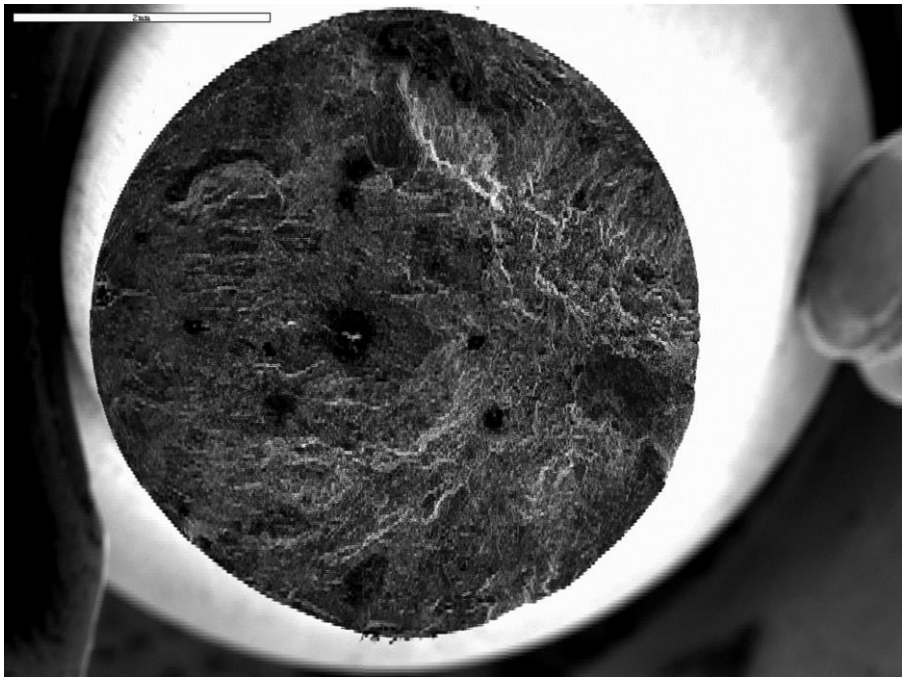

Figure 57. Overall view of the fracture surface of A356 rotating bending alloy specimen.

Unlike in uniaxial fatigue test, fatigue cracks initiated and propagated simultaneously at different sites in the specimen. Similar results were reported for ablated 6061 aluminum alloy casting [155]. A closer view of one of the fatigue crack initiator is given in Figure 56. As it was in uniaxial type specimen, the pore is located on the surface. The beach marks around the pore are also visible in Figure 56 and proof that remaining parts showed ductile failure in Figure 57.

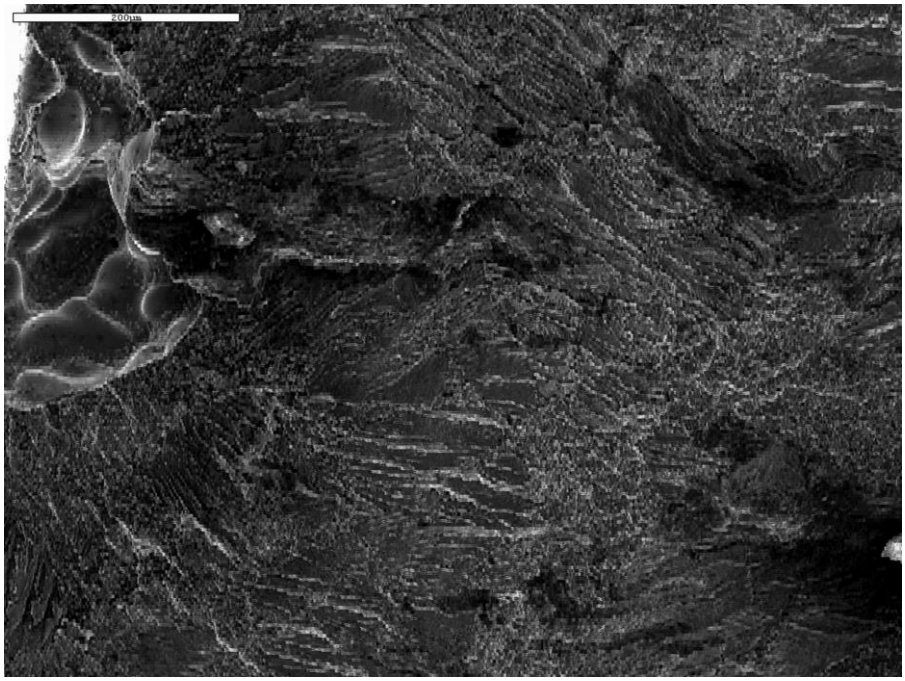

Figure 58. Close-up look at the fatigue initiating pore right below the specimen surface in rotating bending fatigue specimen.

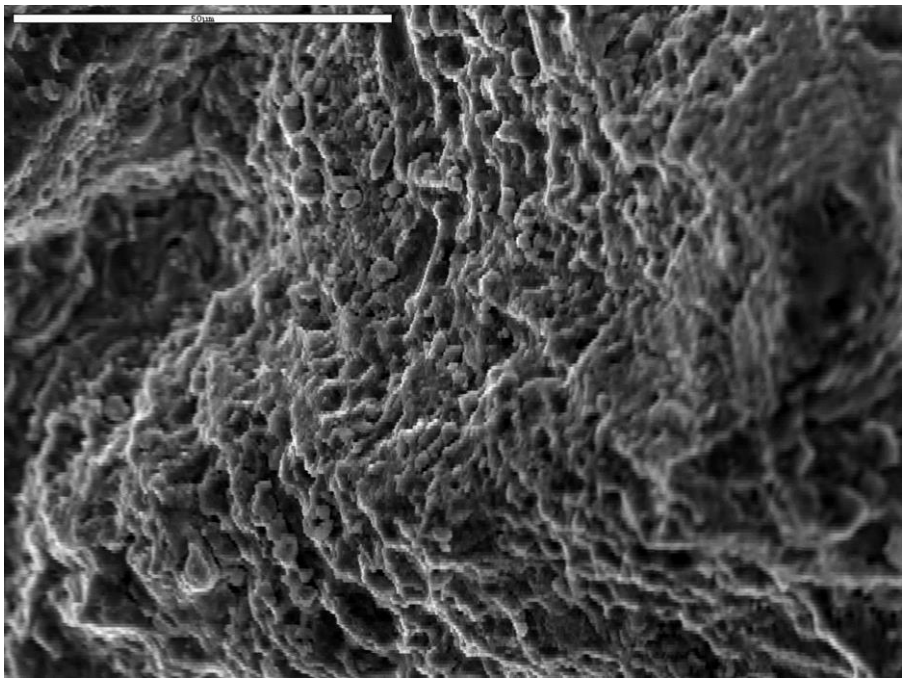

Figure 59. SEM fractography indicating the ductile fracture for the remaining parts of A356 alloy rotating bending specimen.

The six methods of estimating HCF behavior from tensile data presented in section 2.9 were tested on the axial fatigue data. The Basquin parameters estimated by the six methods are listed in Table 20 and the estimates are presented in Figure 60. It is clear that none of the six methods perform well enough to estimate the S-N curve for A356 aluminum hub castings. The closest line among the six methods is Method 1 but the R^2 was still found to be less than 0 for methods 3,4,5 and 6.

Table 20. Basquin parameter estimates by the six methods.

Parameter	Best fit	Method 1	Method 2	Method 3	Method 4	Method 5	Method 6
σ_f'	491.4	442.2	281.2	383.5	388.7	442.2	328.8
b	-0.141	-0.120	-0.081	-0.090	-0.095	-0.110	-0.073
R^2	0.910	**0.668**	0.472	< 0	< 0	< 0	< 0

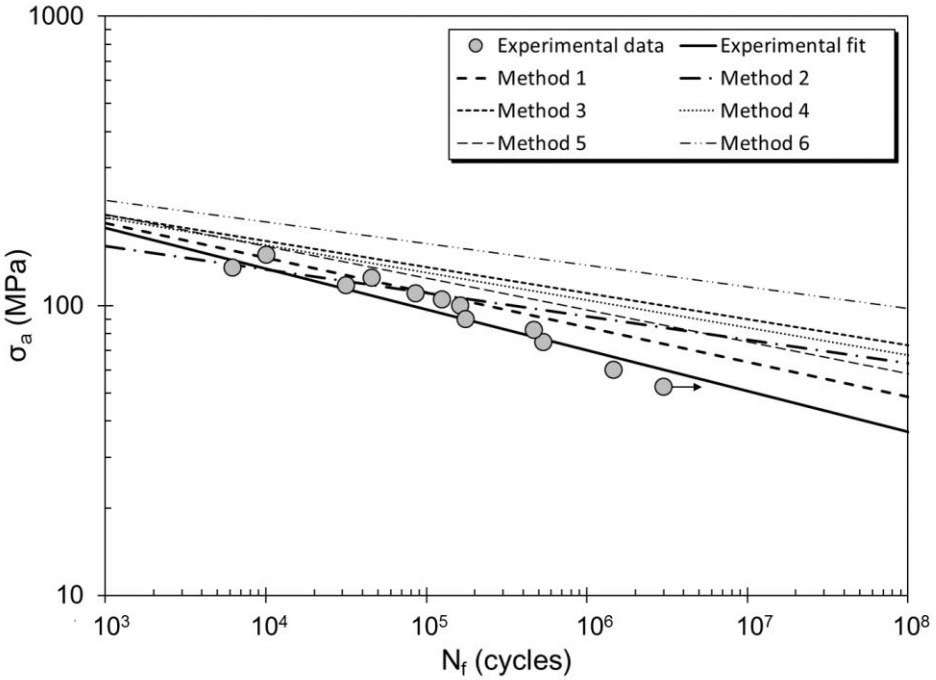

Figure 60. Estimated S-N curves by using the six methods for A356 alloy.

The method developed in this study was also tested. Because of its low elongation, the structural quality of the casting is less than 0.10. As a result, the scatter in estimated *b* is high at that level of structural quality, Figure 42. For that reason, upper and lower estimates were also determined. The results are summarized in Table 21. For each estimated Basquin exponent, a separate $\sigma_f / S_{T(max)}$ was found by using Equation (43) and Figure 46.

Table 21. Estimates for HCF of the A356 Aluminum Alloy.

Estimate	Q_T	b	$\sigma_f/S_{T(max)}$	$S_{T(max)}$ (MPa)	σ_f' (MPa)
Nominal	0.098	-0.120	0.330	298.3	519.4
Upper		-0.090	0.418		433.6
Lower		-0.159	0.217		582.6

The three fits are presented in Figure 61. The nominal and upper limit estimates by the new method overestimate the fatigue performance. The lower limit estimate however accurately describes the fatigue performance. The R^2 for the lower limit is 0.882.

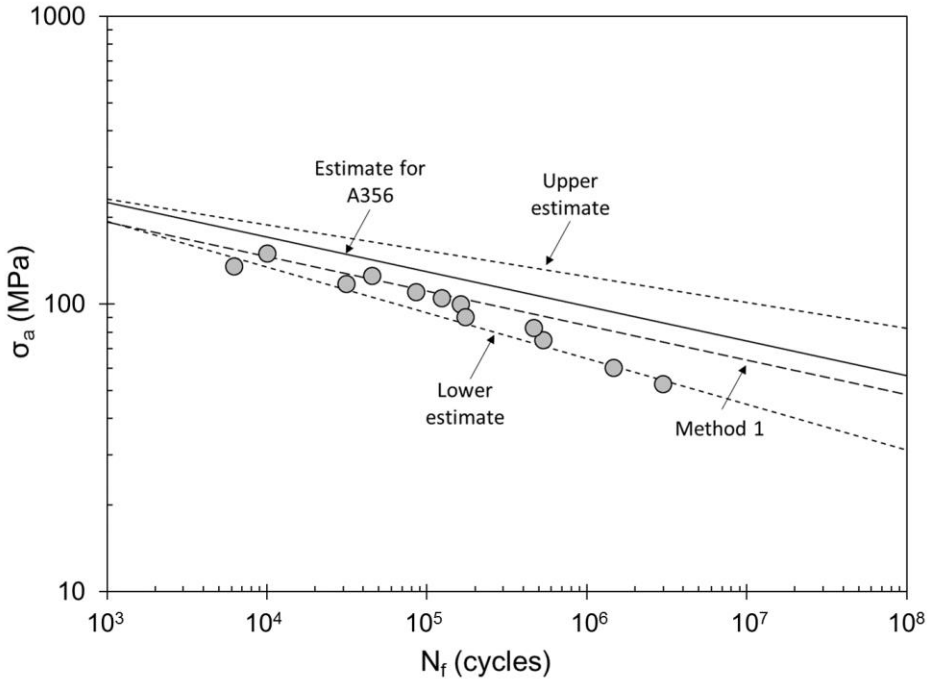

Figure 61. The three estimates made by the new method along with method 1 for A356 alloy wheels.

Finally, the effectiveness of the three methods to estimate axial fatigue performance from rotating beam fatigue data, outlined in section 2.10, were evaluated. The results are presented in Figure 62. The simple method of multiplying maximum stress in rotating beam fatigue testing by 0.59 surprisingly provides a respectable fit, as can be seen in Figure 62.a. Because this method was based on observations made on fatigue strengths of steels, it is not clear at this point whether the fit is due to a fundamental relationship or by chance.

The method proposed by Manson and Muralidharan (Figure 62.b) overestimates the fatigue performance of A356 alloy wheels. This result is not surprising because Manson and Muralidharan stated in their paper that their model provides better fits in the plastic (low cycle) region.

The method developed by Esin based on micro strains (Figure 62.c) also provided a very respectable estimate of the axial fatigue performance. Because Esin's model requires an endurance limit which is not visible in aluminum alloys, the alternating stress level corresponding to a fatigue life of 10^8 was taken as the endurance limit, which is consistent with the results of Yi et al. [156] for 319 aluminum alloy castings. Based on these results, the method proposed by Esin is recommended for estimating axial S-N curves at R=-1 from rotating beam fatigue data.

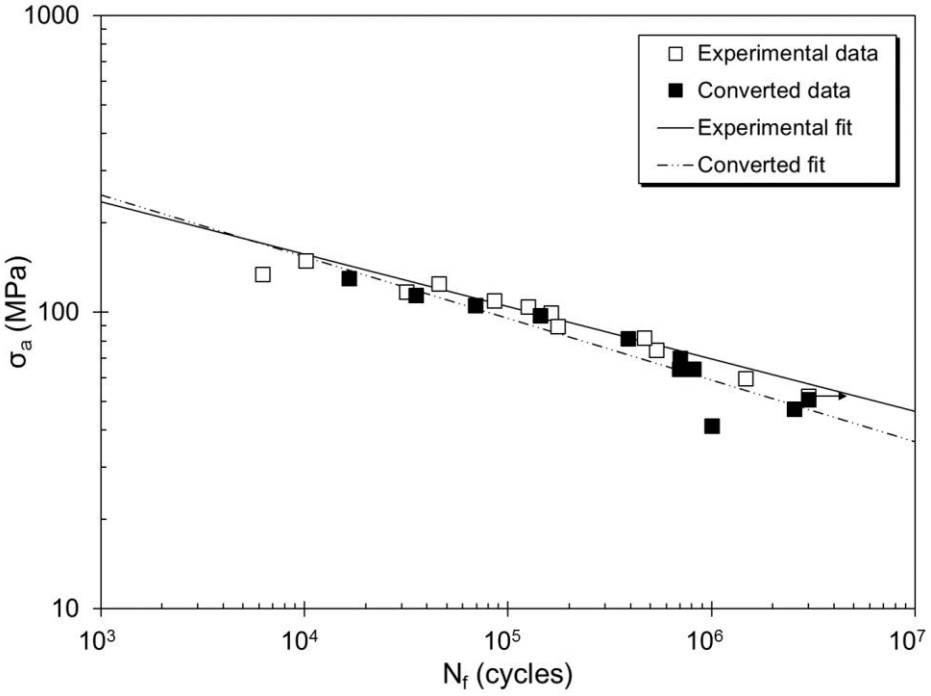

(a)

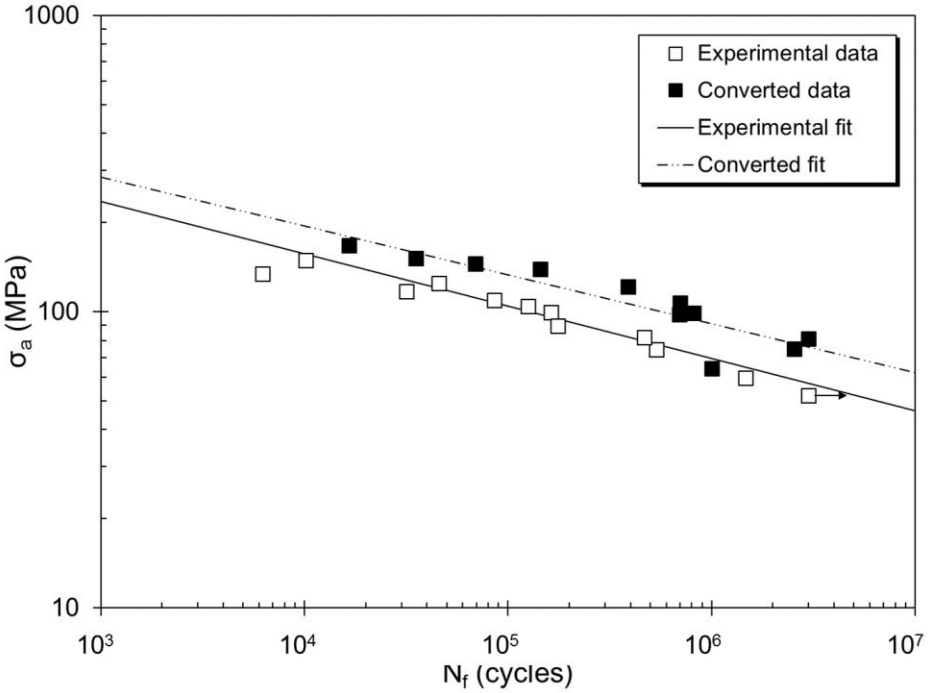

(b)

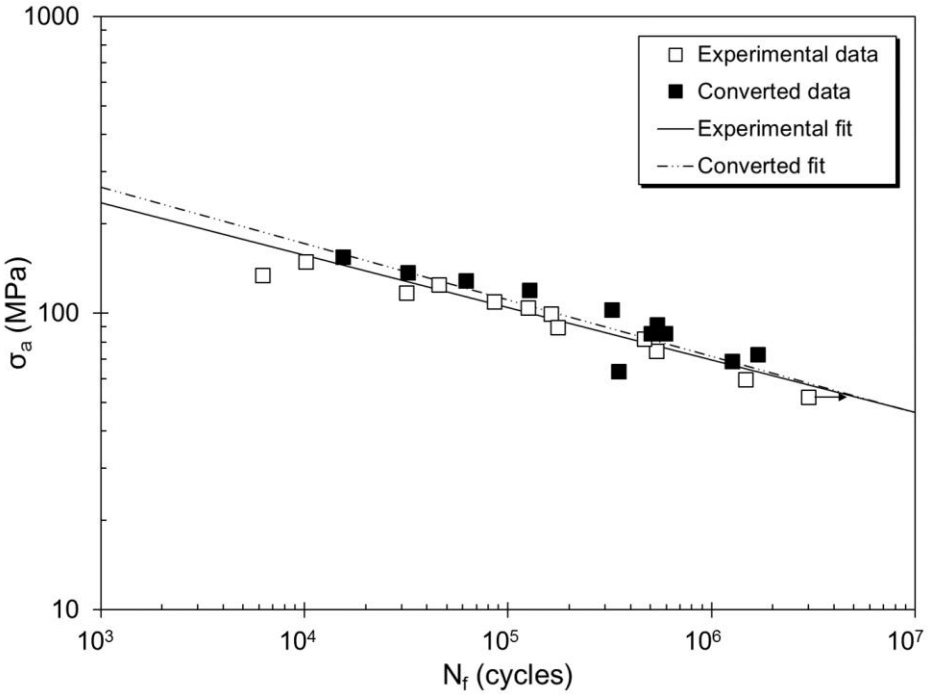

(c)

Figure 62. Uniaxial HCF performance estimated from rotating beam fatigue tests by using the methods by (a) Sors, (b) Manson and Muralidharan, and (c) Esin.

6. Conclusions

Following conclusions have been reached for research questions presented in section 2.12.

Question 1: *How well do selected mean stress correction equations perform in cast aluminum alloys, especially in datasets with various levels of structural quality? Is the Walker parameter a function of structural quality?*

- A new procedure to correct for mean stress in fatigue testing that can accommodate the run-outs in fatigue datasets while calculating Basquin parameters and estimating Weibull parameters has been developed.
- It is recommended that the Weibull probability plots for N_{eq} be developed for verifying the mean stress correction model of choice.
- The Walker correction method provided the best fits to the Basquin law. However, the Walker parameter is strongly affected by the structural quality of the aluminum castings. An empirical relationship between the Walker parameter and the quality index, Q_T was developed in this study.
- The Weibull distribution for N_{eq} was found to affect by the selection of the mean stress correction method to a great extent.

Question 2: *Is there more evidence for Q_T-N_f relationship from the aerospace and automotive castings literature?*

- A comprehensive approach that incorporates the inclusion of runouts in estimating Basquin and Weibull parameters, mean stress correction and volumetric correction for different specimen sizes was developed and applied to four independent datasets. Results have shown that there is consistency between the data included in this study in

terms of the relationship between structural quality as measured in tensile tests and fatigue life.

- The quality index, Q_T, can be used to characterize the structural integrity of 319, D357 and B201 type cast aluminum alloys from tensile tests. A strong relationship has been found between the expected Q_T and fatigue life of 319, D357 and B201 aluminum alloy castings.
- The Q_T-N_f relationship for 319 is quite different from that of B201 and D357 due to the different specimen geometries used.
- The fatigue life expectancy of 319 alloy at R=-1, σ_a=100 MPa and at Q_T=1.0, i.e., defect-free casting, is at least 2.2×10^{14} which, in practice, can be considered infinite fatigue life.
- Probability plots for both Q_T and N_f distributions for B201 showed strong indications of Weibull mixtures, providing yet another proof that the two properties are linked to each other.
- There is a strong negative correlation between the proportion of Q_T in Region 1 and probability of survival for 10^5 cycles. Similarly, a strong positive correlation exists between the proportion of Q_T in Region 3 and probability of survival for 10^5 cycles, providing further evidence for the strong link between elongation and fatigue performance.
- It is significant that B201 and D357 specimens followed the same Q_T-N_f relationship, despite different microstructures. This finding provides further proof that fatigue behavior in cast aluminum alloys is determined by the size and location of defects, and not by the microstructure.

- The statement by Tiryakioğlu that the elongation requirement in industrial specifications is a *de facto* fatigue life specification is justified.

Question 3: *How do methods to estimate high cycle fatigue perform with aluminum castings? If they do not perform well, can a new model for aluminum castings be developed?*

- Among all six methods available in the literature to predict S-N curves from tensile properties, none of them provided reliable estimates for five datasets from two independent studies including E319 and A356 alloy castings. This is attributed to the effect of structural defects on fatigue properties which made it impossible for the six methods built on intrinsic tensile and fatigue behavior.
- A new method to estimate Basquin parameters as a function of Q_T has been developed. By using this method, the fatigue life of a sand-cast A356 alloy casting as well as the five datasets could be estimated accurately.
- Ratio of fatigue strength at 10^6 cycles to tensile strength resulted in lower coefficient of determination value than ratio of fatigue strength at 10^6 cycles to defect-free tensile strength.
- Strong correlation observed between elastic exponent and the ratio of fatigue strength at 10^6 cycles to defect-free tensile strength.

Question 4: *What is the fatigue performance of an A356-T6 casting in rotating beam and axial fatigue testing? Can axial fatigue be predicted from rotating beam fatigue test data? If so, what model among the existing ones provides the best fit?*

- As expected, Manson and Muralidharan's conversion method resulted in overestimated high-cycle fatigue region for A356 aluminum alloy.
- Even though conversion method by Sors made acceptable predictions for A356 aluminum alloy, precautions should be taken due to its small number of parameters involved.
- Taking fatigue strength at 10^8 cycles as true elastic limit for A356 aluminum cast alloy in Esin's method is recommended for its simplicity.
- Esin's method gives the closest fit for converted data to experimental data among all three models available.

7. Future Work

Upon observing the reasonable predictions of fatigue life from tensile properties, it is the purpose of the future work:

- to extend the analyses that were made on mean stress correction, including those that are made in pure tension and pure compression data,
- to determine with more data from rotating bending and uniaxial fatigue that Esin's method is the most reliable among the ones in the literature.
- to develop closed-form method to predict both rotating beam and uniaxial fatigue properties from tensile data.

References

1. Özdeş, H. and M. Tiryakioğlu, *On the Relationship between Structural Quality Index and Fatigue Life Distributions in Aluminum Aerospace Castings.* Metals, 2016. **6**(4): p. 81.
2. Schütz, W., *A history of fatigue.* Engineering Fracture Mechanics, 1996. **54**(2): p. 263-300.
3. Dieter, G.E., *Mechanical metallurgy*. 2nd ed. McGraw-Hill series in materials science and engineering. 1976, New York: McGraw-Hill. xxi, 774 p.
4. Reed-Hill, R.E., *Physical metallurgy principles*. 1964, Princeton, N.J.: Van Nostrand.
5. *MIL-A-21180 D: Aluminum-Alloy Castings*. 1984: Department of Defense.
6. Lee, Y.-L., *Fatigue testing and analysis: theory and practice*. Vol. 13. 2005: Butterworth-Heinemann.
7. Manson, S.S., *Fatigue: a complex subject—some simple approximations.* Experimental mechanics, 1965. **5**(7): p. 193-226.
8. Muralidharan, U. and S.S. Manson, *A Modified Universal Slopes Equation for Estimation of Fatigue Characteristics of Metals.* Journal of Engineering Materials and Technology, 1988. **110**(1): p. 55-58.
9. Baumel Jr, A. and T. Seeger, *Materials data for cyclic loading. Supplement 1*. Elsevier Science Publishers, 1990.
10. Meggiolaro, M. and J. Castro, *Statistical evaluation of strain-life fatigue crack initiation predictions.* International Journal of Fatigue, 2004. **26**(5): p. 463-476.
11. Lopez, Z. and A. Fatemi, *A method of predicting cyclic stress–strain curve from tensile properties for steels.* Materials Science and Engineering: A, 2012. **556**: p. 540-550.
12. Heywood, R., *Designing against fatigue*. Chapman and Hall Limited, London. Vol. 5. 1962.
13. Stephens, R.I., et al., *Metal fatigue in engineering*. 2000: John Wiley & Sons.
14. Dowling, N.E., *Mean stress effects in strain–life fatigue.* Fatigue & Fracture of Engineering Materials & Structures, 2009. **32**(12): p. 1004-1019.
15. Dowling, N.E., C.A. Calhoun, and A. Arcari, *Mean stress effects in stress-life fatigue and the Walker equation.* Fatigue & Fracture of Engineering Materials & Structures, 2009. **32**(3): p. 163-179.
16. E. Dowling, N., *Mean Stress Effects in Stress-Life and Strain-Life Fatigue.* Society of Automotie Engineers, Inc., 2004. **51**.
17. Ince, A. and G. Glinka, *A modification of Morrow and Smith-Watson-Topper mean stress correction models.* Fatigue & Fracture of Engineering Materials & Structures, 2011. **34**(11): p. 854-867.
18. Niesłony, A. and M. Böhm, *Mean Stress Effect Correction in Frequency-domain Methods for Fatigue Life Assessment.* Procedia Engineering, 2015. **101**: p. 347-354.
19. Özdeş, H. and M. Tiryakioğlu, *On The Mean Stress Correction in Fatigue Life Assessment in Cast Aluminum Alloys*, in *Shape Casting: 6th International Symposium*. 2016, John Wiley & Sons, Inc. p. 125-132.

20. Smith, K., T. Topper, and P. Watson, *A stress-strain function for the fatigue of metals(Stress-strain function for metal fatigue including mean stress effect).* Journal of materials, 1970. **5**: p. 767-778.
21. *Fatigue curve*. Available from: http://www.expertsmind.com/topic/fatigue/fatigue-curve-914333.aspx.
22. *ISO 1099:2006 Metallic materials — Fatigue testing — Axial force-controlled method*.
23. Wöhler, A., *Über die Festigkeits-versuche mit Eisen und Stahl.* Zeitschrift für Bauwesen, 1870. **20**: p. 74-106.
24. Basquin, O. *The exponential law of endurance tests*. in *Proc. Astm*. 1910.
25. Kun, F., et al., *Universality behind Basquin's Law of Fatigue.* Phys Rev Lett, 2008. **100**(9): p. 094301.
26. Collins, J.A., *Failure of materials in mechanical design: analysis, prediction, prevention*. 1993: John Wiley & Sons.
27. Kalpakjian, S., S.R. Schmid, and K.V. Sekar, *Mechanical Behavior, Testing and Manufacturing Properties of Materials*, in *Manufacturing engineering and technology*. 2014, Prentice Hall. p. 56-87.
28. Soderberg, C.R., *Factor of safety and working stress.* Transactions of ASME, 1930. **52**(2): p. 13-28.
29. Walker, K., *The effect of stress ratio during crack propagation and fatigue for 2024-T3 and 7075-T6 aluminum*, in *Effects of environment and complex load history on fatigue life*. 1970, ASTM International.
30. *MIL-HDBK-5J: Metallic Materials and Elements for Aerospace Vehicle Structures*. 2003: Department of Defense.
31. Campbell, J., *Entrainment defects.* Materials Science and Technology, 2006. **22**(2): p. 127-145.
32. Tiryakioğlu, M., J. Campbell, and J.T. Staley, *Evaluating structural integrity of cast Al–7% Si–Mg alloys via work hardening characteristics.* Materials Science and Engineering: A, 2004. **368**(1-2): p. 205-211.
33. Tiryakioğlu, M., *On estimating the fracture stress and elongation of Al–7%Si–0.3%Mg alloy castings with single pores.* Materials Science and Engineering A, 2010. **527**(18–19): p. 4546-4549.
34. Wang, Q.G., D. Apelian, and D.A. Lados, *Fatigue behavior of A356-T6 aluminum cast alloys. Part I. Effect of casting defects.* Journal of Light Metals, 2001. **1**(1): p. 73-84.
35. Nyahumwa, C., N. Green, and J. Campbell, *Effect of Mold-Filling Turbulence on Fatigue Properties of Cast Aluminum Alloys (98-58).* Transactions of the American Foundrymen's Society, 1998. **106**: p. 215-223.
36. Tiryakioğlu, M., J. Campbell, and C. Nyahumwa, *Fracture Surface Facets and Fatigue Life Potential of Castings.* Metallurgical and Materials Transactions B, 2011. **42**(6): p. 1098-1103.
37. Nyahumwa, C., N.R. Green, and J. Campbell, *Influence of casting technique and hot isostatic pressing on the fatigue of an Al-7Si-Mg alloy.* Metallurgical and Materials Transactions A, 2001. **32**(2): p. 349-358.

38. Mayer, H., C. Ede, and J. Allison, *Influence of cyclic loads below endurance limit or threshold stress intensity on fatigue damage in cast aluminium alloy 319-T7.* International journal of fatigue, 2005. **27**(2): p. 129-141.
39. Promisel, N. *Evaluation of Non-Ferrous Materials*. in *Materials Evaluation in Relation to Component Behavior, Proc. Third Sagamore Ordnance Materials Research Conference*. 1956.
40. Wang, Q.G., et al., *Oxide films, pores and the fatigue lives of cast aluminum alloys.* Metallurgical and Materials Transactions B, 2006. **37**(6): p. 887-895.
41. Murakami, Y. and M. Endo, *Effects of defects, inclusions and inhomogeneities on fatigue strength.* International Journal of Fatigue, 1994. **16**(3): p. 163-182.
42. Murakami, Y., *Metal fatigue: effects of small defects and nonmetallic inclusions*. 2002: Elsevier.
43. Murakami, Y. and S. Beretta, *Small defects and inhomogeneities in fatigue strength: experiments, models and statistical implications.* Extremes, 1999. **2**(2): p. 123-147.
44. Kobayashi, M. and T. Matsui, *Prediction of fatigue strength of aluminum casting alloys by the√ area parameter model.* Trans. JSME, ser. A, 1996. **62**(594): p. 341-346.
45. Tiryakioğlu, M., *Relationship between Defect Size and Fatigue Life Distributions in Al-7 Pct Si-Mg Alloy Castings.* Metallurgical and Materials Transactions A, 2009. **40**(7): p. 1623-1630.
46. Iben Houria, M., et al., *Influence of casting defect and SDAS on the multiaxial fatigue behaviour of A356-T6 alloy including mean stress effect.* International Journal of Fatigue, 2015. **80**: p. 90-102.
47. Gall, K., et al., *On the driving force for fatigue crack formation from inclusions and voids in a cast A356 aluminum alloy.* International Journal of Fracture, 2001. **108**(3): p. 207-233.
48. Wicke, M., et al., *Characterization of Casting Pores in Fe-rich Al-Si-Cu Alloys by Microtomography and Finite Element Analysis.* Procedia Structural Integrity, 2016. **2**: p. 2643-2649.
49. Nicoletto, G., et al., *Casting Porosity and Long-Life Fatigue Strength of a Cast Al-Alloy.* Materials Science Forum, 2008. **567-568**: p. 393-396.
50. Raske, D. and J. Morrow, *Mechanics of materials in low cycle fatigue testing*, in *Manual on Low Cycle Fatigue Testing*. 1969, ASTM International.
51. Bathias, C., *There is no infinite fatigue life in metallic materials.* Fatigue and Fracture of Engineering Materials and structures, 1999. **22**(7): p. 559-566.
52. Mughrabi, H., *Microstructural mechanisms of cyclic deformation, fatigue crack initiation and early crack growth.* Philosophical Transactions of the Royal Society of London A: Mathematical, Physical and Engineering Sciences, 2015. **373**(2038).
53. Courtney, T.H., *Mechanical behavior of materials*. 2005: Waveland Press.
54. Tiryakioğlu, M., J.T. Staley, and J. Campbell, *Evaluating structural integrity of cast Al–7% Si–Mg alloys via work hardening characteristics: II. A new quality index.* Materials Science and Engineering: A, 2004. **368**(1): p. 231-238.
55. Alexopoulos, N.D. and M. Tiryakioglu, *Relationship between Fracture Toughness and Tensile Properties of A357 Cast Aluminum Alloy.* Metallurgical and Materials

Transactions a-Physical Metallurgy and Materials Science, 2009. **40a**(3): p. 702-716.
56. Tiryakioğlu, M., J.T. Staley, and J. Campbell, *The effect of structural integrity on the tensile deformation characteristics of A206-T71 alloy castings.* Materials Science and Engineering: A, 2008. **487**(1-2): p. 383-387.
57. Wertz, J., et al., *An Energy-Based Axial Isothermal-Mechanical Fatigue Lifing Procedure.* Journal of Engineering for Gas Turbines and Power, 2012. **134**(2): p. 024502.
58. Scott-Emuakpor, O.E., et al., *Analysis of Strain Energy Behavior Throughout a Fatigue Process.* Experimental Mechanics, 2011. **51**(8): p. 1317-1323.
59. Esin, A. and W. Jones, *A mathematical model for generating microplastic hysteresis loops.* The Journal of Strain Analysis for Engineering Design, 1968. **3**(1): p. 50-56.
60. Esin, A., *The Microplastic Strain Energy Criterion Applied to Fatigue.* Journal of Basic Engineering, 1968. **90**(1): p. 28-36.
61. Esin, A. and W.D. Jones, *A theory of fatigue based on the microstructural accumulation of strain energy.* Nuclear Engineering and Design, 1966. **4**(3): p. 292-298.
62. Duyi, Y. and W. Zhenlin, *A new approach to low-cycle fatigue damage based on exhaustion of static toughness and dissipation of cyclic plastic strain energy during fatigue.* International Journal of Fatigue, 2001. **23**(8): p. 679-687.
63. Tiryakioglu, M., J. Campbell, and N.D. Alexopoulos, *Quality Indices for Aluminum Alloy Castings: A Critical Review.* Metallurgical and Materials Transactions B, 2009. **40**: p. 802-811.
64. Tiryakioğlu, M. and J. Campbell, *Quality Index for Aluminum Alloy Castings.* International Journal of Metalcasting, 2014. **8**(3): p. 39-42.
65. Tiryakioğlu, M., J. Campbell, and N.D. Alexopoulos, *On the ductility potential of cast Al–Cu–Mg (206) alloys.* Materials Science and Engineering: A, 2009. **506**(1–2): p. 23-26.
66. Tiryakioğlu, M., J. Campbell, and N.D. Alexopoulos, *On the ductility of cast Al-7 pct Si-Mg alloys.* Metallurgical and Materials Transactions A, 2009. **40**(4): p. 1000-1007.
67. Tiryakioglu, M. and J. Campbell, *Ductility, structural quality, and fracture toughness of Al–Cu–Mg–Ag (A201) alloy castings.* Materials Science and Technology, 2009. **25**(6): p. 784-789.
68. Ünal, O. and M. Tiryakioğlu, *On the ductility potential and assessment of structural quality in Mg alloy castings.* Materials Science and Engineering: A, 2015. **643**: p. 51-54.
69. Tiryakioğlu, M., J. Campbell, and N.D. Alexopoulos, *Quality Indices for Aluminum Alloy Castings: A Critical Review.* Metallurgical and Materials Transactions B, 2009. **40**(6): p. 802-811.
70. Alexopoulos, N.D. and M. Tiryakioğlu, *On the uniform elongation of cast Al–7%Si–0.6%Mg (A357) alloys.* Materials Science and Engineering: A, 2009. **507**(1-2): p. 236-240.

71. Pang, J.C., et al., *Relations between fatigue strength and other mechanical properties of metallic materials.* Fatigue & Fracture of Engineering Materials & Structures, 2014. **37**(9): p. 958-976.
72. Pang, J.C., et al., *General relation between tensile strength and fatigue strength of metallic materials.* Materials Science and Engineering: A, 2013. **564**: p. 331-341.
73. Tiryakioğlu, M., *On the relationship between elongation and fatigue life in A206-T71 aluminum castings.* Materials Science and Engineering: A, 2014. **601**: p. 116-122.
74. Coffin Jr, L.F., *A study of the effects of cyclic thermal stresses on a ductile metal*. 1953, Knolls Atomic Power Lab.
75. Manson, S.S., *Behavior of materials under conditions of thermal stress.* 1954.
76. McLellan, D., *Tensile Properties of A357-T6 Aluminum Castings.* Journal of Testing and Evaluation, 1980. **8**(4): p. 170-176.
77. Sors, L., *Fatigue design of machine components*. Vol. 1. 1971: Pergamon.
78. Manson, S.S. and U. Muralidharan, *Fatigue Life Prediction in Bending from Axial Fatigue Information.* Fatigue & Fracture of Engineering Materials & Structures, 1987. **9**(5): p. 357-372.
79. Esin, A., *A Method for Correlating Different Types of Fatigue Curve.* International Journal of Fatigue, 1980. **2**(4): p. 153-158.
80. Esin, A. and W.J.D. Jones, *The Effect of Strain on the A.C. Resistance of a Metal: a Method of Studying Microplasticity.* British Journal of Applied Physics, 1967. **18**: p. 1251-1257.
81. Weibull, W., *A statistical theory of the strength of materials*. 1939: Generalstabens litografiska anstalts förlag.
82. Weibull, W., *The phenomenon of rupture in solids*. 1939, Stockholm: Generalstabens litografiska anstalts förlag.
83. Weibull, W., *A statistical distribution function of wide applicability.* Journal of Applied Mechanics, 1951. **18**: p. 293-297.
84. Peirce, F.T., *Tensile Tests for Cotton Yarns–"The Weakest Link" Theorems on the Strength of Long and of Composite Specimens.* Journal of the Textile Institute, 1926. **17**: p. T355-368.
85. Tiryakioğlu, M., *Weibull Analysis of Mechanical Data for Castings II: Weibull Mixtures and Their Interpretation.* Metallurgical and Materials Transactions A, 2015. **46**(1): p. 270-280.
86. Tiryakioğlu, M. and J. Campbell, *Weibull Analysis of Mechanical Data for Castings: A Guide to the Interpretation of Probability Plots.* Metallurgical and Materials Transactions A, 2010. **41**(12): p. 3121-3129.
87. Goodman, J. and . *Mechanics Applied to Engineering*. 9th edition ed. Vol. 1. 1930, London: Longmans Green and Co.
88. Jana, S., et al., *Effect of stress ratio on the fatigue behavior of a friction stir processed cast Al–Si–Mg alloy.* Scripta Materialia, 2009. **61**(10): p. 992-995.
89. Oswalt, K., *A Comparison of the Fatigue Behavior of High Strength Cast Aluminum Alloys 201 and A357*. 1971, DTIC Document.
90. Koutiri, I., et al., *High cycle fatigue damage mechanisms in cast aluminium subject to complex loads.* International Journal of Fatigue, 2013. **47**: p. 44-57.

91. Mu, P., et al., *Influence of casting defects on the fatigue behavior of cast aluminum AS7G06-T6.* International Journal of Fatigue, 2014. **63**: p. 97-109.
92. Serrano Munoz, I., *Influence of casting defects on the fatigue behaviour of an A357-T6 aerospace alloy*. 2014, Lyon, INSA.
93. Sarkani, S., et al., *Runout analysis in fatigue investigation.* Engineering Fracture Mechanics, 2007. **74**(18): p. 2971-2980.
94. Boileau, J.M., *The Effect of Solidification Time on the Mechanical Properties of a Cast 319 Aluminum Alloy*, in *Materials Science and Engineering*. 2000, Wayne State University.
95. Byczynski, G., *The Strength and Fatigue Performance of 319 Aluminum Alloy Castings*, in *School of Metallurgy and Materials*. 2002, University of Birmingham.
96. Chaudhury, S.K., et al., *Fatigue Performance of Fluidized Bed Heat Treated 319 Alloy Diesel Cylinder Heads.* Metallurgical and Materials Transactions A, 2015. **46**(7): p. 3015-3027.
97. Chaudhury, S.K., et al., *Microstructure and Mechanical Properties of Heat-Treated B319 Alloy Diesel Cylinder Heads.* Metallurgical and Materials Transactions A, 2015. **46**(7): p. 3276-3286.
98. Zhu, X., *Ultrasonic Fatigue of E319 Cast Aluminum Alloy in the Long Lifetime Regime*, in *Materials Science and Engineering*. 2007, The University of Michigan.
99. Rincon, E., et al., *Temperature effects on the tensile properties of cast and heat treated aluminum alloy A319.* Materials Science and Engineering: A, 2009. **519**(1-2): p. 128-140.
100. Stephens, R.I., et al., *Low Cycle Fatigue of A356-T6 Cast Aluminum Alloy - A Round-Robin Test Program.* SAE Technical Paper 881701, 1988.
101. Kaplan, E.L. and P. Meier, *Nonparametric Estimation from Incomplete Observations.* Journal of the American Statistical Association, 1958. **53**(282): p. 457-481.
102. Tiryakioğlu, M., D. Hudak, and G. Ökten, *On evaluating Weibull fits to mechanical testing data.* Materials Science and Engineering: A, 2009. **527**(1–2): p. 397-399.
103. Eisaabadi B, G., et al., *The effect of melt quality and filtering on the Weibull distributions of tensile properties in Al–7%Si–Mg alloy castings.* Materials Science and Engineering: A, 2013. **579**: p. 64-70.
104. Skallerud, B., T. Iveland, and G. Härkegård, *Fatigue life assessment of aluminum alloys with casting defects.* Engineering Fracture Mechanics, 1993. **44**(6): p. 857-874.
105. Barter, S., et al., *An experimental evaluation of fatigue crack growth.* Engineering failure analysis, 2005. **12**(1): p. 99-128.
106. Rading, G., J. Berry, and J. Li, *Fatigue crack growth in cast Al-Cu alloy A206 with different levels of porosity.* AFS Transactions, 1994. **102**: p. 57-61.
107. Crawford, B.R., et al., *The EIFS distribution for anodized and pre-corroded 7010-T7651 under constant amplitude loading.* Fatigue & Fracture of Engineering Materials & Structures, 2005. **28**(9): p. 795-808.
108. Tiryakioğlu, M., *On the relationship between statistical distributions of defect size and fatigue life in 7050-T7451 thick plate and A356-T6 castings.* Materials Science and Engineering: A, 2009. **520**(1): p. 114-120.

109. Jiang, H., P. Bowen, and J.F. Knott, *Fatigue performance of a cast aluminium alloy Al-7Si-Mg with surface defects.* Journal of Materials Science, 1999. **34**(4): p. 719-725.
110. Farahmand, B. and K. Nikbin, *Predicting fracture and fatigue crack growth properties using tensile properties.* Engineering Fracture Mechanics, 2008. **75**(8): p. 2144-2155.
111. Han, S.-W., S. Kumai, and A. Sato, *Fatigue crack growth behavior in semi-liquid die-cast Al-7% Si-0.4% Mg alloys with fine effective grain structure.* Materials Science and Engineering: A, 2001. **308**(1): p. 225-232.
112. Umezawa, O., K. Nagai, and K. Ishikawa, *Internal crack initiation in high cycle fatigue for Ti-5 Al-2.5 Sn ELI alloy at cryogenic temperatures.* Tetsu-To-Hagane/Journal of the Iron and Steel Institute of Japan, 1989: p. 159-166.
113. Mughrabi, H., *On 'multi-stage' fatigue life diagrams and the relevant life-controlling mechanisms in ultrahigh-cycle fatigue.* Fatigue & Fracture of Engineering Materials & Structures, 2002. **25**(8-9): p. 755-764.
114. Sadananda, K., A. Vasudevan, and N. Phan, *Analysis of endurance limits under very high cycle fatigue using a unified damage approach.* International Journal of Fatigue, 2007. **29**(9): p. 2060-2071.
115. Przybyla, C., et al., *Microstructure-sensitive modeling of high cycle fatigue.* International Journal of Fatigue, 2010. **32**(3): p. 512-525.
116. Nakamura, Y., et al., *Effect of alumite surface treatments on long-life fatigue behavior of a cast aluminum in rotating bending.* International Journal of Fatigue, 2010. **32**(3): p. 621-626.
117. Bathias, C., *There is no infinite fatigue life in metallic materials.* Fatigue & Fracture of Engineering Materials & Structures, 1999. **22**(7): p. 559-565.
118. Wang, Q.Y., et al., *Gigacycle fatigue of ferrous alloys.* Fatigue & Fracture of Engineering Materials & Structures, 1999. **22**(8): p. 667-672.
119. do Lee, C., *Effect of T6 heat treatment on the defect susceptibility of fatigue properties to microporosity variations in a low-pressure die-cast A356 alloy.* Materials Science and Engineering: A, 2013. **559**: p. 496-505.
120. Özdeş, H. and M. Tiryakioğlu, *On The Relationship Between Quality Index and Fatigue Life Distributions in B201 and D357 Alloy Aerospace Castings*, in *Shape Casting: 6th International Symposium*. 2016, John Wiley & Sons, Inc. p. 85-92.
121. Ozelton, M., S. Mocarski, and P. Porter, *Durability and damage tolerance of aluminum castings*. 1991, DTIC Document.
122. Anderson, T.W. and D.A. Darling, *A Test of Goodness of Fit.* Journal of the American Statistical Association, 1954. **49**(268): p. 765-769.
123. Jiang, S. and D. Kececioglu, *Maximum likelihood estimates, from censored data, for mixed-Weibull distributions.* IEEE Transactions on Reliability, 1992. **41**(2): p. 248-255.
124. Staley Jr, J.T., M. Tiryakioğlu, and J. Campbell, *The effect of hot isostatic pressing (HIP) on the fatigue life of A206-T71 aluminum castings.* Materials Science and Engineering: A, 2007. **465**(1–2): p. 136-145.
125. Staley Jr, J.T., M. Tiryakioğlu, and J. Campbell, *The effect of increased HIP temperatures on bifilms and tensile properties of A206-T71 aluminum castings.* Materials Science and Engineering: A, 2007. **460–461**: p. 324-334.

126. Campbell, J., *Castings*. 2nd edition ed. 2003: Elsevier.
127. Nayhumwa, C., N.R. Green, and J. Campbell, *Influence of casting technique and hot isostatic pressing on the fatigue of an Al-7Si-Mg alloy.* Metallurgical and Materials Transactions A, 2001. **32**(2): p. 349-358.
128. Zhang, B., D.R. Poirier, and W. Chen, *Microstructural effects on high-cycle fatigue-crack initiation in A356.2 casting alloy.* Metallurgical and Materials Transactions A, 1999. **30**(10): p. 2659-2666.
129. Couper, M.J., A.E. Neeson, and J.R. Griffiths, *Casting defects and the fatigue behaviour of an aluminium casting alloy.* Fatigue & Fracture of Engineering Materials & Structures, 1990. **13**(3): p. 213-227.
130. Stephens, R., *The influence of microstructure on the fatigue behavior of A356-T6 cast aluminium alloy.* Materials science monographs, 1988. **46**: p. 185-195.
131. Song, J.-Y., J.-C. Park, and Y.-S. Ahn, *Effect of Cast Microstructure on Fatigue Behaviors of A356 Aluminum Alloy for Automotive Wheel.* Journal of Korea Foundry Society, 2010. **30**(1): p. 46-51.
132. Palmer, D.E., *Stress ratio effects in fatigue of lost foam cast aluminum alloy 356*. 2014, THE UNIVERSITY OF WISCONSIN-MILWAUKEE.
133. Jiang, X.-S., et al., *Microstructure-based analysis of fatigue behaviour of Al-Si-Mg alloy*. Transactions of Nonferrous Metals Society of China, 2011. **21**(3): p. 443-448.
134. Song, M., et al., *Cyclic stress–strain behavior and low cycle fatigue life of cast A356 alloys.* International Journal of Fatigue, 2011. **33**(12): p. 1600-1607.
135. Davidson, C., et al., *Fatigue properties of a semi-solid cast Al–7Si–0.3 Mg–T6 alloy*. Metallurgical Science and Technology, 2000. **18**(2).
136. Davidson, C., J. Griffiths, and A. Zanada. *Fatigue Properties Of Squeeze, Semisolid And Gravity Diecast Al-Si-Mg Alloy*. in *Structural Integrity and Fracture International Conference (SIF'04)*. 2004.
137. Bergsma, S., X. Li, and M. Kassner, *Semi-solid thermal transformations in Al–Si alloys: II. the optimized tensile and fatigue properties of semi-solid 357 and modified 319 aluminum alloys.* Materials Science and Engineering: A, 2001. **297**(1): p. 69-77.
138. Uematsu, Y., et al. *Effect of friction stir processing on the fatigue behaviour of cast aluminium alloy*. in *ICF12, Ottawa 2009*. 2013.
139. Lee, M.H., et al., *Effects of HIPping on high-cycle fatigue properties of investment cast A356 aluminum alloys.* Materials Science and Engineering: A, 2003. **340**(1): p. 123-129.
140. Cao, X., et al., *Influence of casting defects on fatigue behaviour of A356 aluminium alloy*. International Journal of Cast Metals Research, 2014. **27**(6): p. 362-368.
141. Siegfanz, S., et al., *Influence of the microstructure on the fatigue damage behaviour of the aluminium cast alloy AlSi7Mg0.3.* Materials Science and Engineering: A, 2013. **565**: p. 21-26.
142. Gao, Y.X., et al., *A micro-cell model of the effect of microstructure and defects on fatigue resistance in cast aluminum alloys.* Acta Materialia, 2004. **52**(19): p. 5435-5449.
143. Kuwazuru, O., et al., *Quantitative evaluation of porosity effect on fatigue strength of high pressure die cast aluminum alloy (Part 2, fatigue strength prediction based*

on elastic stress field around pores). Nihon Kikai Gakkai Ronbunshu, A Hen/Transactions of the Japan Society of Mechanical Engineers, Part A, 2011. **77**(773): p. 48-57.
144. Shaha, S., et al., *Effect of Cr, Ti, V, and Zr Micro-additions on Microstructure and Mechanical Properties of the Al-Si-Cu-Mg Cast Alloy.* Metallurgical and Materials Transactions A, 2016. **47**(5): p. 2396-2409.
145. Shaha, S., et al., *Monotonic and cyclic deformation behavior of the Al–Si–Cu–Mg cast alloy with micro-additions of Ti, V and Zr.* International Journal of Fatigue, 2015. **70**: p. 383-394.
146. Elhadari, H., et al., *Tensile and fatigue properties of a cast aluminum alloy with Ti, Zr and V additions.* Materials Science and Engineering: A, 2011. **528**(28): p. 8128-8138.
147. Ammar, H.R., A.M. Samuel, and F.H. Samuel, *Porosity and the fatigue behavior of hypoeutectic and hypereutectic aluminum–silicon casting alloys.* International Journal of Fatigue, 2008. **30**(6): p. 1024-1035.
148. González, R., et al., *Experimental investigation for fatigue strength of a cast aluminium alloy.* International Journal of Fatigue, 2011. **33**(2): p. 273-278.
149. Tian, D., et al., *Low cycle fatigue behavior of casting A319 alloy under two different aging conditions.* Materials Science and Engineering: A, 2016. **654**: p. 60-68.
150. Caton, M., et al., *Demonstration of an endurance limit in cast 319 aluminum.* Metallurgical and Materials Transactions A, 2003. **34**(1): p. 33-41.
151. Ceschini, L., et al., *Microstructure, tensile and fatigue properties of the Al–10% Si–2% Cu alloy with different Fe and Mn content cast under controlled conditions.* Journal of Materials Processing Technology, 2009. **209**(15): p. 5669-5679.
152. Fan, K., et al., *Tensile and fatigue properties of gravity casting aluminum alloys for engine cylinder heads.* Materials Science and Engineering: A, 2013. **586**: p. 78-85.
153. González, R., et al., *Fatigue of an aluminium cast alloy used in the manufacture of automotive engine blocks.* International Journal of Fatigue, 2013. **54**: p. 118-126.
154. Tiryakioğlu, M., J. Campbell, and J.T. Staley, *The influence of structural integrity on the tensile deformation of cast Al–7wt.%Si–0.6wt.%Mg alloys.* Scripta Materialia, 2003. **49**(9): p. 873-878.
155. Tiryakioğlu, M., P.D. Eason, and J. Campbell, *Fatigue life of ablation-cast 6061-T6 components.* Materials Science and Engineering: A, 2013. **559**: p. 447-452.
156. Yi, J.Z., et al., *A Probabilistic Model of Fatigue Strength Controlled by Porosity Population in a 319-Type Cast Aluminum Alloy: Part II. Monte-Carlo Simulation.* Metallurgical and Materials Transactions A, 2007. **38**(5): p. 1123-1135.
157. Spindel, J.E. and E. Haibach, *The method of maximum likelihood applied to the statistical analysis of fatigue data.* International Journal of Fatigue, 1979. **1**(2): p. 81-88.
158. Spindel, J.E. and E. Haibach, *Some considerations in the statistical determination of the shape of SN curves*, in *Statistical analysis of fatigue data*. 1981, ASTM International.

APPENDIX

In HCF testing, it is common to have a combination of failure and survival data, i.e., run-outs in the same dataset. When that is the case, the data become "censored on the right tail of the distribution" and the analysis becomes more complex.

There are several procedures to take runouts into account during the analysis of fatigue test results [93, 157, 158]. One such method has been recently introduced by Sarkani *et al.* [93] who, with the assumption of the underlying distribution of fatigue life is Weibull, used the maximum likelihood method to estimate the coefficients in the Basquin law, by maximizing Equation A.1 with notation below.

$$\Lambda(b, m, \sigma, D)=-\ln(\sigma)\sum_{j=1}^{h} r_j+\sum_{j=1}^{h}\sum_{i=1}^{r_j} z_{ij}-\sum_{j=1}^{h}\sum_{i=1}^{r_j} e^{z_{ij}}-\sum_{j=1}^{h}(l_j-r_j)e^{z_j^*} \tag{A.1}$$

where,

$$z_{ij}=\frac{y_{ij}-\ln(-b)+m\ln(S_j)}{\sigma} \tag{A.2}$$

$$z_j^*=\frac{y_j^*-\ln(-b)+m\ln(S_j)}{\sigma} \tag{A.3}$$

h: number of stress levels tested

l: total number tested

l_j: total number tested at stress level S_j

r_j: number of failures observed at stress level S_j

y_{ij}: *i*th log failure cycle count at stress level j, $i=1,2,\ldots,r_j$; $y_{ij}=\ln(N_{ij})$

y^*_j: log of the run-out cycle at stress level *j*